Development of Semiconducting Polymers with Acid-Cleavable Side Chains for Size-Selective Gas Sensors Based on Organic Thin-Film Transistors

by

YuFang Zhong

A thesis

presented to the University of Waterloo

in fulfilment of the

thesis requirement for the degree of

Master of Applied Science

in

Chemical Engineering

Waterloo, Ontario, Canada, 2024

© YuFang Zhong 2024

Author's Declaration

I hereby declare that I am the sole author of this thesis. This is a true copy of the thesis, including any required final revisions, as accepted by my examiners.

I understand that my thesis may be made electronically available to the public.

Abstract

Organic thin-film transistor (OTFT) based gas sensors have gained research interests due to their promising performance and potential for integration into flexible and wearable electronic devices, characterized by low cost, light weight, and ease of fabrication. Herein, a series of novel semiconducting polymers with acid-cleavable side chains were synthesized for application as OTFT based gas sensors employing a size-selective approach. We first established a cost-effective and simple synthetic route to obtain acetal substituted thiophene based polymers. Subsequent conversion of acetal side chains to aldehydes was achieved through a simple acid treatment process applied to the coated polymer film by HCl vapor to generate nanopores. The pore sizes could be tuned by varying the lengths of the acetal side chains used. Screening of suitable polymer structures with desired pore sizes and adequate performance was accomplished by altering the acetal side chain lengths and the comonomer units. Overall results revealed that the aldehyde substituted polymer generated by acid treatment to OC21T polymer demonstrated the least sacrifice in OTFT performance upon side chain cleavage and the best stability under ambient conditions, which makes it the optimal candidate for OTFT based gas sensor material among all the polymers synthesized. The resulting aldehyde substituted thiophene based polymer (OCH1T) showed great sensitivity to methanol and ethanol vapors. Slight sensitivity of OCH1T polymer toward isopropanol vapor was also observed, which could be attributed to the grain boundaries of the polymer film. The promising size-selective effect was further confirmed by exposure of the device to other volatile organic compound vapors with various molecular sizes.

Acknowledgements

I would like to express my deepest gratitude to Professor Yuning Li for offering me the opportunity to join the Printable Electronic Materials Laboratory and pursue my graduate studies. I am truly thankful for his constructive advice and insightful feedback, which have guided me through the challenges I encountered during my master's studies. His mentorship has enabled me to enhance both my academic and personal skills, which is extremely beneficial for my future career and life. I deeply appreciate all the support I have received from him.

I would also like to thank my committee members, Professor Elisabeth Prince and Professor Ting Tsui, for taking the time to review this work and provide constructive suggestions.

Moreover, I would like to thank my colleagues, Dr. Ravinder Singh, Dr. Samala Venkateswarlu, Dr. Sung Jae Jeon, Dr. Xiguang Gao, Dr. Yas Fazaeli, Naixin Zhao, Scott Flynn, Andrew Stella, Songbo Cui, Jiayi Song, Jimmy Papazotos, Yi Yuan, Zhe Huang, and Yonglin Wang for assisting me with experiments, characterizations and device fabrications with valuable advice and suggestions.

I would also like to acknowledge the support provided by Natural Sciences and Engineering Research Council of Canada (NSERC) and the NSERC Green Electronics Network (GreEN).

Lastly, I would like to thank my family and friends who have provided continuous support and encouragement throughout my master's program.

Table of Contents

Author's Declaration ii

Abstract iii

Acknowledgements iv

List of Figures viii

List of Tables x

List of Schemes xi

List of Abbreviations xii

List of Symbols xiv

Chapter 1 Introduction to Organic Electronics 1

1.1 Semiconductors 1

1.2 Organic Electronics 3

1.3 Objectives and Thesis Outline 4

1.3.1 Objectives 4

1.3.2 Thesis Outline 4

Chapter 2 Background 6

2.1 Conducting Polymers 6

2.2 Organic Thin Film Transistor 7

2.2.1 Organic Field Effect Transistor Principles 7

2.2.2 Key Parameters 11

2.2.2.1 Charge Carrier Mobility 11

2.2.2.2 Threshold Voltage 11

2.2.2.3 Current On/Off Ratio 12

2.3 OTFT Based Gas Sensors 12

2.4 OTFT Device Preparation Methods 15

2.5 Gas Preparation 17

2.6 Characterization Methods 18

2.6.1 Nuclear Magnetic Resonance 18

2.6.2 Gel Permeation Chromatography 19

2.6.3 Thermogravimetric Analysis 20
2.6.4 Ultraviolet and Visible Spectroscopy 20
2.6.5 Cyclic Voltammetry 21
2.6.6 X-Ray Diffraction 22
2.6.7 Fourier Transform Infrared Spectroscopy 24

Chapter 3 Synthesis and Characterization of Acetal-Substituted Thiophene Polymers with Different Comonomer Units and the Corresponding Aldehyde-Based Polymers 25
3.1 Introduction of Polythiophenes 25
3.2 Bithiophene and Thienthiophene Series 26
3.2.1 Synthesis of Bithiophene and Thienthiophene Series of Polymers 27
3.2.2 Opto-electrochemical Properties 29
3.2.3 Physical Properties 36
3.2.4 Morphology and Crystallinity 38
3.2.5 OTFT Performance 41
3.3 One-Thiophene Series 48
3.3.1 Synthesis Method 48
3.3.2 Opto-electrochemical Properties 49
3.3.3 Physical and Chemical Properties 53
3.3.4 Morphology and Crystallinity 55
3.3.5 OTFT Performance 59
3.4 Experimental Section 63

Chapter 4 OTFT Based Gas Sensor Performances Using OMe1T and OC21T Polymers 72
4.1 Introduction 72
4.2 Stability of 1T Polymers in Air 72
4.3 OTFT Based Sensing Performances 74
4.3.1 Gas Injection Method 75
4.3.2 Results and Discussion 75
4.4 Real Time Sensing of OC21T Polymer Pair 77
4.4.1 Sensing Method 77
4.4.2 OC21T Polymer Sensitivity (Before Acid Treatment) 77
4.4.3 OCH1T based OTFT Sensor Performance 80
4.4.3.1 Alcohol Vapor Sensing 80

4.4.3.2 Other Solvent Sensing 86
4.5 Conclusions 88
Chapter 5 Conclusions and Future Steps 90
5.1 Conclusions 90
5.2 Future Steps 91
References 92

List of Figures

Figure 1-1. Energy levels of a semiconductor.[4] 2
Figure 2-1. Structures of some commonly used conducting polymers.[24] 6
Figure 2-2. Illustration of four types of OTFT structures: **a)** bottom-gate, bottom contact (BGBC), **b)** bottom-gate, top contact (BGTC), **c)** top-gate, bottom contact (TGBC), and **d)** top-gate, top contact (TGTC).[36] 8
Figure 2-3. Illustration of gas detection mechanism for a p-type OTFT device. [48] 14
Figure 2-4. BGBC OTFT devices with **a)** straight channel (smaller one); **b)** amplified channel with interdigitated electrodes (larger one). 16
Figure 2-5. Electrochemical cell setup for CV measurement. [60] 22
Figure 2-6. Demonstration of different polymer chain orientations with respect to the substrate: **a)** edge-on; **b)** face-on; **c)** end-on.[63] 23
Figure 3-1. Acid treatment setup of polymer film using HCl vapor for conversion of acetal group to aldehyde group. 31
Figure 3-2. Polymer films coated on glass substrate before acid treatment (left) and after acid treatment (right). 32
Figure 3-3. UV-vis absorption spectra of polymer solution, as-cast thin film, annealed thin film and acid-treated thin films with various conditions: **a)** OC4BT; **b)** OC8BT; **c)** OC4TT; and **d)** OC8TT. 34
Figure 3-4. CV profiles of OC4BT polymer: **a)** without acid treatment**; b)** with acid treatment (which is the OCHBT polymer). 34
Figure 3-5. CV profiles of OC8BT polymer: **a)** without acid treatment**; b)** with acid treatment (which is the OCHBT polymer). 35
Figure 3-6. CV profiles of OC4TT polymer: **a)** without acid treatment**; b)** with acid treatment (which is the OCHTT polymer). 35
Figure 3-7. CV profiles of OC8TT polymer: **a)** without acid treatment**; b)** with acid treatment (which is the OCHTT polymer). 35
Figure 3-8. TGA curves for polymers: **a)** OC4BT; **b)** OC8BT; **c)** OC4TT; and **d)** OC8TT. 37
Figure 3-9. GIXD of OC4BT film (without acid treatment) after annealed at various temperatures: **a)** in-plane; **b)** out-of-plane; **c)** 2D image of polymer film annealed at 150 °C which demonstrates the best crystallinity. 39
Figure 3-10. GIXD of OC8BT film (without acid treatment) after annealed at various temperatures: **a)** in-plane; **b)** out-of-plane; **c)** 2D image of OC8BT film annealed at 200 °C which demonstrates the best crystallinity. 40
Figure 3-11. GIXD of OC8TT film (without acid treatment) after annealed at various temperatures: **a)** in-plane; **b)** out-of-plane; **c)** 2D image of OC8TT film annealed at 200 °C. 40
Figure 3-12. OTFT transfer curve comparisons before and after acid treatment for polymers: **a)** OC4BT and **b)** OC8BT. 42
Figure 3-13. **(a&b)** OTFT transfer curves for OC4BT without and with acid treatment (OCHBT), respectively, at 100 ºC; **(c&d)** OTFT output curves for OC4BT without and with acid treatment (OCHBT), respectively, at 100 ºC. 43
Figure 3-14. **(a&b)** OTFT transfer curves for OC8BT without and with acid treatment (OCHBT), respectively, at 150 ºC; **(c&d)** OTFT output curves for OC8BT without and with acid treatment (OCHBT), respectively, at 150 ºC. 44
Figure 3-15. OTFT transfer curve comparisons before and after acid treatment for polymers: **a)** OC4TT and **b)** OC8TT. 45

Figure 3-16. **(a&b)** OTFT transfer curves for OC4TT without and with acid treatment (OCHTT), respectively, at 250 ºC and 100 ºC; **(c&d)** OTFT output curves for OC4TT without and with acid treatment (OCHTT), respectively, at 250 ºC and 100 ºC. 46
Figure 3-17. **(a&b)** OTFT transfer curves for OC8TT without and with acid treatment (OCHTT), respectively, at 250 ºC and 150 ºC; **(c&d)** OTFT output curves for OC8TT without and with acid treatment (OCHTT), respectively, at 250 ºC and 150 ºC. 47
Figure 3-18. UV-vis absorption spectra of polymer solution, as-cast thin film, annealed thin film and acid-treated thin films with various conditions: **a)** OMe1T; **b)** OC21T; and **c)** OC41T. 51
Figure 3-19. CV profiles of OMe1T polymer: **a)** non-acid treated; **b)** acid treated (which is the OCH1T polymer). 52
Figure 3-20. CV profiles of OC21T polymer: **a)** non-acid treated; **b)** acid treated (which is the OCH1T polymer). 52
Figure 3-21. CV profiles of OC41T polymer**: a)** non-acid treated; **b)** acid treated (which is the OCH1T polymer). 52
Figure 3-22. TGA curves for polymers: **a)** OMe1T; **b)** OC21T; and **c)** OC41T. 54
Figure 3-23. FTIR spectra of OC21T polymer before and after acid treatment. 55
Figure 3-24. GIXD of OC21T polymer: **a)** no acid, in-plane**, b)** no acid, out-of-plane**; c)** acid, in-plane**, d)** acid, out-of-plane**, e)** 2D images for OC21T before acid treatment at 150 °C (left) and after acid at 150 °C (right). 56
Figure 3-25. GIXD of OC41T polymer: **a)** no acid, in-plane**, b)** no acid, out-of-plane; **c)** acid, in-plane**, d)** acid, out-of-plane**, e)** 2D images for OC41T before acid treatmnet at 150 °C (left) and after acid at 150 °C (right). 57
Figure 3-26. AFM images of **a)** OC21T thin film annealed at 100 °C and; **b)** OCH1T thin film which was obtained by acid treatment to OC21T film, annealed at 100 °C. 58
Figure 3-27. OTFT transfer curve comparisons before and after acid treatment for polymers: **a)** OMe1T; **b)** OC21T; and **c)** OC41T. 60
Figure 3-28. (**a-c)** OTFT transfer curves and **(d-e)** output curves for OMe1T, OC21T and OC41T at RT, 150 °C and 150 °C, respectively. 61
Figure 4-1. Mobilities of OTFT device measured in N_2 glovebox and air for polymers before acid treatment (left) and after acid treatment (right): **a)** OMe1T; **b)** OC21T. 73
Figure 4-2. Threshold voltages of OTFT device measured in N_2 glovebox and air for polymer before acid treatment (left) and after acid treatment (right): **a)** OMe1T; **b)** OC21T. 73
Figure 4-3. Gas sensing profiles of OC21T based OTFT sensor being exposed to various gas vapors. 79
Figure 4-4. Relative response ratio summary of OCH1T based OTFT device (from OC21T polymer) towards methanol, ethanol, and IPA gases with different concentrations. 82
Figure 4-5. Sensitivity summary for OCH1T (from OC21T polymer) based OTFT device upon exposure to methanol, ethanol and IPA gases. 82
Figure 4-6. I_{DS} vs. time measurment of OCH1T polymer being exposed to various concentrations of methanol vapors. 83
Figure 4-7. I_{DS} vs. time measurment of OCH1T polymer being exposed to various concentrations of ethanol vapors. 84
Figure 4-8. I_{DS} vs. time measurment of OCH1T polymer being exposed to various concentrations of ispropanol vapors. 85
Figure 4-9. Real-time gas sensing profiles of OCH1T based OTFT sensor being exposed to various gas vapors. 87

List of Tables

Table 3-1. Summary of optical and electrochemical properties of BT and TT series polymers.. 36
Table 3-2. Summary of optical and electrochemical properties of OCHBT polymer through acid treatment to OC4BT and OC8BT polymers, correspondingly. 36
Table 3-3. Summary of optical and electrochemical properties of OCHTT polymer through acid treatment to OC4TT and OC8TT polymers, correspondingly. 36
Table 3-4. OTFT Performance Summary for OC4BT polymer. 44
Table 3-5. OTFT Performance Summary for OC4BT polymer after acid treatment. 44
Table 3-6. OTFT Performance Summary for OC8BT polymer. 45
Table 3-7. OTFT performance summary for OC8BT polymer after acid treatment. 45
Table 3-8. OTFT performance summary for OC4TT polymer. 47
Table 3-9. OTFT performance summary for OC4TT polymer after acid treatment. 47
Table 3-10. OTFT performance summary for OC8TT polymer. 48
Table 3-11. OTFT performance summary for OC8TT polymer after acid treatment. 48
Table 3-12. Summary of optical and electrochemical properties for 1T series polymers. 53
Table 3-13. Summary of optical and electrochemical properties for 1T series polymers after acid treatment. 53
Table 3-14. OTFT performance summary for OMe1T polymer. 61
Table 3-15. OTFT performance summary for OC21T polymer. 62
Table 3-16. OTFT performance summary for OC41T polymer. 62
Table 4-1. OMe1T OTFT performance comparison in glovebox and air. 74
Table 4-2. OC21T OTFT performance comparison in glovebox and air. 74
Table 4-3. OTFT Summary for OCH1T polymer (converted from OMe1T) with injection of various gases. 76
Table 4-4. OTFT Summary of OCH1T polymer (converted from OC21T) with injection of various gases. 76

List of Schemes

Scheme 1. Synthesis schemes of OC4BT and OC4TT polymers and the corresponding aldehyde forms. 28
Scheme 2. Synthesis schemes of OC8BT and OC8TT polymers and the corresponding aldehyde forms. 28
Scheme 3. Synthesis scheme for 1T series of polymer and conversion to aldehyde-substituted thiophene-based polymer. 49

List of Abbreviations

1T: One thiophene

2D: Two-dimensional

AFM: Atomic force microscopy

BT: Bithiophene

CP: Conducting polymer

CV: Cyclic voltammetry

$CDCl_3$: Deuterated chloroform

D-A: Donor-acceptor

DCM: Dichloromethane

DDTS: Dodecyltrichlorosilane

EtOH: Ethanol

FET: Field-effect transistor

FTIR: Fourier transform infrared

GIXD: Grazing incidence X-ray diffraction

GPC: Gel permeation chromatography

HOMO: Highest occupied molecular orbital

IPA: Isopropanol

IP: In-plane

LUMO: Lowest unoccupied molecular orbital

MeOH: Methanol

NBS: N-bromosuccinimide

NMR: Nuclear magnetic resonance

OFET: Organic field-effect transistor

OLED: Organic light-emitting diode

OOP: Out-of-plane

OPV: Organic photovoltaics

OSC: Organic solar cell

OTFT: Organic thin-film transistor

PDI: Polydispersity index

PTSA: p-Toluenesulfonic acid

RT: Room temperature

SAM: Self-assembled monolayer

SEM: Scanning electron microscopy

TEM: Transmission electron microscopy

TGA: Thermogravimetric analysis

THF: Tetrahydrofuran

TLC: Thin layer chromatography

TT: Thieno[3,2-b]thiophene

UV-vis: Ultraviolet-visible

VOC: Volatile organic compound

XRD: X-ray diffraction

List of Symbols

ε: Molar absorptivity

$\lambda_{max,100}$: Maximum absorbance of thin film annealed at 100 °C

$\lambda_{max,RT}$: Maximum absorbance of as-cast thin film

$\lambda_{max,sol}$: Maximum absorbance in solution

λ_{onset}: Onset absorption wavelength

μ: Mobility

A: Absorbance

Ag: Silver

Au: Gold

c: Concentration

E_{HOMO}: HOMO energy level

E_{LUMO}: LUMO energy level

E_g^{opt}: Optical band gap

$I_{ON/OFF}$: Current ON/OFF ratio

ℓ: Path length of light

M_n: Number-average molecular weight

M_w: Weight-average molecular weight

N_i: Number of molecules of i, where i is the polymer being measured

Pt: Platinum

W_i: Weight of i, where i is the polymer being measured

V_{DS}: Drain-source voltage

V_{GS}: Gate-source voltage

V_{th}: Threshold voltage

Chapter 1 Introduction to Organic Electronics

1.1 Semiconductors

Semiconductor materials are extensively used in the contemporary electronics industry and have garnered significant attention. Semiconductor materials exhibit conductivity that falls between that of insulators and conductors, due to the differences in energy band gaps among these materials.[1] The excitation of electrons from the valence band to the conduction band due to the absorption of energy provides conductivity to the material, while the energy difference between the two bands corresponds to the energy band gap. Electrons being promoted to the conduction band will leave holes in the valence band, thus generating charge carriers that govern the conductivity of the material. Metals typically have a band gap equal to 0 eV, indicating that electrons can move freely between the two bands, resulting in high conductivities. On the other hand, insulators have wide band gaps that prohibit electron promotion thus having no conductivity. Semiconductors possess narrow band gaps, typically greater than 0 eV and smaller than 3 eV, with some absorbing visible light and demonstrating important optical properties.[2,3] Specifically, certain semiconductors in which electrons relax from the excited state by emitting light instead of producing heat are used to make light-emitting diodes. An illustration of the energy band gap of a semiconductor is shown in **Figure 1-1**. It is worth mentioning that semiconductors in pure state have poor conductivity, but the introduction of dopants, exposure to light and modulation of temperature can lead to change in conductivity of the semiconducting material, allowing for control over the current flow.[1]

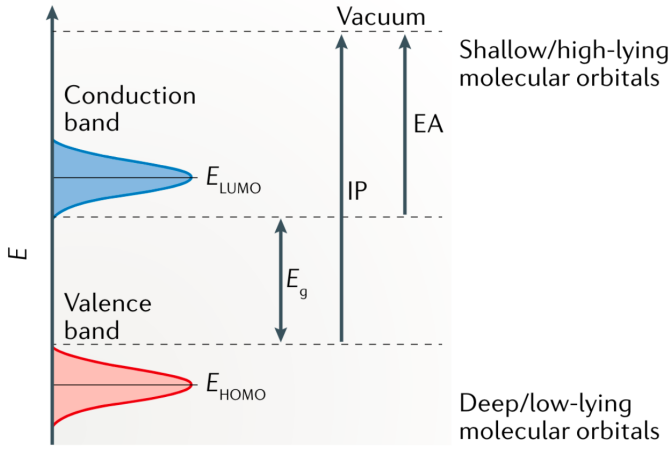


Figure 1-1. Energy levels of a semiconductor.[4]

Semiconductors can be categorized into inorganic and organic types based on their composition. Silicon (Si) and germanium (Ge) are dominantly used inorganic semiconductor materials for electronic devices and components with promising performances and high stability.[5–7] Nevertheless, such inorganic semiconductors have low flexibility, high production costs and heavyweight. In addition, high purity of raw materials is essential for achieving better and more reliable performance. Consequently, exploration of potential alternatives is crucial to address these challenges. In recent years, significant attention has been drawn to the research and development of organic semiconductors as they are more flexible, easy to fabricate, portable, and lightweight with low production costs.[5,8] Compared to the inorganic counterpart, organic semiconductors offer structure diversity, providing more control over the shape and morphology with adjustable conductivity.[5] Most organic semiconductors, either polymers or small molecules, have an extended π conjugation that allows for electrons to move along the molecular backbone and π stacks thus conducting electricity.[9] Applications based on organic semiconductors include integrated circuits, transistors, diodes, electronic displays, sensors, and solar cells. [3,5,10–16]

1.2 Organic Electronics

The field of organic electronics, including organic light-emitting diodes (OLEDs), organic field-effect transistors (OFETs), and organic photovoltaic (OPV) solar cells, has gained significant attention due to the direct impact of easily adjustable chemical structures in organic semiconductors on their optoelectronic properties.[17] Organic electronics exhibit advantages as they are flexible, wearable, low cost and more sustainable. Furthermore, high-throughput processing methods can be employed for device fabrication, including spin-coating, inkjet printing, gravure and flexographic printing.[18–21] The structural design of organic semiconductors aims to achieve good solution processability, suitable highest occupied molecular orbital (HOMO) and lowest unoccupied molecular orbital (LUMO) energy levels, high charge carrier mobilities and good stability in air.[18] High solubility of material in solvents facilitates the easy fabrication of devices using printing techniques, which is advantageous for industrial production. Side chain engineering is often employed to improve the solubility of polymers in solvents.[22] For HOMO and LUMO energy levels, they are directly related to the optical and electrical properties of the material. Introducing electron-withdrawing or electron-donating groups to the backbone structure can adjust the material's energy levels, thereby facilitating efficient charge transfer processes. Moreover, the air stability of organic semiconductor devices is critical because they are typically processed and utilized in ambient conditions. Enhancing the air stability of organic semiconductors is essential to mitigate adverse effects on device performance caused by interactions between air and the active materials in electronics, and to prevent device degradation over time.

1.3 Objectives and Thesis Outline

1.3.1 Objectives

This thesis aims to synthesize polymers with a nanoporous structure which can be potentially used for organic thin-film transistor (OTFT) based gas sensors with good sensitivity and selectivity based on a size-selective approach. Several targets regarding the polymer structure design and gas sensing performance include:

1. Cost-effective and simple synthetic routes that reduce synthesis challenges, costs, and batch to batch variations.
2. Adjustable pore sizes that enable high selectivity based on the size of analyte molecules.
3. Adequate OTFT performances, including high mobility, high current, low threshold voltage and a high current on-off ratio.
4. Good air stability, high sensitivity, and selectivity towards target alcohol gases.

1.3.2 Thesis Outline

This thesis focuses on the synthesis of a series of polymers containing aldehyde substituted thiophene units for potential OTFT based gas sensor applications. An alcohol-addition method was employed to synthesize acetal monomers with various chain lengths by changing the types of alcohol used. Subsequently, the monomers would undergo polymerization with different thiophene based comonomers including thiophene, bithiophene, and thieno[3,2-b]thiophene for screening of structures with the best performance and potential to be used as gas sensors. Easy conversion of the acetal side chains back to aldehyde groups was achieved through a post-modification process involving acid treatment of the coated polymer film, which generated nanopores and enhanced solvent resistance. The size of acetal chains determines the dimension

of the subsequent nanopores created, achieving high selectivity for sensors based on the size of analyte molecules. The structure of this thesis is outlined as follows:

Chapter 1 provides a brief overview of semiconductors and organic electronics along with the objectives of this work.

Chapter 2 introduces the background of conducting polymers, working principles and key parameters of OTFTs, and OTFT based gas sensors. Polymer characterization methods and OTFT based gas sensing platform setup will also be described in detail.

Chapter 3 presents the experimental synthesis of acetal and aldehyde substituted thiophene polymers with thiophene, bithiophene, and thieno[3,2-b]thiophene comonomer units for screening purpose. It also covers the characterizations and OTFT performances of these polymers before and after acid treatment.

Chapter 4 focuses on the air stability and OTFT based gas sensing performance of two selected polymers, which are OMe1T and OC21T specifically. These two polymers are comprised of one-thiophene (1T) comonomer unit and acetal substituted thiophene having chain length of one carbon and two carbons, correspondingly. They exhibited less molecular weight loss and drop in mobility upon acid treatment compared to other polymers. OTFT based gas sensor performances of the selected polymers after exposure to both alcohol and non-alcohol analytes are studied. Particularly, the selectivity and sensitivity of the OCH1T polymer (through conversion from OC21T specifically) are evaluated.

Chapter 5 concludes the findings and suggests future directions related to this study.

Chapter 2 Background

2.1 Conducting Polymers

The origin of conducting polymers (CPs) could be traced back to 1977 when Hideki Shirakawa, Alan MacDiarmid, and Alan Heeger discovered polyacetylene, which exhibited high conductivity after doping with halogen or halides.[23] Other conducting polymers were developed thereafter including polypyrrole, polythiophene, poly(3,4-ethylene dioxythiophene) (PEDOT), and polyaniline (PANI) with the structures shown in ***Figure 2-1***.[24] Attributed to their electrical, optical, electro-chemical and mechanical properties, conducting polymers serve as a promising candidate for applications as sensors, solar cells, electronic devices, batteries, fuel cells and medical diagnostics.[25] Common advantages associated with conducting polymer materials include but not limit to lightweight, flexibility, low production cost, easy fabrication, and adjustable conductivity.[26]

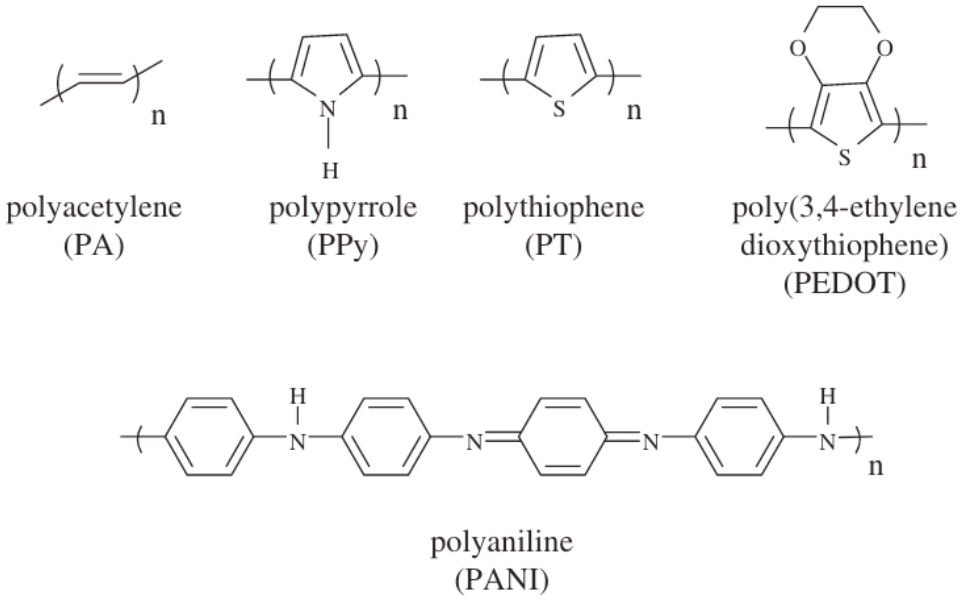


Figure 2-1. Structures of some commonly used conducting polymers.[24]

Conducting polymer structures consist of alternating single and double bonds which provide π-conjugation through continuous overlapping of p_z orbitals, thus allowing for delocalization of electrons. However, these conjugated double bonds are not enough to generate high conductivity for the material. Conducting polymers are insulators in their original states which have considerably large band gaps, but they can demonstrate high conductivity like metals after doping by oxidants or reductants.[24] Oxidants are p-type dopants which remove electrons from the highest occupied molecular orbital (HOMO) of the polymer thus generating holes as positive charge carriers. On the other hand, reductants are n-dopants which provide additional electrons to the structure and create negative charge carriers.[27] N-type doping are less stable than p-type doping in general.[9] Moreover, a small amount of dopant can usually lead to drastic change in conductivity of the material.[9] Attributed to this unique property, control over conductivity can be accomplished which makes this material suitable for various types of electronic device as the flow of current can be easily tuned through the doping process.

2.2 Organic Thin Film Transistor

2.2.1 Organic Field Effect Transistor Principles

Organic thin film transistor (OTFT) is classified as a type of field effect transistor (FET) which uses organic semiconductors adopting a thin film morphology as the conducting channel.[28]
The first organic field effect transistor (OFET) was synthesized by Koezuka and coworkers in 1987 with the use of polythiophene as the organic semiconductor material.[29] OFETs demonstrate excellent potential in the field of flexible and large-area devices as they are stretchable, flexible, light weight which can also be processed in solutions. [4,30–32,14,33]

In general, a field effect transistor consists of different layers of material which include a substrate, a dielectric layer, a semiconducting channel, and three electrodes.[34,35] Two of the electrodes are attached to each end of the channel serving as the source and drain electrodes, while the third electrode works as the gate electrode governing the current flow of the channel. OTFT device structures can adopt four types of structures as indicated in ***Figure 2-2*** including bottom-gate, top-contact (BGTC), bottom-gate, bottom-contact (BGBC), top-gate, top-contact (TGTC), and top-gate, bottom-contact (TGBC) based on the different alignments of each layer of material.

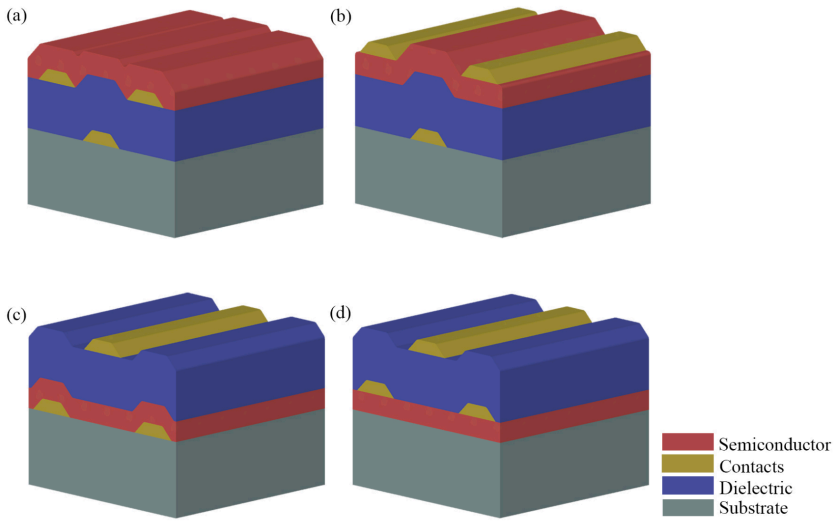


Figure 2-2. Illustration of four types of OTFT structures: **a)** bottom-gate, bottom contact (BGBC), **b)** bottom-gate, top contact (BGTC), **c)** top-gate, bottom contact (TGBC), and **d)** top-gate, top contact (TGTC).[36]

In general, the gate electrode is always separated from the semiconducting channel by a dielectric layer with a thickness x_i, while source and drain electrodes are in direct contact with the semiconductor layer being responsible for injection or extraction of charge carriers. The

charge carrier transport process takes place at the contact surface between semiconducting channel and dielectric layer, where the channel area is determined by the width (W) and length (L), which is limited by the gate electrode dimension.[36] For OTFT, accumulation of charge carriers is crucial to generate flow of current. When a gate voltage is applied, a thin layer of charge carriers with opposite charge relative to the gate voltage is collected on the interface between the semiconductor and dielectric layer. Additional injection of charge carriers leads to further accumulation of charges, which will result in bending of the energy level towards the Fermi level to facilitate the charge transport process. Therefore, the charge carriers will be localized through hopping along the conductive channel and generate electrical current. The adjustment of gate voltage results in change of charge carrier density within the active channel, thus allowing for control over the conductivity and electrical current of the device.[31,37]

In general, there are two types of FETs which are p-type and n-type, where holes or electrons are the corresponding charge carriers that move along the channel, respectively. Materials that can be used following both types of conducting mechanism are classified as ambipolar.[36] For p-type FETs, a negative bias is introduced by applying a negative gate-to-source voltage (V_{GS}) at the gate electrode. Therefore, holes of the semiconducting material will accumulate on the semiconductor/dielectric layer interface. Additional holes are injected from the source electrode by applying a negative source-drain voltage (V_{DS}). Accumulated holes will bend the HOMO of the semiconductor towards the fermi level and transport holes along the channel, making the channel positively charged. N-type FETs operate in a similar way, except that positive source and gate voltages are applied for injection and accumulation of electrons, which cause bending

of LUMO level of semiconductor towards Fermi level, and leads to flow of electrons, thus acquiring a negatively charged active channel.

The operating modes of OTFT will be discussed below using p-type OTFT as an example which has negative gate and source voltages. The gate-to-source voltage (V_{GS}) with respect to threshold voltage (V_{th}) and the source-drain voltage (V_{DS}) are important factors that affect the operating mode of the device. When V_{GS} is below the threshold voltage (a less negative value comparing to V_{th}), the channel doesn't have enough holes to form a conductive pathway, hence no current flow and $I_D = 0$ A. Only when the V_{GS} has passed the threshold voltage (V_{th}) (with more negative values), I_{DS} increases linearly with respect to V_{DS} based the following equation[32]:

$$I_D = \mu C_i (\frac{W}{L})(V_{GS} - V_{th})V_{DS} \qquad \textit{Eq. 1}$$

Where C_i corresponds to the gate capacitance density which can be calculated by dividing the gate dielectric permittivity by the thickness of the dielectric layer, and W and L are the width and length of the active channel. At this stage, current is controlled by voltage. The source-drain voltage has a linear relationship with I_{DS} following Ohm's law. The transconductance (g_m) demonstrated the relationship between the change in I_{DS} and change in V_{GS} under constant V_{DS} as follows[36]:

$$g_m = \mu C_i (\frac{W}{L}) V_{DS} \qquad \textit{Eq. 2}$$

Eventually, a saturation mode will be reached during which the charge carrier concentration is no longer uniform, and more charges are accumulated at the source than at the drain. Then I_D has a parabolic relationship with V_{DS} as below[36]:

$$I_D = \mu C_i \left(\frac{W}{L}\right) V_{DS}[(V_{GS} - V_{th}) - \frac{V_{DS}}{2}] \qquad \textit{Eq. 3}$$

I-V characterizations regarding both output and transfer modes are often conducted to evaluate the OTFT performance.

2.2.2 Key Parameters

2.2.2.1 Charge Carrier Mobility

Charge carrier mobility (μ) describes the efficiency of charge carriers moving along the channel with an equation listed as below:[36]

$$\mu = v_{drift} / E_{DS} \qquad \textit{Eq. 4}$$

where v_{drift} is the drift velocity and E_{DS} is the electric field strength. Charge carrier mobility gives information on how fast the charge carriers can move under the electric field. At the saturation region, mobility can be calculated using the slope of $\sqrt{I_{DS}}$ versus V_{GS} graph.

2.2.2.2 Threshold Voltage

Threshold voltage (V_{th}) refers to the minimum gate-to-source voltage needed for accumulation and transport of charge carriers to establish the conductive channel. It can be strongly influenced by the concentration of dopant, active channel dimension and thickness, dielectric layer thickness and dielectric constant.[38] It is ideal to have a V_{th} value as close as possible to zero which means that less voltage is needed to form the conducting pathway, thus requiring a lower operation voltage and less energy consumption.[36] Threshold voltage, in other words, is the turning point when the OTFT device switches from depletion to accumulation capacitance.[36]

V_{th} is a parameter that can be used for evaluation of sensor performance, therefore it is essential to eliminate other factors that may cause a shift in V_{th} to avoid confusion, which may be improved by surface treatment of semiconductor and dielectric interface to remove charge trapping in the semiconducting film.[36]

2.2.2.3 Current On/Off Ratio

The current of OTFT device at accumulation mode is I_{on}, while current at depletion mode is I_{off} and can be illustrated as below[36]:

$$I_{OFF} = \sigma_s \, x_s \frac{W}{L} V_{DS} \qquad \textit{Eq.5}$$

The on/off ratio provides information related to the current change when the OTFT device is switched from cut-off to saturation as indicated below:

$$I_{ON/OFF} = \frac{\mu C_i (V_{GS-} V_T)^2}{\sigma_s \, x_s V_{DS}} \qquad \textit{Eq.6}$$

High on/off ratio (~10^8) is desirable for application as optical displays, but it may not necessarily be required for sensor applications.[36]

2.3 OTFT Based Gas Sensors

OTFT based gas sensor devices are light weighted, portable, and easy to fabricate, which demonstrated advantages over other gas sensing methodologies including gas chromatography, mass spectrometry and optical chemical sensing as they require longer processing time and relevant expertise to operate.[39,40] The portable OTFT gas sensors can be wearable which allow for on-site and real-time detection with ease of operation.[41] These OTFT sensor may serve as the

electronic nose for detection of target analytes simultaneously with amplified signals.[36] Crone and coworkers explored the potential of OTFTs being employed as gas sensors due to their sensitivity and reproducibility.[42] Conjugated polymers are commonly used as the active channel material in OTFT sensors due to their tunable conductivity. General mechanism for gas detection using semiconductors is based on the interaction of analytes with the trapping sites in the active material which may lead to polarization or charge transfer.[36] The diffusion and absorption of analytes into the semiconductive material (see **Figure 2-3**) will affect the charge carrier mobility, hence changing the channel's conductivity. Common gas analytes that can be detected by OTFT-based sensors include volatile organic compounds (VOCs), poisonous gases and atmospheric gases.[36] For OTFT devices, larger switching speeds of circuits can be accomplished by larger mobilities, shorter length of channel and thinner dielectric layer, but might not be beneficial for sensing applications in terms of sensitivity and response time.[43] Among the four types of OTFT configuration mentioned in **Section 2.2.1,** bottom gate structure is more ideal for sensor applications because the semiconducting layer is placed at top which allows for direct interaction of the active material with analytes.[36] Attributed to the accumulation of charge carriers near the semiconductor/dielectric interface induced by the additional gate electrode, OTFT based sensors can achieve high sensitivity even with the use of thin layer of semiconducting film. Structural design and engineering of organic semiconductors can be used to enhance the sensitivity and selectivity of material towards desired analytes.[44–47] However, using organic semiconductors in transistors poses a significant challenge due to the relatively poor air stability of the material compared to their inorganic counterparts.

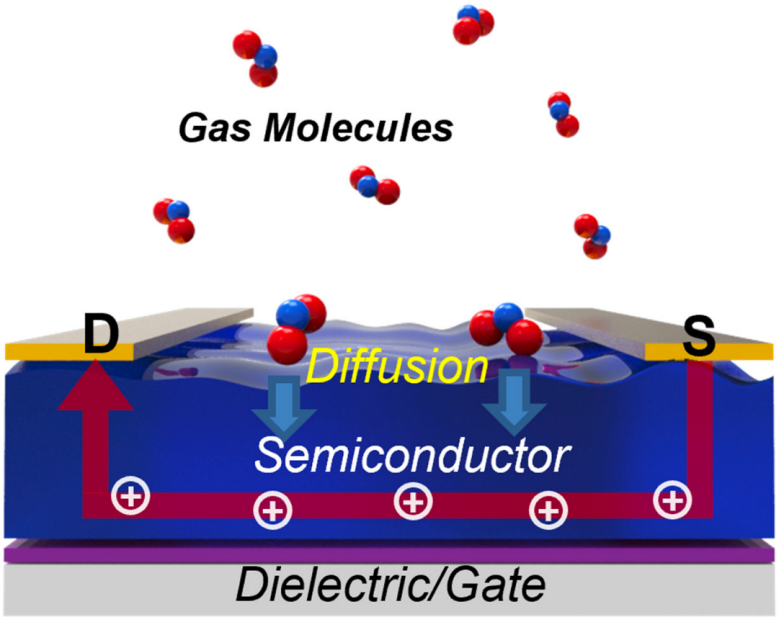


Figure 2-3. Illustration of gas detection mechanism for a p-type OTFT device. [48]

The analyte can undergo chemical and physical interaction with the sensor material thus leading to changes in the OTFT performances as illustrated in **Figure 2-3**.[39,46,48,49] Mobility, threshold voltage and current on/off ratio are key parameters to evaluate the sensing responses. In general, relative response is used to determine the sensing performance of the material which can be calculated by dividing the change in response by the initial response as listed below:

$$Relative\ response = \frac{(R - R_0)}{R_0} \times 100\% \qquad \textit{Eq.7}$$

It is ideal to have a linear correlation between the relative response and analyte concentration with high response ratio. Moreover, a promising sensor material should also exhibit fast response and recovery time, sensitivity, and selectivity with stability in air for long period of time.[49]

2.4 OTFT Device Preparation Methods

Two types of BGBC transistors were used for OTFT measurements in this work with different patterns indicated in **Figure 2-4.** The smaller one (with W=1,000 μm and L = 30 μm) was used to obtain OTFT transfer and output curves, while the other larger device (W= 15,800 μm and L= 30 μm) with interdigitated electrodes was mainly used for I_{DS} vs. t measurements for real-time sensing profiles and sensitivity determinations. The transistor patterns on the silicon wafer were obtained through photolithography. Transistors were cut into desired sizes, cleaned by sonication using DI water, acetone, and IPA (20 minutes each), and dried using nitrogen gas.

For preparation of the small OTFT device, $C_{18}SH$ on a glass substrate was first placed into a plasma chamber and treated for 2 minutes, then it was removed from the chamber with replacement of the cleaned transistors for another 2 minutes of plasma. After this, transistors were taken out and put into a solution containing 20 mL DI water with 2-3 drops of 1:10:10 ratio of HNO_3: HCl: H_2O acid mixture for 5 minutes, rinsed with DI water and IPA, then dried using N_2 gas. To ensure complete drying of the devices, they were heated on a hotplate at 120 °C for 15 minutes before proceeding to the next step. After cooling down to room temperature, the transistors were placed into a solution of 20 mL toluene with 8 drops of dodecyltrichlorosilane (DDTS) for 20 minutes to form the self-assembled monolayer (SAM) on the dielectric layer. Transistors were then rinsed with toluene, dried using nitrogen gas and ready for coating.

Polymer solution with a concentration of 5 mg/mL in chloroform was prepared for spin-coating. 50 μL of polymer solution was casted onto the transistor at 3000 rpm for 80s. The concentration and spin rate can be adjusted accordingly to coat film with other thicknesses. Annealing of device was performed inside of N_2 glovebox for 20 minutes at the desired temperature. Acid

treatment of the device was performed the same way as for the UV thin films which will be discussed in **Section 3.2.2**. The device was exposed to HCl vapor for 7 minutes for complete side chain conversion. Brief heating of device was performed in air for 3 minutes to remove potential HCl residue on the surface without exposing the device to air for too long before testing. Then the device was transferred into glovebox for an additional 20 minutes of annealing.

The larger transistor with interdigitated electrodes was used to study the real time gas sensing performance, which was cleaned by sonication using DI water, acetone, and IPA (20 min each) before use. Polymer solution with a concentration of 10 mg/mL was prepared and spin coated to the surface of the substrate at 3000 rpm for 80s. Subsequent acid treatment and acid residue vapor removal process were conducted the same way as for the smaller ones.

Electrical performances of OTFT were characterized using Agilent B2912A Semiconductor Analyzer, with the transfer and output curves measured using QuickIV software. C_i has a value of 11.6 $nFcm^{-2}$ for the smaller devices used in this thesis, which can be substituted into the mobility equation for further calculation. For this thesis, as all polymers were p-type materials, both $V_{GS\ and}$ V_{DS} were scanned over the range from 0 V to -100 V. For I_{DS} vs. T measurement, gate voltage was fixed at -100 V with a source-drain voltage at -50 V.

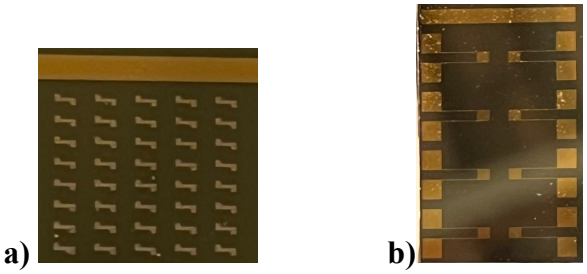


Figure 2-4. BGBC OTFT devices with **a)** straight channel (smaller one); **b)** amplified channel with interdigitated electrodes (larger one).

2.5 Gas Preparation

Analyte gas with various concentrations should be prepared to examine the influence on OTFT performances. Since no pure analyte gas was available in our lab, the saturated vapor was obtained by evaporation of solvent in a closed system with further dilution. For this method, only volatile solvents were used including acetone, ethyl acetate, diethyl ether, dichloromethane, hexane, toluene, methanol, ethanol, and isopropanol. To a 25 mL round-bottom flask, 15 mL of the solvent of interest was added and sealed with a septum stopper. Then the flask was purged with nitrogen and let stay at room temperature for the solvent to evaporate and generate vapor. The gas portion above the liquid level was the corresponding saturated vapor which was subjected for injection or further dilution. The concentration of saturated vapor was calculated by using Antoine equation as shown below[50]:

$$log_{10}P = A - B/(C + T) \qquad \textit{Eq. 8}$$

Where P is the vapor pressure, T is temperature, and A, B, and C are empirical values which are compound specific. The temperature in our lab was approximately 22 °C while the experiments were performed. Then ideal gas law was employed to calculate the gas concentration based on vapor pressure:

$$PV = nRT \qquad \textit{Eq. 9}$$

Where P, V, n, R and T are pressure, volume, number of moles, ideal gas constant and temperature, respectively. Since n/V is also the concentration in mol/L, then the above equation can be rearranged into the following format for determination of concentration:

$$\frac{n}{V} = \frac{P}{RT}$$

Taking methanol for example, the saturated vapor pressure of methanol at 22 °C is 14.4461 kPa, then the value was substituted into ***Eq. 9*** and rearranged as follows[51]:

$$c = \frac{n}{V} = \frac{P}{RT} = \frac{14.4461\ kPa}{8.314\ L \cdot \frac{kPa}{mol \cdot K} \times 295.15K} = 0.0059 \frac{mol}{L}$$

The calculated saturated vapor concentration of methanol is in mole per liter, which can be converted into mg/L using the molecular weight of methanol as follows:

$$0.0059 \frac{mol}{L} \times \frac{32.04\ g}{mol} \times 1000 \frac{mg}{g} = 189.04 \frac{mg}{L}$$

To test solvent vapor with various concentrations, dilution was performed using nitrogen gas based on volume percentage. Another one-neck flask was filled with nitrogen by strong blowing of nitrogen gas for 30 s and sealed with a septum stopper. To prepare 20% of methanol vapor in nitrogen, 1 mL of saturated vapor was taken out from the flask containing the methanol solvent using a 5 mL syringe, followed by additional measurement of 4 mL nitrogen gas from the other flask using the same syringe to prepare a 5 mL of gas mixture containing 20 % of methanol (37.72 mg/L). Similarly, 40%, 60% and 80% of diluted gas samples can be prepared the same way.

2.6 Characterization Methods

2.6.1 Nuclear Magnetic Resonance

Nuclear magnetic resonance (NMR) is a crucial technique used to determinate the chemical structure of organic compounds.[52] With a strong magnetic field, the nucleus will absorb radio frequency energy and lead to a spin state change.[53] Nuclei in a molecule may experience different electronic environments, indicating that they will absorb radiation at various frequencies, thus resulting in different chemical shifts with respect to the reference.[54] For ^{1}H

NMR, proton can sense other protons located on the adjacent carbons, which causes splitting of the corresponding resonance peak. Integration of peaks indicates the number of protons that are chemically equivalent. As a result, the combination of information allows for determination of both the chemical structure and purity of the synthetic compounds.

2.6.2 Gel Permeation Chromatography

Gel permeation chromatography (GPC) is used to measure the molecular weight of polymers and molecular weight distribution based on a size separation principle.[55,56] The stationary phase of GPC column consists of porous particles with various pore sizes, and a dilute polymer solution is introduced to the column and eluted by a solvent. The retention time of polymer is directly proportional to the size of polymer: polymer with smaller molecular weight can go through more pores inside of the column, thus requiring longer retention time and larger elution volume, which are the two parameters to distinguish various sizes of polymer chains.[55] GPC can be used to measure both weight-average molecular weight M_w and number-average molecular weight M_n with the following equations:

$$M_n = \frac{\sum N_i M_i}{\sum N_i} \qquad \textit{Eq. 10}$$

$$M_w = \frac{\sum W_i M_i}{\sum W_i} \qquad \textit{Eq. 11}$$

Where N represents the number of molecules in the polymer having a molecular weight of M, and W is the total mass of molecules with molecular weight M. Based on the two types of molecular weights obtained, polydispersity index (PDI) of polymer can also be calculated based on the following equation:

$$PDI = \frac{M_w}{M_n} \qquad \textit{Eq. 12}$$

PDI represents molecular weight distribution, and the closer of PDI to 1 indicates a narrower distribution of polymer molecular weights, which is more ideal yet hard to accomplish.

2.6.3 Thermogravimetric Analysis

Thermogravimetric analysis (TGA) allows for determination of a sample's composition and thermal stability.[57] TGA measures the weight change of sample in response to various temperatures and time. During TGA measurement, the sample being analyzed is heated under a controlled environment at a constant heating rate with the weight change being monitored over time. Mass drops may be observed due to decomposition of sample, evaporation of volatile compounds, or decrease in oxidation state responding to the temperature change.[57,58]

2.6.4 Ultraviolet and Visible Spectroscopy

Ultraviolet and visible (UV-Vis) spectroscopy is an essential tool for determination of the optical band gaps for organic semiconductors and identification of functional groups. Beer-Lambert law illustrates the relationship between absorbance and concentration of analyte in solution as follows:

$$A = \varepsilon lc \qquad \textit{Eq. 13}$$

Where A represents absorbance, ε is the molar attenuation/absorptivity coefficient, l is the optical path length and c is the concentration of analyte in solution. With the absorption of photons, electrons at ground state can jump to the excitation state. Different functional groups of molecule will absorb lights of various wavelength, thus causing different electronic transitions.[59]

For conductive polymers bearing conjugated double bonds as the backbone structure, both π → π* and n→ π* transitions are possible.[59] Polymer backbones in solution are more twisted than in solid state, thus resulting in a decreased extent of π conjugation with less coplanar structure and leading to a shorter absorption wavelength. Moreover, formation of polymers is always related to the extension of π conjugation, which usually leads to red (bathochromic) shift of absorbance peak to longer wavelength (lower energy) and increase in absorption (hyperchromic). The onset wavelength is used for calculation of the optical band gap (E_g) using the following equation:

$$E_g(eV) = hf = h\frac{c}{\lambda_{onset}} \qquad \textit{Eq. 14}$$

Where h is Planck's constant and c is the speed of light. Therefore, the above equation can be further simplified for estimation of the optical band gap between HOMO and LUMO levels:

$$E_g(eV) \approx \frac{1240}{\lambda_{onset}}$$

2.6.5 Cyclic Voltammetry

Cyclic voltammetry (CV) is an electrochemical measurement to examine the reduction and oxidation reactions of an analyte. Both forward and reverse sweep scans are conducted to generate the cyclic voltammograms, which demonstrates the current change at the working electrode as a response to the applied potential.[60] The rate of voltage change over time is the scan rate, which is constant during the scanning process. The generated profile provides information regarding the reduction and oxidation potential relative to the reference electrode (which is a silver electrode for this thesis), which can be further converted to HOMO and LUMO energy levels of the polymer. Oxidation onset of the CV diagram corresponds to the energy for electron removal from HOMO, where E_{HOMO} can be calculated based on the following equation:

$$E_{HOMO}(eV) = -e(E_{ox}^{onset} - E_{\frac{FC}{FC^+}}) - 4.8eV \qquad \textbf{Eq.15}$$

Where E_{FC/FC^+} is the potential of ferrocene which serves as the internal standard of the electrolyte for calibration. E_{LUMO} is associated with the reduction process of polymer during which electrons are injected to the LUMO, and can be calculated as follows:

$$E_{LUMO}(eV) = -e(E_{red}^{onset} - E_{\frac{FC}{FC^+}}) - 4.8eV \qquad \textbf{Eq.16}$$

A typical scheme of an electrochemical cell is illustrated below:

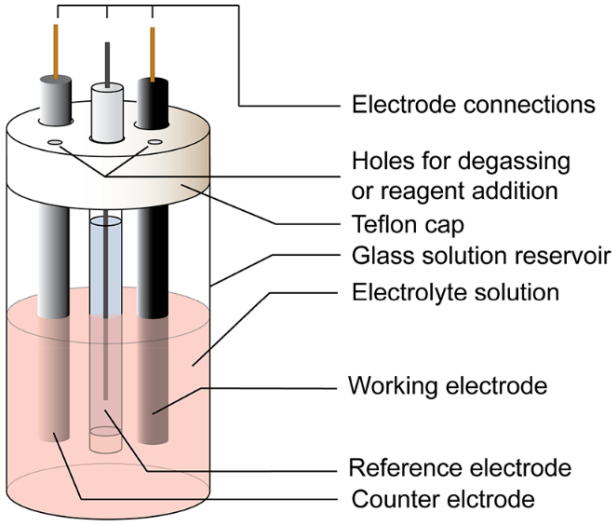


Figure 2-5. Electrochemical cell setup for CV measurement. [60]

2.6.6 X-Ray Diffraction

X-ray diffraction (XRD) helps to determine the crystallinity of polymers and provides information on polymer chain ordering. Monochromatic X-ray radiations being generated by a cathode ray tube after filtration are directed towards the sample, diffracted and collected by the detector.[61] XRD signal follows Bragg's Law for constructive interference thus allowing for d-spacing calculation:

$$2dsin\theta = n\lambda \qquad \textit{Eq. 17}$$

Where d corresponds to plane spacing, λ represents X-ray's wavelength and θ is the incident angle of X-ray beam. If no peaks are shown in the collected diagram, then it suggests that the polymer adopts an amorphous morphology, and the polymer chains are randomly ordered. While if peaks are observed, it could be due to π–π stacking or lamellar packing of polymer chains based on the location (2θ) of peaks. [62] The optical and electronic performances of conjugated polymers are highly affected by the ordering of the polymer chains.[62] Moreover, the orientation of backbone motif with respect to the substrate can influence the charge carrier transport and device performance.[63] The possible orientations of polymer backbone with respect to the substrate are illustrated in **Figure 2-6**. For this thesis, grazing incidence X-ray diffraction (GIXD) measurement with a 2D detector was used to examine the polymer chain packing in thin film on silicon substrate.

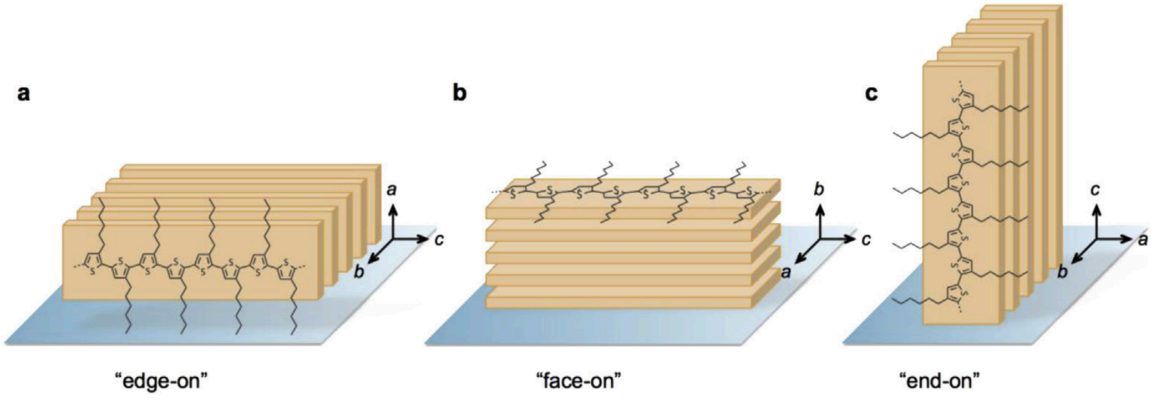


Figure 2-6. Demonstration of different polymer chain orientations with respect to the substrate: **a)** edge-on; **b)** face-on; **c)** end-on.[63]

2.6.7 Fourier Transform Infrared Spectroscopy

Fourier transform infrared (FTIR) spectroscopy is a vibrational spectroscopic technique used to examine the chemical properties of a compound based on its infrared absorption spectra.[64] Different chemical bonds will absorb infrared light at different frequencies, resulting in distinct characteristic peaks/bands with unique shape and intensity. FTIR provides information on the chemical functionalities of a sample, enabling the identification of molecular structures or functional groups, as well as the analysis of molecular interactions. Such method is fast and non-destructive with high sensitivity and accuracy.

Chapter 3 Synthesis and Characterization of Acetal-Substituted Thiophene Polymers with Different Comonomer Units and the Corresponding Aldehyde-Based Polymers

3.1 Introduction of Polythiophenes

Conjugated polymers containing thiophenes and derivatives have been widely studied and explored, with applications in the field of organic electronics. Thiophene is a readily available compound with well-established chemistry, which allows for facile functionalization of the core with various substituents and easy incorporation into the polymer backbones. [65–68] It is also worth mentioning that the sulfur atom in the thiophene backbone can facilitate the charge transport process due to its relativity high polarizability.[65] The choice of substituent groups and comonomers can lead to various optical, morphological, and electronic properties of the resulting conducting polymer, thereby broadening the potential applications.

Backbone coplanarity might be affected by the comonomer unit employed, which leads to variations in molecular packing of polymer chains in solid state and influences the performance. Commonly used thiophene based comonomers include unsubstituted one-thiophene (1T), thienothiophene (TT) and bithiophene (BT). In general, bithiophene unit can afford a more coplanar and rigid polymer backbone structure but leads to a decrease in polymer solubility as a compromise.[65,69] On the other hand, unsubstituted one-thiophene comonomer exhibits better solubility but also forms a more twisted backbone, and sometimes with lower molecular weight. Solubility of polymers is an essential factor affecting the processability of polymers for practical uses, which can be improved by incorporation of solubilizing alkyl chains to the monomer structure. [22]

Owing to the electron withdrawing property, carbonyl groups are commonly used substituent groups for synthesis of D-A type polymers. 3-thiophenecarboxaldehyde is a commercially available compound which contains an aldehyde group and can be potentially used to copolymerize with different thiophene based comonomers to compare properties and performance.[70] A side chain modification process involving the addition of alcohols to convert the aldehyde into acetal groups can offer better solubility to the monomer, facilitating the subsequent polymerization process with different comonomer units. Furthermore, the alkoxy chains of acetal group can readily revert to the aldehyde form via acid cleavage, creating pores within the coated film which can be potentially used as size-selective gas sensors. In other words, the acetal chain length influences both the solubility of the pristine acetal polymer and the pore size of the corresponding aldehyde polymer after side chain conversion. In this chapter, polymerizations of acetal substituted thiophene monomers with three different comonomer units were investigated. Moreover, various acetal chain lengths were employed aiming for preparing the resulting aldehyde polymers with various nanopore sizes.

3.2 Bithiophene and Thienthiophene Series

Bithiophene (BT) and thienothiophene (TT) polymers were investigated first as they could provide extended conjugations comparing to one-thiophene (1T) based polymers, which could potentially improve the coplanarity and rigidity of the polymer structures to achieve better electronic performances.[65,68] As a result, improved charge mobility and conductivity would be expected. They may also provide enhanced environmental stability which is favorable for sensor applications. Acetal substituted thiophene monomers with C4 and C8 chain lengths were used to

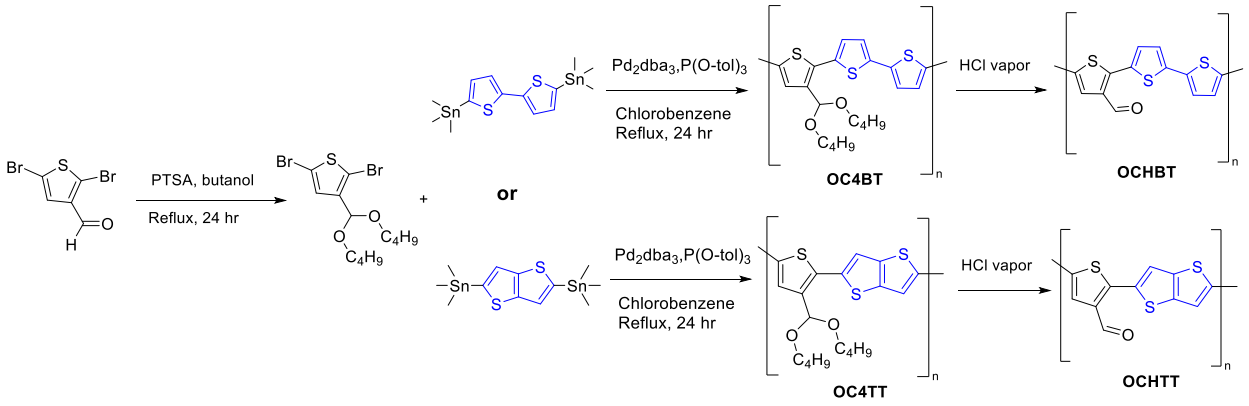
help solubilize the polymers, which can be converted back to aldehyde after simple exposure to HCl vapor for a short period of time.

3.2.1 Synthesis of Bithiophene and Thienthiophene Series of Polymers

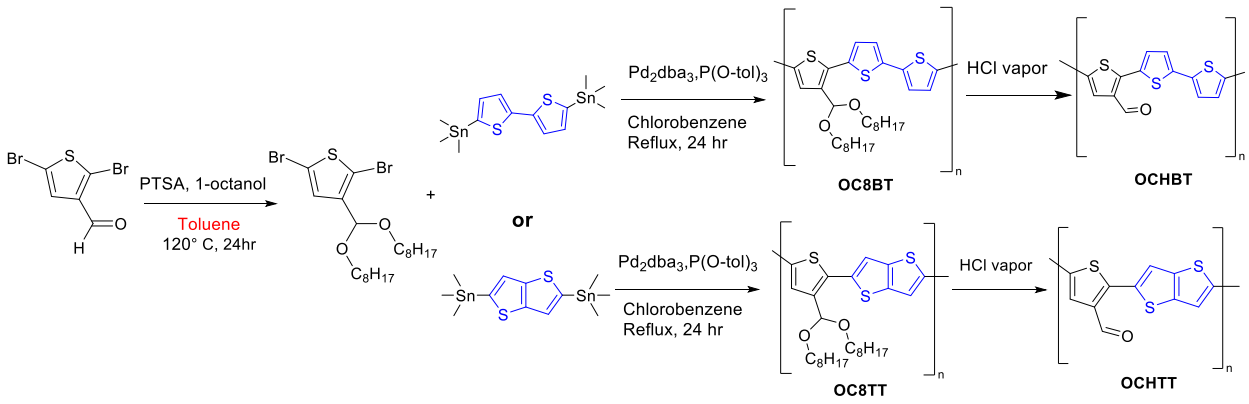
Scheme 1 and ***Scheme 2*** illustrate the reaction steps to obtain polymer OC4BT, OC8BT, OC4TT and OC8TT. In general, synthesis of acetal substituted thiophene monomer can be accomplished by a simple reaction between an aldehyde containing compound and two equivalents (or excess) of alcohols. This reaction works under the presence of an acid catalyst which protonates the oxygen on the carbonyl and increases the electrophilicity of the carbon on the carbonyl. It is noteworthy that water will be generated as a side product of the reaction which will lead to reverse reaction. As a result, if only two equivalents of alcohol were used, a Dean-Stark apparatus should be utilized to eliminate the water formed, thus pushing the reaction to the product side. Such setup is usually required for alcohols that are hard to be removed during work-up process. For this work, the monomer with acetal group having a length of 8 carbons was synthesized by reacting 2,5-dibromothiophene-3-carbaldehyde with 1-octanol. Octanol has a high boiling point of 195°C, thus the use of Dean-Stark reactor became essential. Toluene was selected as the solvent as it has higher boiling point yet lower density than water. It indicates that while the water and toluene mixture was refluxed and condensed in the burette at the side, phase separation would occur. Since water is heavier than toluene, water would allocate at the bottom of the condenser, which could be drained out constantly by opening the tab.

On the other hand, acetals having dimethoxy, diethoxy and dibutoxy side chains could be obtained using the corresponding alcohols directly as they could be effectively removed by rotary evaporation during the work-up process. In these cases, alcohols served both as the

reagent and reaction solvent without the need to remove water, since the excess amount of reactant was already enough to push the reaction to completion. In this work, the acid catalyst selected was p-toluenesulfonic acid (PTSA). The obtained acetal monomers through addition of alcohol were then subjected to polymerize with 5,5'-bis(trimethylstannyl)-2,2'-bithiophene or 2,5-bis(trimethylstannyl)thieno[3,2-*b*]thiophene via Stille coupling method. The detailed polymerization method was discussed in **Section 3.4.**



Scheme 1. Synthesis schemes of OC4BT and OC4TT polymers and the corresponding aldehyde forms.



Scheme 2. Synthesis schemes of OC8BT and OC8TT polymers and the corresponding aldehyde forms.

For BT series of polymers, OC8BT polymer exhibited good solubility even in hexane, while the majority of OC4BT polymer was collected from the chloroform portion of Soxhlet extraction. TT based copolymers were both obtained from the chloroform fraction of Soxhlet extraction. Probably due to the increased polymerization temperature, OC4TT required longer time to be fully dissolved in chloroform while preparing the polymer solution for subsequent characterizations. Therefore, C4 was the shortest length of side chain attempted for copolymerization with the TT comonomer. Moreover, due to the limited solubility of OC4TT, XRD and GPC data were not collected.

3.2.2 Opto-electrochemical Properties

UV-vis absorption measurements were conducted for both solution and thin films of polymers with acetal side chains. A stock polymer solution in chloroform with a concentration of 5 mg/mL was prepared. 15 μL of the stock polymer solution was then added to a cuvette and diluted using 3 mL of chloroform for measurement of polymer absorbance in solution. Polymer thin film was obtained by spin-coating 50 μL of the stock solution onto a glass substrate with a spin rate of 1000 rpm for 60 s. The absorption spectra of polymer thin films both at room temperature and annealed at 100 °C for 20 minutes were measured. For the aldehyde substituted thiophene polymer OCHBT and OCHTT, an acid treatment was performed using the coated polymer film, as after the cleavage of side chains by acid, the polymers were no longer soluble in solution. A glass slide with the coated polymer thin film was placed into a round-bottom petri dish which contained 5 drops of HCl acid (37%), then covered with a lid as indicated in **Figure 3-1.** The film was placed in the petri dish for 5 minutes, then taken out, dried and measured UV-vis. The same process was repeated for several time intervals until no further shift or change of

absorbance peak was observed. After complete removal of side chains, the film was annealed at 100 °C for 10 minutes to further compare the difference. Solvent resistance of the acid-treated film was investigated by dipping the film into various solvents for 3 times with gentle shaking. Then the film was removed from the solvent and dried using nitrogen gas for UV measurement again.

CV measurement of these polymers was obtained using a solution of acetonitrile with 0.1 M tetrabutylammonium hexafluorophosphate ($[n\text{-}Bu4N]^+[PF6]^-$) as the electrolyte. The electrolyte solution was purged with nitrogen for 10 minutes to deoxygenate. Then a three-electrode system setup was used, consisting of one silver electrode and two platinum electrodes. Approximately 5 μL of the 5 mg/mL polymer solution which was prepared for UV measurement was drop casted to the tip of one of the platinum electrodes as the working electrode, while the other one served as the auxiliary electrode. After complete evaporation of chloroform solvent, all three electrodes were connected to the measurement device correspondingly, with the tips of electrode completely submerged under the electrolyte solution. I-V scan was then conducted with a scan rate of 20 mV/s. E_{HOMO} of the polymer was obtained by extrapolating the onset oxidation potential and substituting into **Eq.15**. to convert from V to eV**.** The acid treatment process was done the same way as for the UV thin film measurements but with replacement of the polymer film with the coated electrode. Then the electrode was placed into a vacuum oven at 80 °C for 3 minutes to remove acid vapor, dried with nitrogen gas, and subjected to CV measurement.

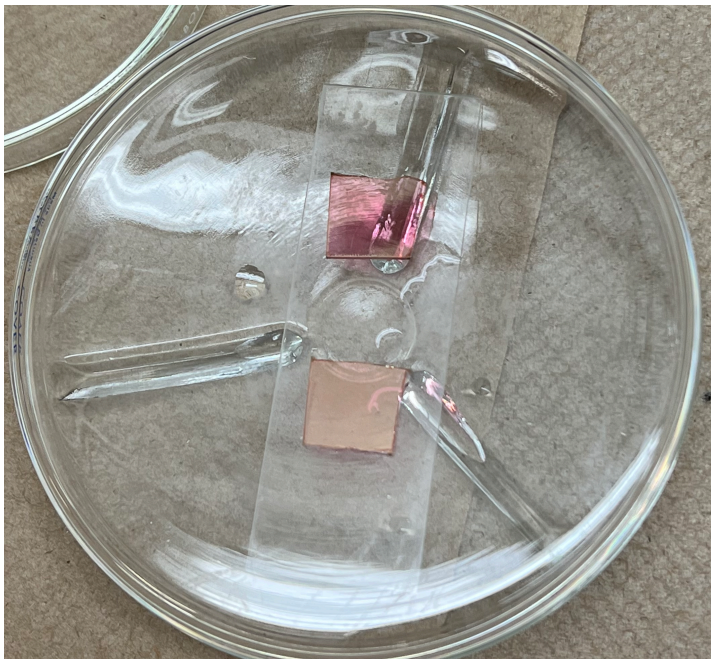


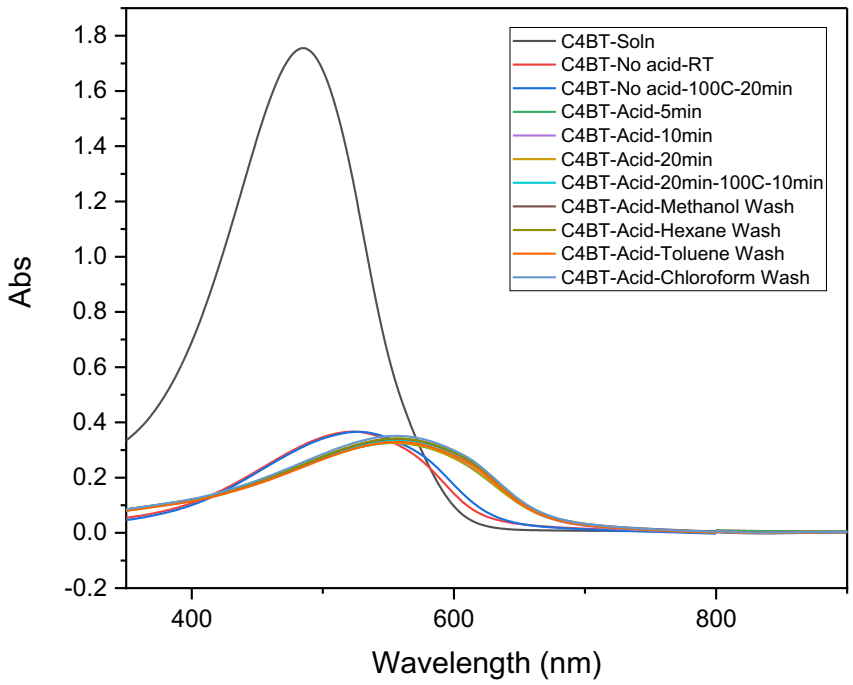
Figure 3-1. Acid treatment setup of polymer film using HCl vapor for conversion of acetal group to aldehyde group.

For all polymer thin films coated using OC4BT, OC8BT, OC4TT and OC8TT, bathochromic shifts (red shifts) were observed after acid treatment as the absorption peaks moved to longer wavelength, hence lower energy band gap. The narrower band gap could facilitate the electron excitation to the conduction band. Even though a 20-minute interval of acid treatment process was monitored, the complete cleavage of side chains was accomplished within 5 minutes. An obvious color change could be observed as indicated in **Figure 3-2.** Further heating did not lead to any significant change in the absorption spectra. Solvent resistance of the acid-treated film was performed by testing the solubility of polymer film in methanol, hexane, toluene, and chloroform. The aldehyde polymer exhibited solubility in none of the solvents listed as the intensity of absorption peak remained the same throughout all tests. It suggested that the aldehyde polymer was robust with promising solvent resistance. The HOMO and LUMO levels of the polymers indicates that they are p-type semiconducting polymers with good air stability.

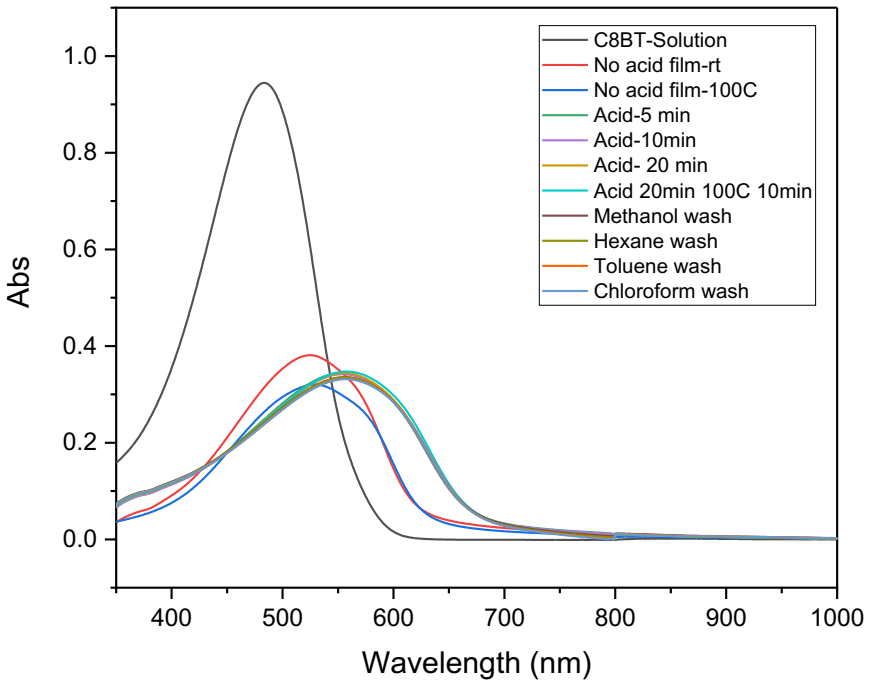
No obvious change in E_{HOMO} was observed after acid treatment. The optical and electrochemical properties of OC4BT, OC8BT, OC4TT and OC8TT polymers (before and after acid treatment) were summarized in **Table 3-1, 3-2,** and **3-3.**



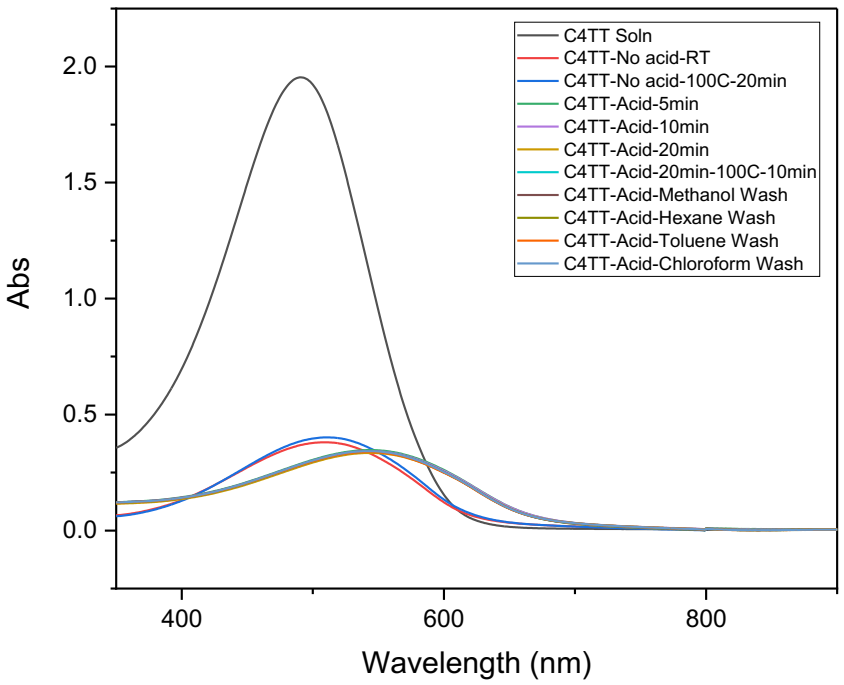
Figure 3-2. Polymer films coated on glass substrate before acid treatment (left) and after acid treatment (right).



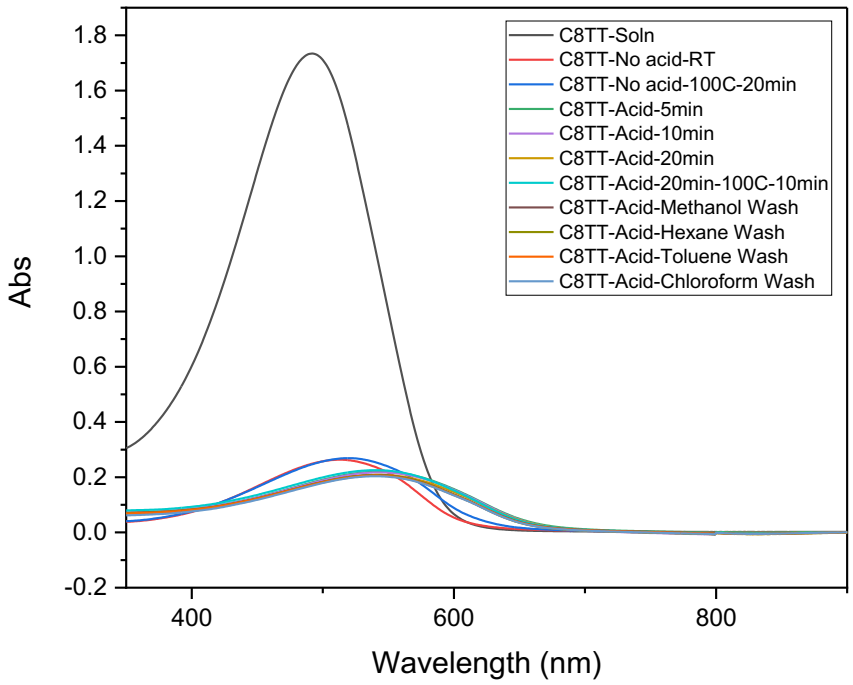
a)


C8BT-Solution
No acid film-rt
No acid film-100C
Acid-5 min
Acid-10min
Acid- 20 min
Acid 20min 100C 10min
Methanol wash
Hexane wash
Toluene wash
Chloroform wash
Abs
Wavelength (nm)
1.0
0.8
0.6
0.4
0.2
0.0
400
500
600
700
800
900
1000

b)

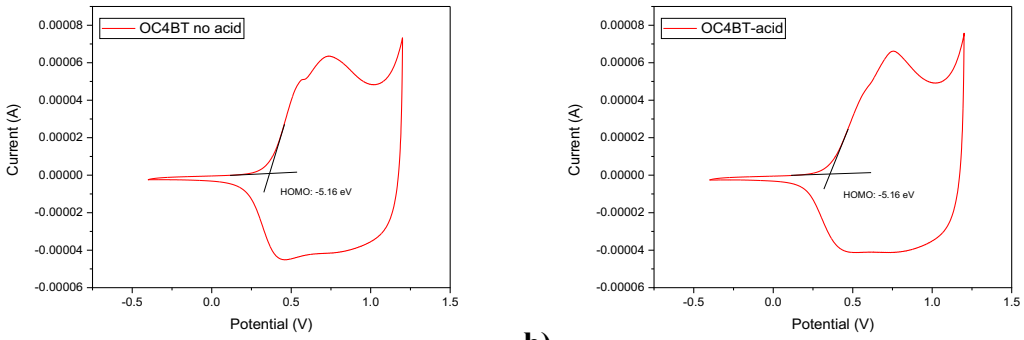

C4TT Soln
C4TT-No acid-RT
C4TT-No acid-100C-20min
C4TT-Acid-5min
C4TT-Acid-10min
C4TT-Acid-20min
C4TT-Acid-20min-100C-10min
C4TT-Acid-Methanol Wash
C4TT-Acid-Hexane Wash
C4TT-Acid-Toluene Wash
C4TT-Acid-Chloroform Wash
Abs
Wavelength (nm)
2.0
1.5
1.0
0.5
0.0
400
600
800

c)



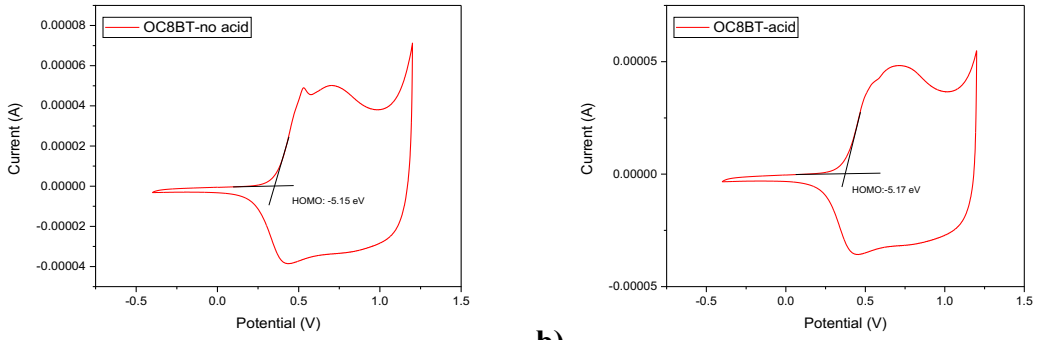
d)

Figure 3-3. UV-vis absorption spectra of polymer solution, as-cast thin film, annealed thin film and acid-treated thin films with various conditions: **a)** OC4BT; **b)** OC8BT; **c)** OC4TT; and **d)** OC8TT.



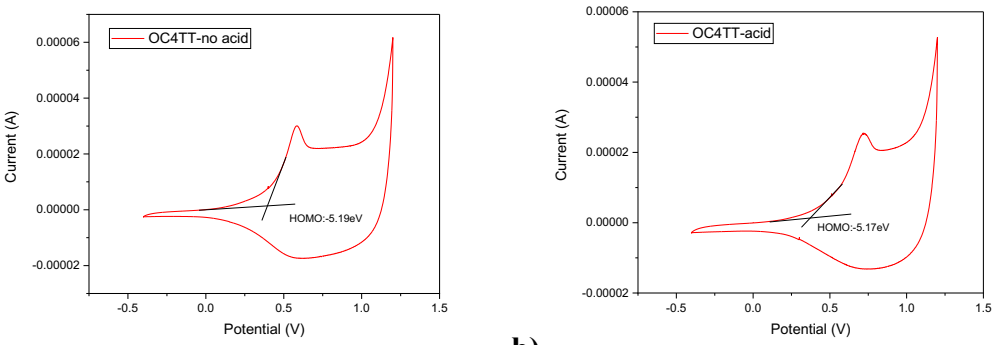
a) **b)**

Figure 3-4. CV profiles of OC4BT polymer: **a)** without acid treatment**; b)** with acid treatment (which is the OCHBT polymer).



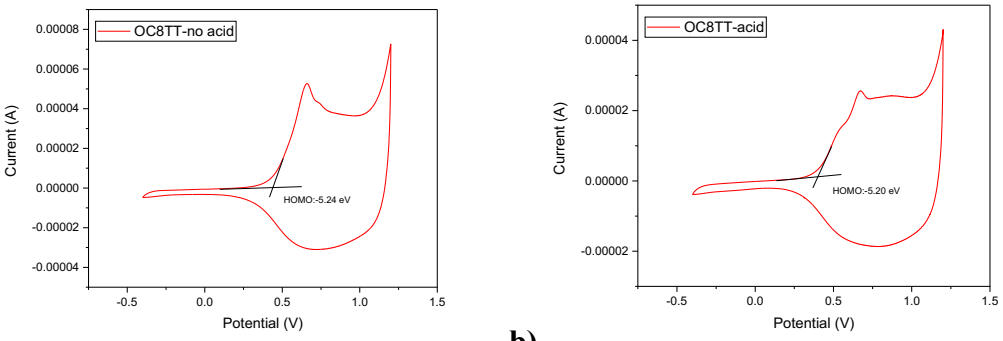
a) **b)**

Figure 3-5. CV profiles of OC8BT polymer: **a)** without acid treatment**; b)** with acid treatment (which is the OCHBT polymer).



a) **b)**

Figure 3-6. CV profiles of OC4TT polymer: **a)** without acid treatment**; b)** with acid treatment (which is the OCHTT polymer).



a) **b)**

Figure 3-7. CV profiles of OC8TT polymer: **a)** without acid treatment**; b)** with acid treatment (which is the OCHTT polymer).

Table 3-1. Summary of optical and electrochemical properties of BT and TT series polymers.

Polymer	$\lambda_{max\text{-}soln}$ (nm)	$\lambda_{max\text{-}TF\text{-}RT}$ (nm)	$\lambda_{max\text{-}TF\text{-}100}$ (nm)	λ_{onset} (nm)	E_g^{opt} (eV)	E_{HOMO} (eV)	E_{LUMO} (eV)
OC4BT	485	523	527	627	1.98	-5.16	-3.18
OC8BT	486	528	533	625	1.98	-5.15	-3.17
OC4TT	491	509	510	624	1.99	-5.19	-3.20
OC8TT	492	510	514	620	2.00	-5.24	-3.24

Table 3-2. Summary of optical and electrochemical properties of OCHBT polymer through acid treatment to OC4BT and OC8BT polymers, correspondingly.

Polymer	Original polymer	$\lambda_{max\text{-}TF}$ (nm)	λ_{onset} (nm)	E_g^{opt} (eV)	E_{HOMO} (eV)	E_{LUMO} (eV)
OCHBT	OC4BT	552	679	1.83	-5.16	-3.33
OCHBT	OC8BT	556	677	1.83	-5.17	-3.34

Table 3-3. Summary of optical and electrochemical properties of OCHTT polymer through acid treatment to OC4TT and OC8TT polymers, correspondingly.

Polymer	Original polymer	$\lambda_{max\text{-}TF}$ (nm)	λ_{onset} (nm)	E_g^{opt} (eV)	E_{HOMO} (eV)	E_{LUMO} (eV)
OCHTT	OC4TT	542	670	1.85	-5.17	-3.32
OCHTT	OC8TT	543	669	1.85	-5.20	-3.35

3.2.3 Physical Properties

Gel Permeation Chromatography (GPC) measurement was conducted using THF as the solvent at 70 °C to determine the molecular weight of the pristine BT and TT polymers. The number-average molecular weight (M_n) of OC4BT was 1429 Da and weight-average molecular weight (M_w) was 2817 Da with a PDI calculated to be 1.97. For OC8BT, M_n was found to be 16544 Daltons and M_w was 251589 Daltons, with a PDI of 15.21. For the TT series of polymer, due to the poor solubility of OC4TT, GPC was not measured to avoid potential obstruction of the GPC

column. OC8TT has a number-average molecular weight M_n of 2659 Da, and a weight average molecular weight of 7811 Da, with the calculated PDI to be 2.94.

Thermogravimetric analysis (TGA) was performed to examine the thermal stability of the synthesized polymers. Polymer samples were heated under nitrogen from 50 ℃ to 600 ℃ with a heating rate of 10 ℃/min. The TGA curves were shown in **Figure 3-8.** The first decomposition step for OC4BT and OC8BT polymers occurred at 305 ℃ and 311℃, respectively, where 5% of weight was lost. For the TT series, the first decomposition step happened at 306 ℃ and 298 ℃ for OC4TT and OC8TT polymers, respectively.

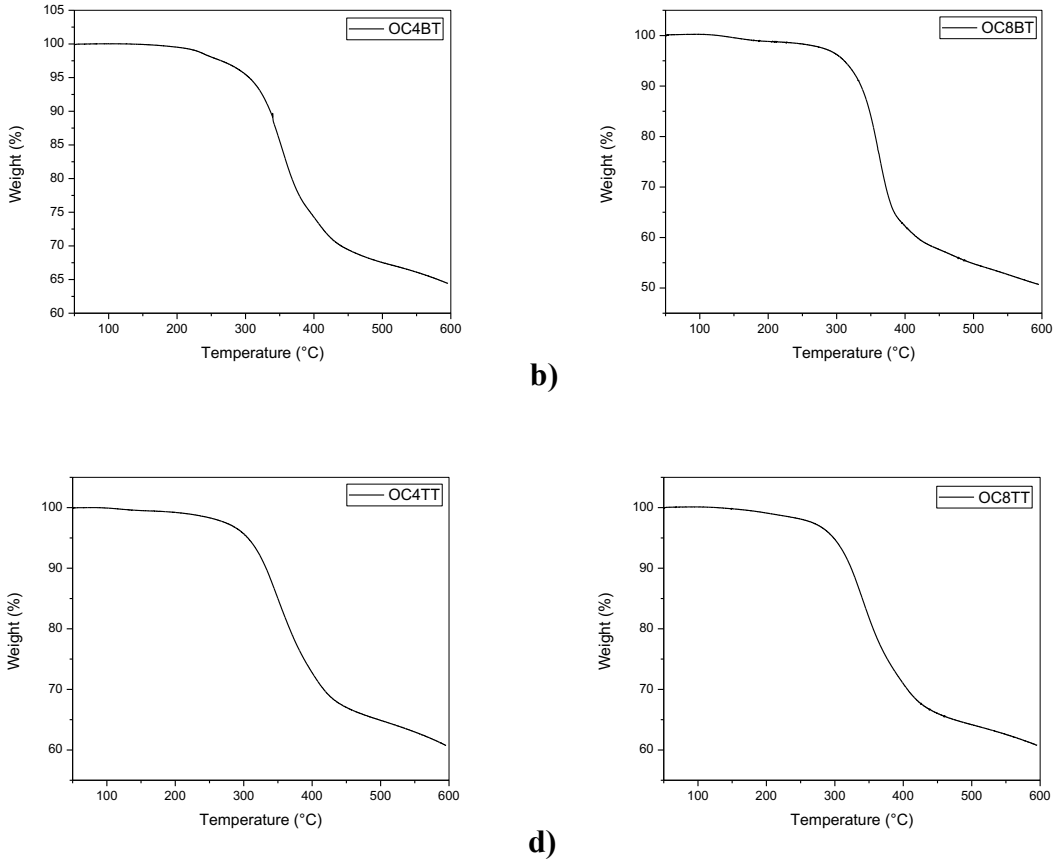


Figure 3-8. TGA curves for polymers: **a)** OC4BT; **b)** OC8BT; **c)** OC4TT; and **d)** OC8TT.

3.2.4 Morphology and Crystallinity

Grazing-incidence X-ray diffraction (GIXD) was performed to examine the morphology of polymer thin films in this thesis. Polymer solution with a concentration of 10 mg/mL was prepared and spin coated to silicon substrate and annealed at different temperatures. ***Figure 3-9*** shows the 1D and 2D XRD for the pristine OC4BT polymer without acid treatment. No obvious peaks are shown at room temperature and annealed at 50 °C for both in-plane and out-of-plane, suggesting that the polymer adopts an amorphous morphology at low temperatures. As the annealing temperature was increased to 100 °C or higher, an obvious peak at around $2\theta = 4.8^{o}$ was observed for out-of-plane data, which corresponds to the lamellar packing of polymer chains. The maximal intensity of the lamellar packing peak was observed when the polymer film was annealed at 150 °C. It indicates that the polymer has an edge-on orientation at high temperature which could potentially facilitate charge carrier transfer between polymer chains. This also explains why higher mobility was observed when the OTFT device was annealed at elevated temperatures. For OC8BT polymer, increased intensity for the lamellar peak (out-of-plane) at around $2\theta = 3.8°$ was observed as annealing temperature was raised, where no peak was observed for temperatures below 100 °C. The best molecular packing of polymer film was found to be at 200 °C (see **Figure 3-10**). OC8TT exhibited similar trend as the OC8BT polymer, which was amorphous at temperature below 100 °C. The intensity of the lamellar packing peak increased with elevated annealing temperatures, with a maximum degree of edge-on orientation reached at 200 °C (see **Figure 3-11**). Due to the solubility issue, XRD of OC4TT was not conducted.

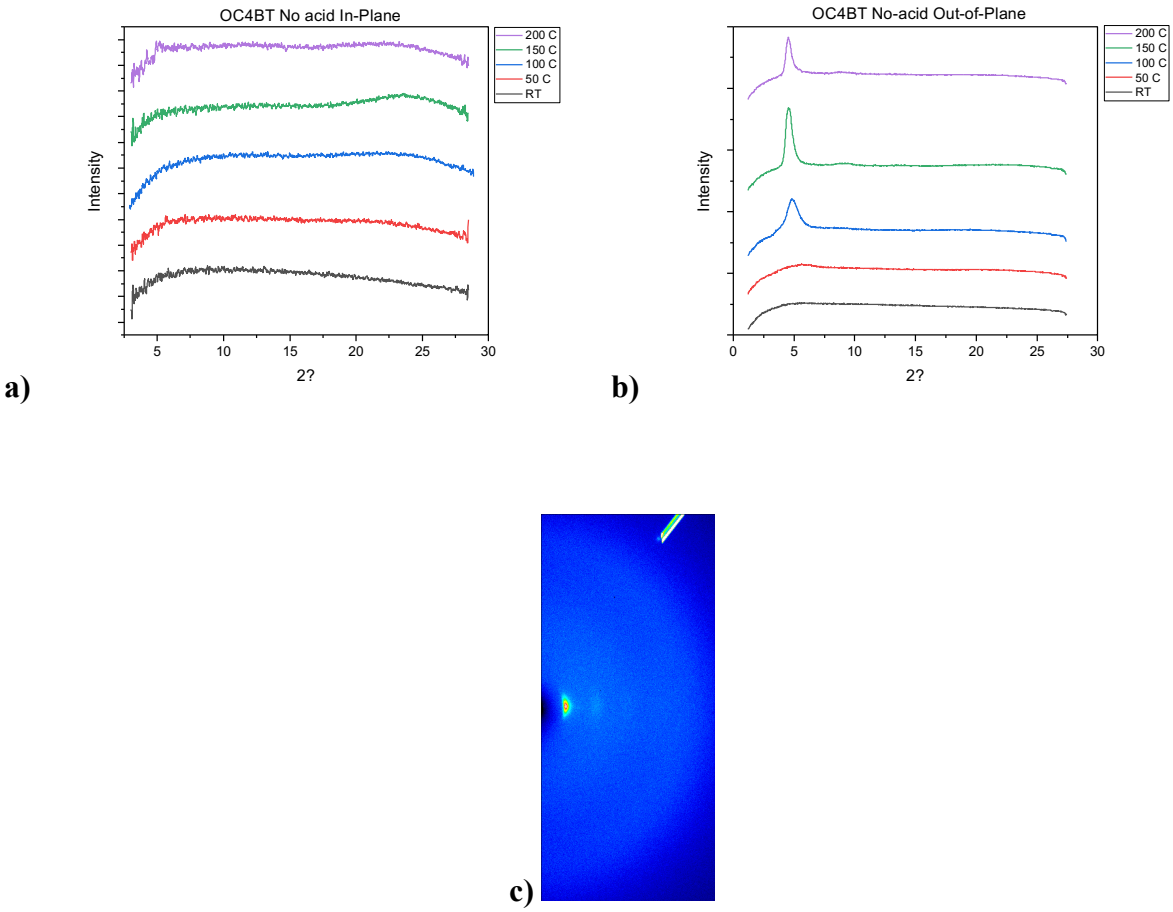
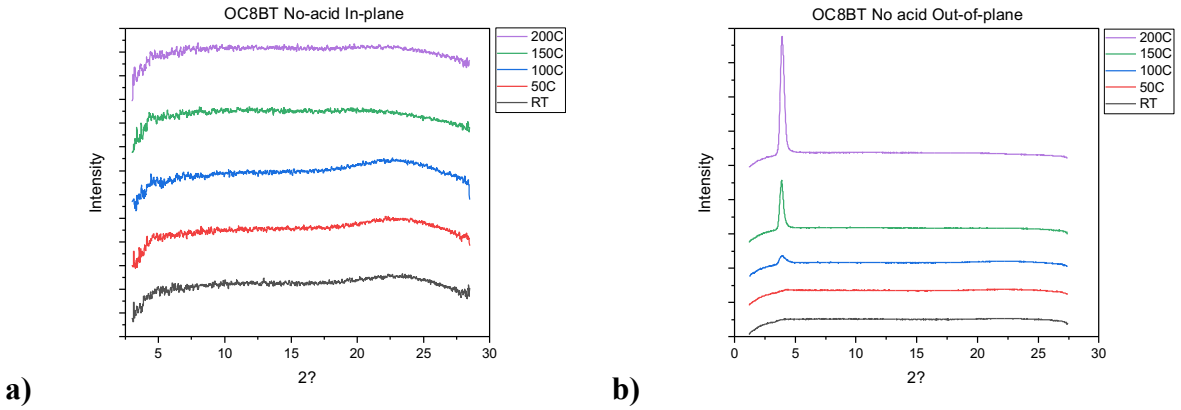
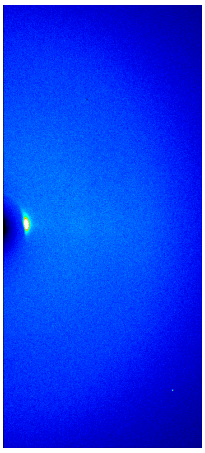


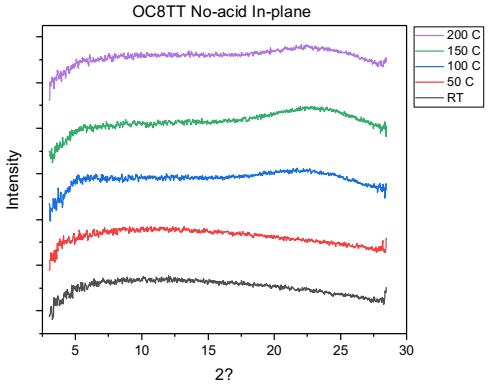
Figure 3-9. GIXD of OC4BT film (without acid treatment) after annealed at various temperatures: **a)** in-plane; **b)** out-of-plane; **c)** 2D image of polymer film annealed at 150 °C which demonstrates the best crystallinity.



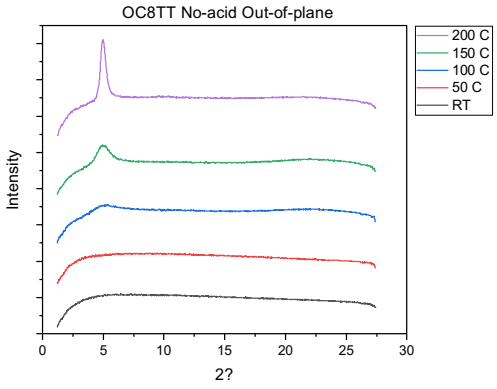


c)

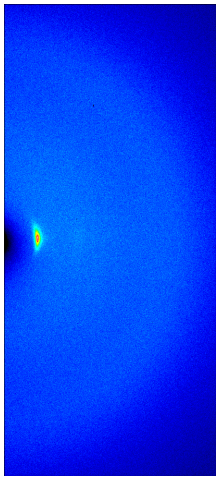
Figure 3-10. GIXD of OC8BT film (without acid treatment) after annealed at various temperatures: **a)** in-plane; **b)** out-of-plane; **c)** 2D image of OC8BT film annealed at 200 °C which demonstrates the best crystallinity.



a)



b)



c)

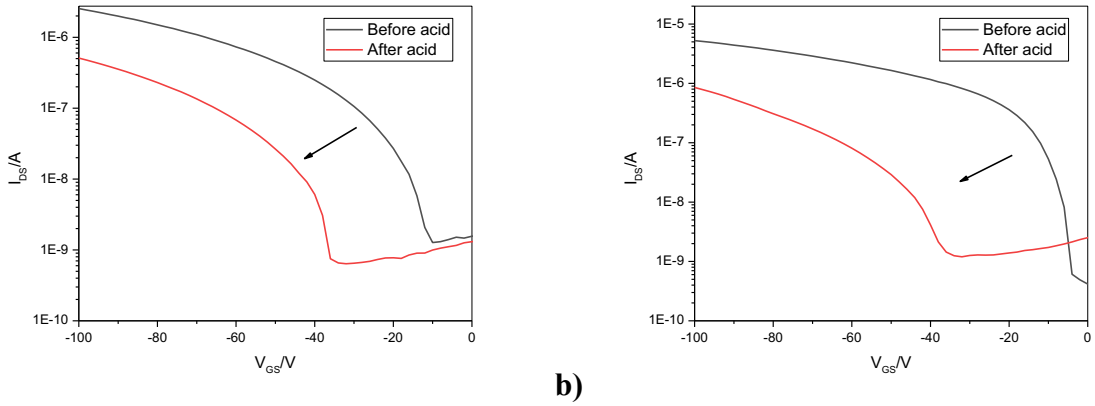
Figure 3-11. GIXD of OC8TT film (without acid treatment) after annealed at various temperatures: **a)** in-plane; **b)** out-of-plane; **c)** 2D image of OC8TT film annealed at 200 °C.

3.2.5 OTFT Performance

OTFT devices were fabricated using the method described in **Section 2.4.** Both bithiophene and thienothiophene based polymers exhibited p-type OTFT performances. Highest hole mobility achieved for OC4BT polymer was 1.75 x 10^{-3} cm^2 $V^{-1}s^{-1}$ after annealed at 100 °C, while OC8BT exhibited best mobility at 150 °C with a value of 2.23 x 10^{-3} $cm^2V^{-1}s^{-1}$. The high mobilities correlate with the XRD results, as better chain ordering was observed at higher annealing temperatures. For TT series of polymers, the mobilities are not as high as the BT series polymers which is likely due to the less conjugation associated with the TT backbone. However, an increasing trend in mobility was observed with the raised annealing temperatures. As a result, annealing of TT based OTFT devices at temperatures ranging from 200°C to 300°C was also performed to further examine the trend. It is found that the highest average hole mobilities for OC4TT and OC8TT polymers are 6.80 x 10^{-4} $cm^2V^{-1}s^{-1}$ and 3.07 x 10^{-3} $cm^2V^{-1}s^{-1}$, respectively, which both occurred at 250 °C. However, such temperature might be too high for practical applications.

It is noteworthy that mobilities of all devices dropped drastically after the acid treatment process. The relative response regarding the average mobility change was calculated by dividing the difference in mobilities between non-acid treated and acid treated polymers by the mobility of non-acid treated polymer. BT series of polymers experienced about an 80% drop in mobility, while the TT series exhibited an even larger decrease, with approximately a 90% loss in mobility. This phenomenon can be possibly explained by the molecular weight loss associated with the conversion of side chains. Due to the high coplanarity and rigidity of polymer chains contributed by the bithiophene and thienothiophene framework, longer acetal side chains were required to afford good polymer solubility. However, larger pores would be generated

consequently when the acetal groups were converted to aldehydes, thus resulting in a large decrease in molecular weight. For acetal group with C8 chain length, 46.91% and 49.40 % molecular weight loss were expected for OC8BT and OC8TT polymers, respectively, indicating that nearly half of the polymer film would be gone after the acid treatment process. For polymers synthesized using the C4 acetal chains, up to 32.19 % and 34.40 % molecular weight loss might happen. Even though desired nano porous structure could be generated by this process, the large interchain spaces created might lead to collapse or aggregation of polymer chains. The conducting pathway of charge carrier transports might be interrupted as a result, thus having a negative impact on the OTFT performance. In addition, the absolute values of V_{th} for devices after acid treatment also increased, indicating more defects and charge traps were generated within the semiconducting channel. As a result, alternate polymer structure design is required to resolve this issue. One-thiophene (1T) usually offers better solubility to the polymer, the chain lengths of acetal group can possibly be shortened to reduce the amount of molecular weight loss associated with the acid treatment step.



a) **b)**

Figure 3-12. OTFT transfer curve comparisons before and after acid treatment for polymers: **a)** OC4BT and **b)** OC8BT.

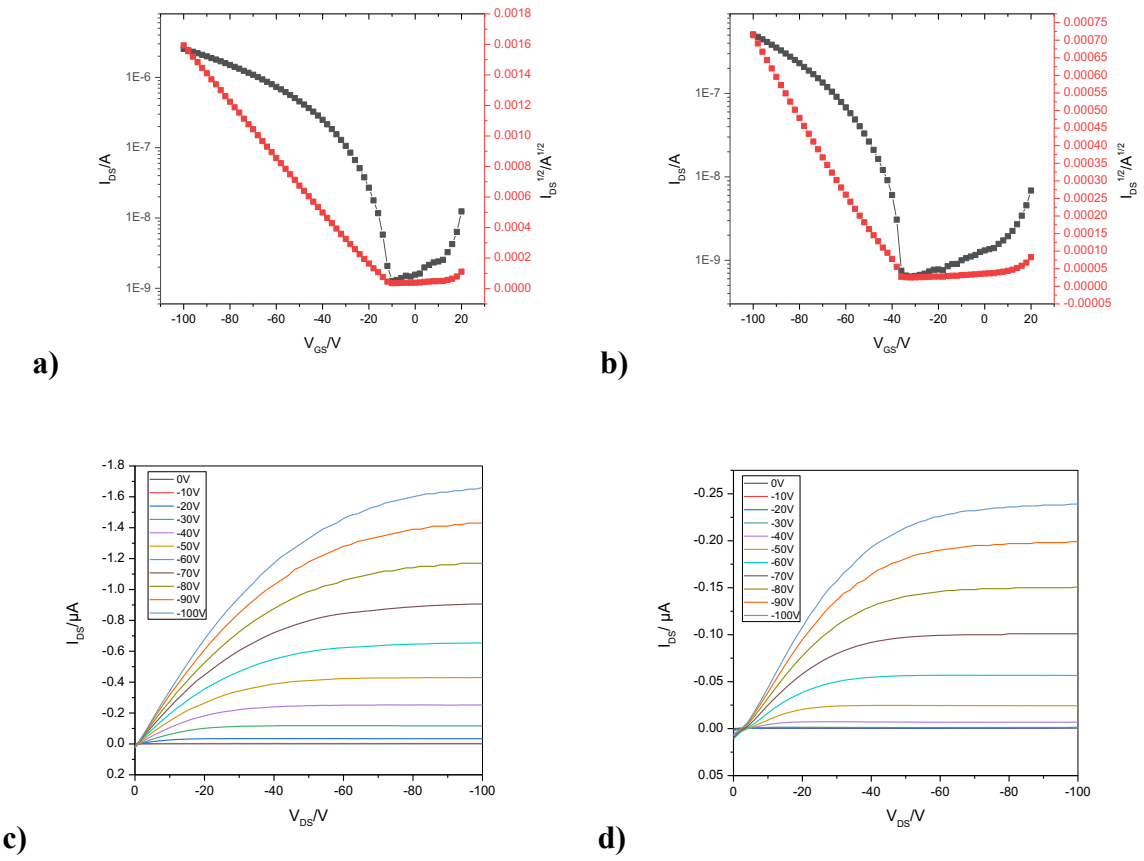
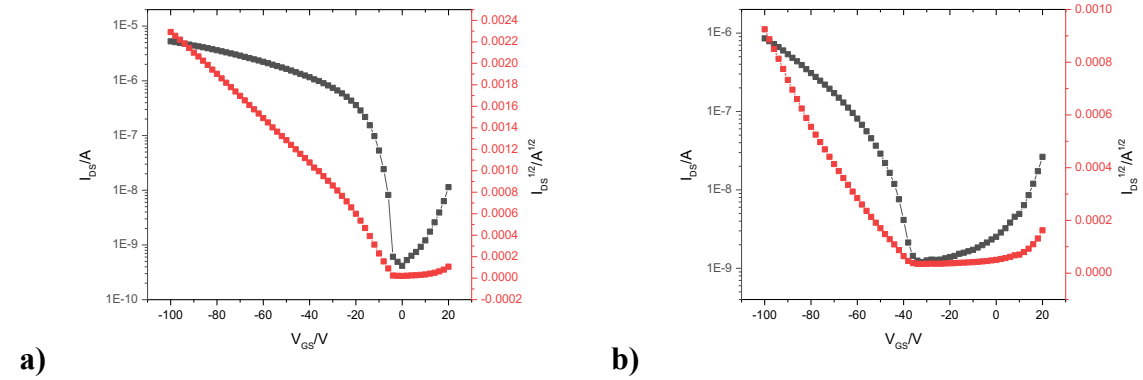


Figure 3-13. **(a&b)** OTFT transfer curves for OC4BT without and with acid treatment (OCHBT), respectively, at 100 ºC; **(c&d)** OTFT output curves for OC4BT without and with acid treatment (OCHBT), respectively, at 100 ºC.



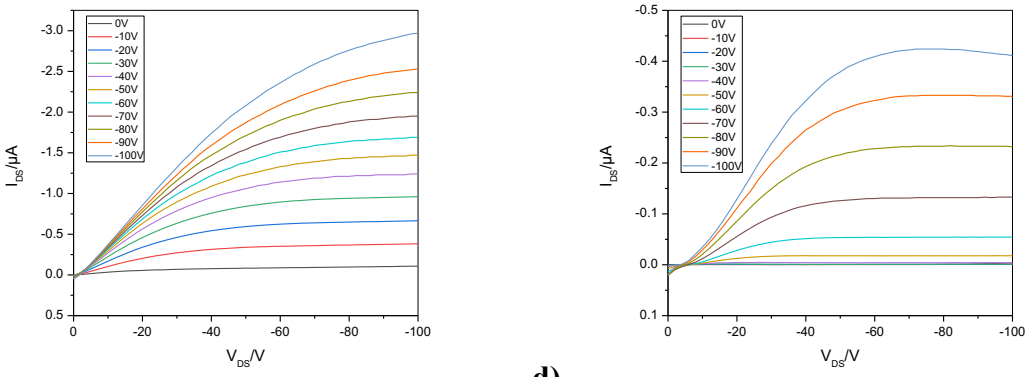


Figure 3-14. **(a&b)** OTFT transfer curves for OC8BT without and with acid treatment (OCHBT), respectively, at 150 ºC; **(c&d)** OTFT output curves for OC8BT without and with acid treatment (OCHBT), respectively, at 150 ºC.

Table 3-4. OTFT Performance Summary for OC4BT polymer.

Polymer	**Type**	**Temperature (°C)**	**Best Mobility ($cm^2V^{-1}s^{-1}$)**	**Avg Mobility ($cm^2V^{-1}s^{-1}$)**	**V_{th} (V)**	**$I_{on/off}$**
OC4BT	P-type	RT	1.08E-03	9.50E-04	-25.52	1000
OC4BT	P-type	50	1.02E-03	8.01E-04	-29.75	1000
OC4BT	***P-type***	***100***	***1.75E-03***	***1.46E-03***	***-13.16***	***1000***
OC4BT	P-type	150	5.61E-04	4.87E-04	0.29	1000
OC4BT	P-type	200	9.05E-04	4.13E-04	-38.88	100000

Table 3-5. OTFT Performance Summary for OC4BT polymer after acid treatment.

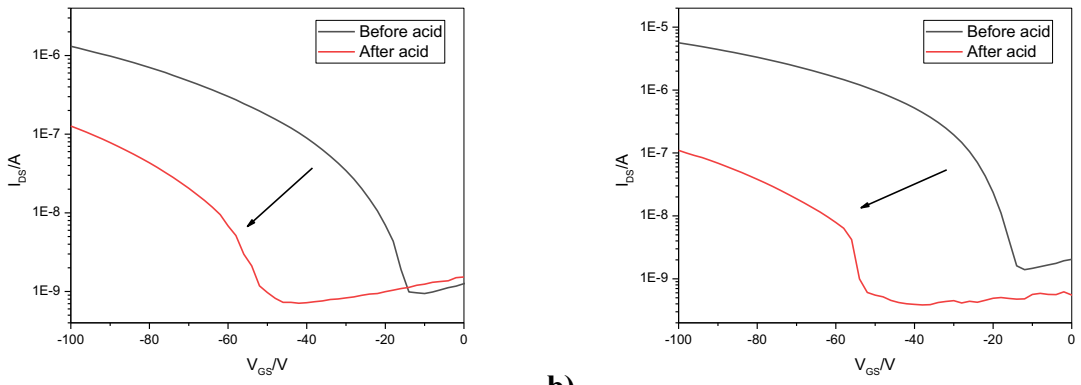
Polymer	**Temperature (°C)**	**Best Mobility ($cm^2V^{-1}s^{-1}$)**	**Avg Mobility ($cm^2V^{-1}s^{-1}$)**	**V_{th}(V)**	**$I_{on/off}$**	**Condition**
OC4BT	100	2.23E-03	2.11E-03	-19.10	1000	No acid
OCHBT	100	6.51E-04	5.82E-04	-37.02	1000	Acid
OCHBT	150	4.86E-04	4.25E-04	-39.27	1000	
OCHBT	200	2.16E-04	1.95E-04	-36.36	1000	

Table 3-6. OTFT Performance Summary for OC8BT polymer.

Polymer	Type	Temperature (°C)	Best Mobility ($cm^2V^{-1}s^{-1}$)	Avg Mobility ($cm^2V^{-1}s^{-1}$)	V_{th} (V)	$I_{on/off}$
OC8BT	P-type	RT	6.81E-04	6.27E-04	-10.34	1000
OC8BT	P-type	50	7.56E-04	6.78E-04	-12.41	1000
OC8BT	P-type	100	1.93E-03	1.67E-03	-8.36	1000
OC8BT	***P-type***	***150***	***2.23E-03***	***1.65E-03***	***12.13***	***10000***
OC8BT	P-type	200	4.80E-04	4.04E-04	24.74	1000

Table 3-7. OTFT performance summary for OC8BT polymer after acid treatment.

Polymer	Temperature (°C)	Best Mobility ($cm^2V^{-1}s^{-1}$)	Avg Mobility ($cm^2V^{-1}s^{-1}$)	V_{th}(V)	$I_{on/off}$	Condition
OC8BT	150	6.14E-03	5.77E-03	1.37	10000	No acid
OCHBT	100	1.04E-03	8.41E-04	-42.75	1000	Acid
OCHBT	150	1.18E-03	8.68E-04	-42.61	1000	
OCHBT	200	5.21E-04	4.86E-04	-37.36	1000	



a) **b)**

Figure 3-15. OTFT transfer curve comparisons before and after acid treatment for polymers: **a)** OC4TT and **b)** OC8TT.

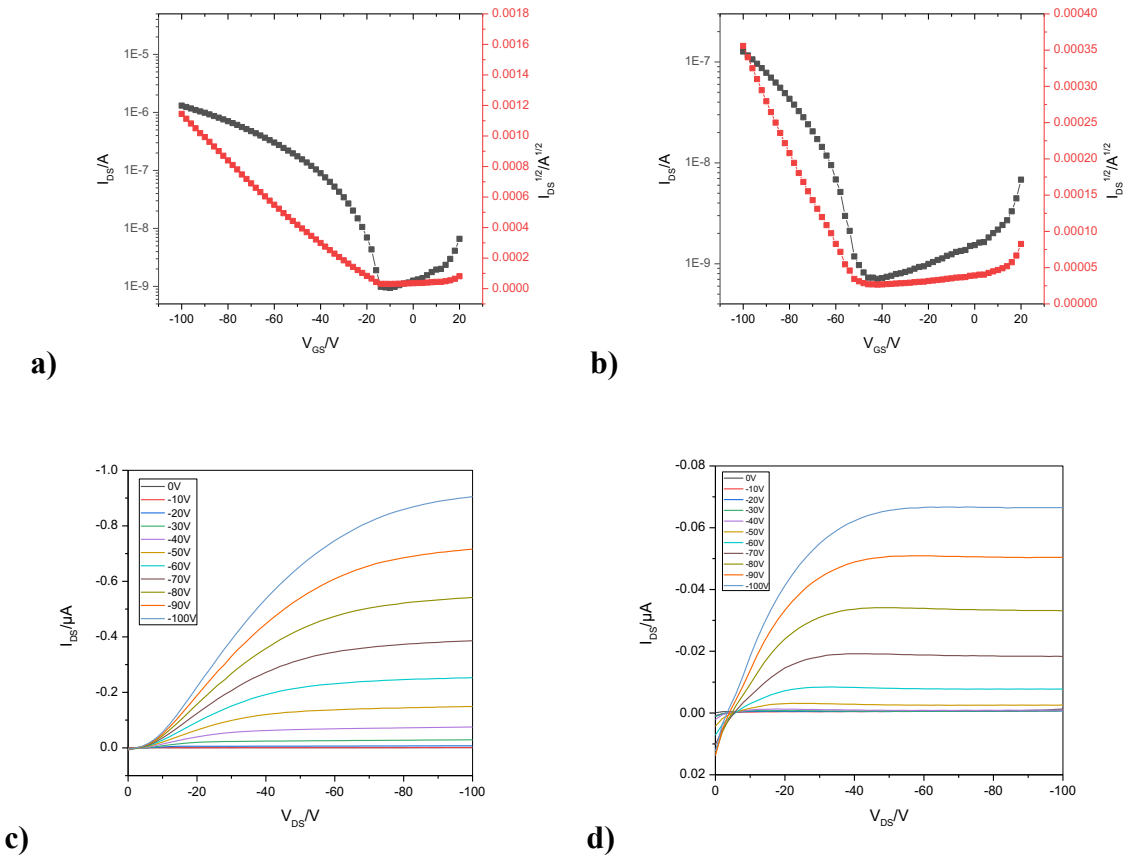
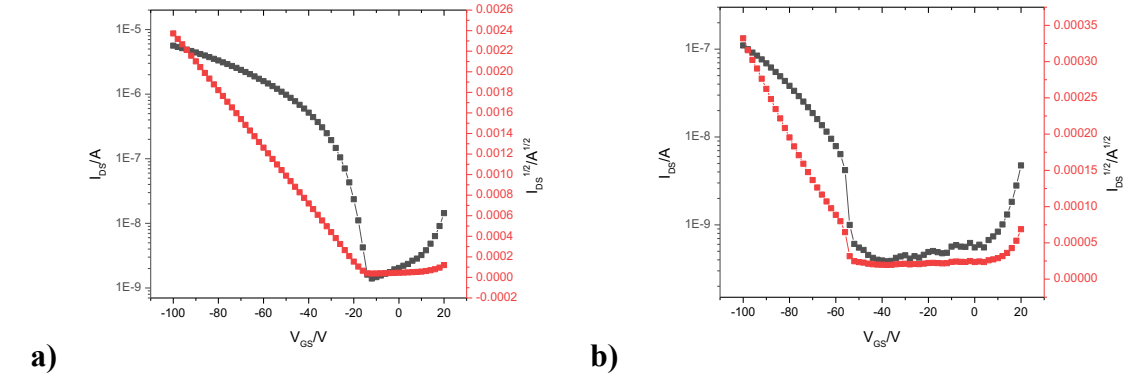
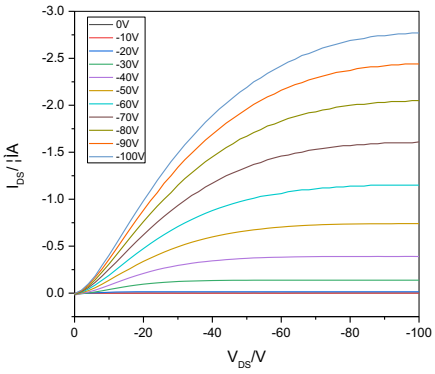
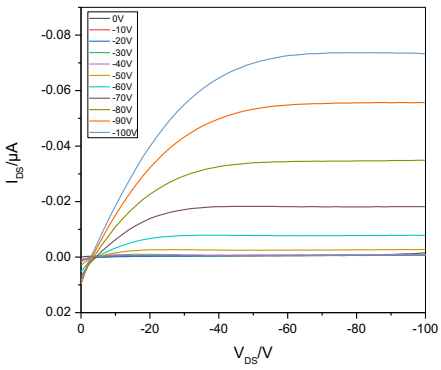


Figure 3-16. **(a&b)** OTFT transfer curves for OC4TT without and with acid treatment (OCHTT), respectively, at 250 ºC and 100 ºC; **(c&d)** OTFT output curves for OC4TT without and with acid treatment (OCHTT), respectively, at 250 ºC and 100 ºC.





c)



d)

Figure 3-17. **(a&b)** OTFT transfer curves for OC8TT without and with acid treatment (OCHTT), respectively, at 250 ºC and 150 ºC; **(c&d)** OTFT output curves for OC8TT without and with acid treatment (OCHTT), respectively, at 250 ºC and 150 ºC.

Table 3-8. OTFT performance summary for OC4TT polymer.

Polymer	Type	Temperature (°C)	Best Mobility ($cm^2V^{-1}s^{-1}$)	Avg Mobility ($cm^2V^{-1}s^{-1}$)	V_{th} (V)	$I_{on/off}$
OC4TT	P-type	RT	1.92E-04	1.67E-04	-34.18	100
OC4TT	P-type	50	1.58E-04	1.31E-04	-31.28	100
OC4TT	P-type	100	2.31E-04	2.23E-04	-26.38	1000
OC4TT	P-type	150	2.61E-04	2.44E-04	-15.67	100
OC4TT	P-type	200	7.81E-04	5.03E-04	-21.77	1000
OC4TT	***P-type***	***250***	***1.01E-03***	***6.80E-04***	***-20.24***	***1000***
OC4TT	P-type	300	1.52E-04	1.20E-04	-10.41	1000

Table 3-9. OTFT performance summary for OC4TT polymer after acid treatment.

Polymer	Temperature (°C)	Best Mobility ($cm^2V^{-1}s^{-1}$)	Avg Mobility ($cm^2V^{-1}s^{-1}$)	V_{th} (V)	$I_{on/off}$	Condition
OC4TT	250	2.60E-03	2.00E-03	-35.43	1000	No acid
OCHTT	100	2.49E-04	2.14E-04	-49.72	100	Acid
OCHTT	150	2.13E-04	1.89E-04	-45.04	1000	
OCHTT	200	1.87E-04	1.65E-04	-47.29	1000	

Table 3-10. OTFT performance summary for OC8TT polymer.

Polymer	Type	Temperature (°C)	Best Mobility ($cm^2V^{-1}s^{-1}$)	Avg Mobility ($cm^2V^{-1}s^{-1}$)	V_{th} (V)	$I_{on/off}$
OC8TT	P-type	RT	1.65E-04	1.55E-04	-21.07	100
OC8TT	P-type	50	1.60E-04	1.49E-04	-21.62	100
OC8TT	P-type	100	4.31E-04	3.63E-04	-24.96	100
OC8TT	P-type	150	1.76E-03	1.35E-03	-26.27	1000
OC8TT	P-type	200	3.02E-03	2.49E-03	-22.85	10000
OC8TT	***P-type***	***250***	***3.98E-03***	***3.07E-03***	***-14.21***	***10000***
OC8TT	P-type	300	9.86E-04	9.21E-04	-13.54	1000

Table 3-11. OTFT performance summary for OC8TT polymer after acid treatment.

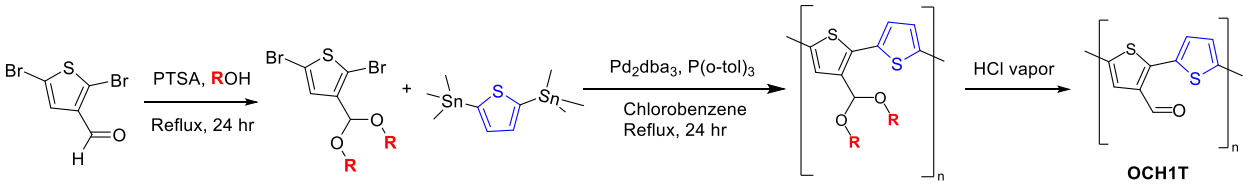
Polymer	Temperature (°C)	Best Mobility ($cm^2V^{-1}s^{-1}$)	Avg Mobility ($cm^2V^{-1}s^{-1}$)	V_{th} (V)	$I_{on/off}$	Condition
OC8TT	250	2.47E-03	2.41E-03	-26.77	1000	No acid
OCHTT	100	1.97E-04	1.70E-04	-54.38	1000	Acid
OCHTT	150	2.12E-04	1.81E-04	-49.21	100	
OCHTT	200	1.91E-04	1.71E-04	-44.63	1000	

3.3 One-Thiophene Series

3.3.1 Synthesis Method

To address the molecular weight loss problem associated with the BT and TT series polymers, copolymerization of acetal substituted thiophene monomers with one-thiophene (1T) unit was performed and studied to explore the possibility of utilizing shorter acetal chains. Same Stille coupling polymerization method was employed with the substitution of 2,5-bis(trimethylstannyl) thiophene as the ditin component. One-thiophene usually exhibits better solubility compared to bithiophene and thienothiophene, so shorter chains may be sufficient to offer good solubility to the polymer. Screening of effective side chain length was performed to explore the limit. Methanol, ethanol, and butanol were used to synthesize the acetal monomers with various chain

lengths. Monomer synthesis can reach quantitative yields when methanol or ethanol was used as the alcohol, attributed to their relative low boiling points and ease for removal. It is found that even the acetal monomer with dimethoxy side chain can afford good solubility in chloroform after polymerization, which makes the polymer synthesis route easier and cost-effective. OC41T exhibited good solubility in hexane while OC21T and OMe1T were mainly soluble in chloroform.



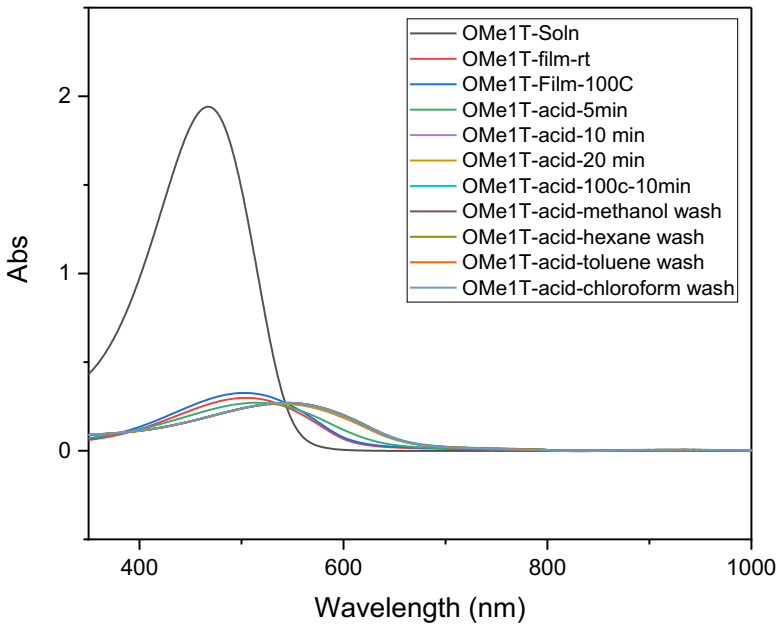
Scheme 3. Synthesis scheme for 1T series of polymer and conversion to aldehyde-substituted thiophene-based polymer.

3.3.2 Opto-electrochemical Properties

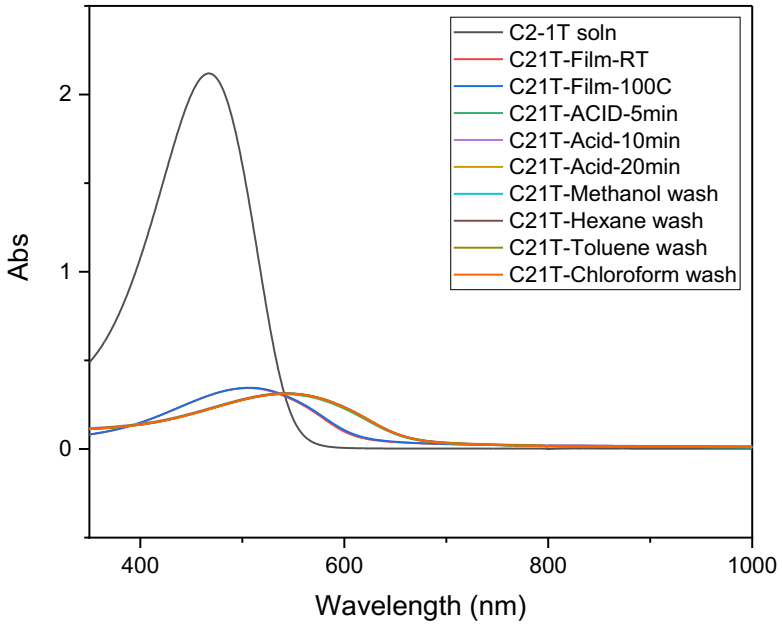
UV-vis spectra for 1T polymers were measured following the procedure outlined in **Section 3.2.2**. Complete side chain removal was again accomplished within 5 minutes. The band gap energies for OMe1T, OC21T, and OC41T are 2.02, 2.26 and 2.03 eV, respectively. Similar phenomenon was observed after the conversion of side chains where the energy band gap became narrower. The band gap energies for OCH1T polymer obtained by acid cleavage from OMe1T, OC21T, and OC41T were 1.84, 1.85 and 1.83 eV, respectively, which showed no significant difference.

CV data were acquired using the same method described in **Section 3.2.2** with comparison of both non-acid treated and acid-treated polymers. Similar to the BT and TT series, 1T series of polymers are also classified as p-type semiconductor materials based on the obtained HOMO and

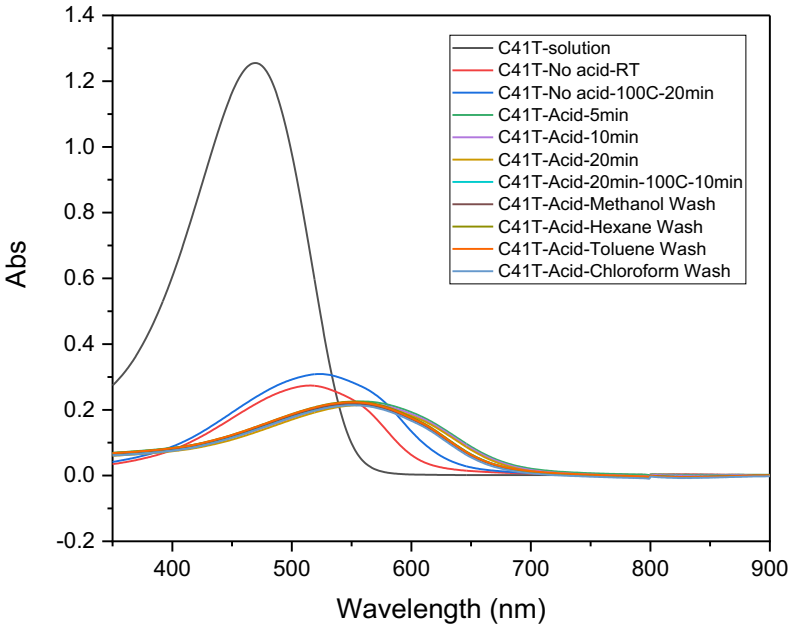
LUMO energy levels. OMe1T, OC21T and OC41T have E_{HOMO} values of -5.25 and -5.29 eV and -5.31eV; while after side chain removal, the E_{HOMO} values were calculated to be -5.39 eV, -5.37 eV and -5.34 eV, respectively. There was a slight difference in E_{HOMO} values for OCH1T obtained from treatment to different 1T pristine polymers. However, since the onset value of oxidation was obtained by extrapolation of the CV scan curve, thus the calculated E_{HOMO} was just an estimated value which might lead to slight deviation. The obtained values still fit in a reasonable range. All opto-electrochemical related data for 1T series of polymers (before and after acid treatment) were summarized in **Table 3-12** and **Table 3-13.**



a)



b)



c)

Figure 3-18. UV-vis absorption spectra of polymer solution, as-cast thin film, annealed thin film and acid-treated thin films with various conditions: **a)** OMe1T; **b)** OC21T; and **c)** OC41T.

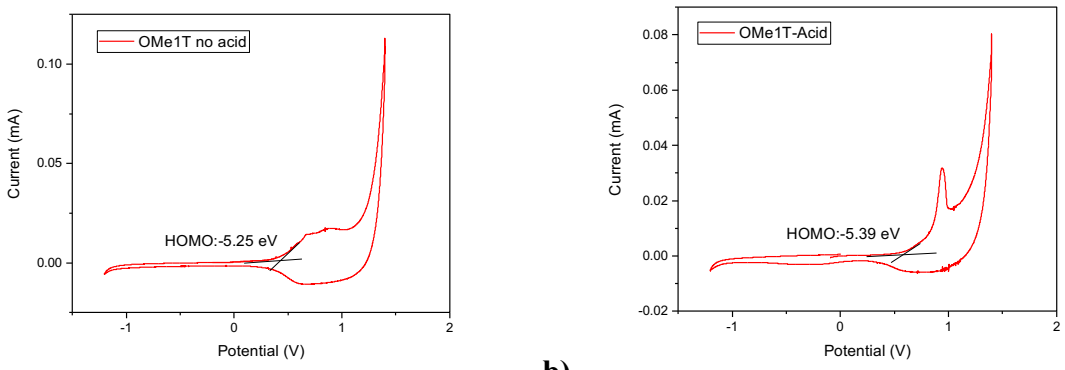


Figure 3-19. CV profiles of OMe1T polymer: **a)** non-acid treated; **b)** acid treated (which is the OCH1T polymer).

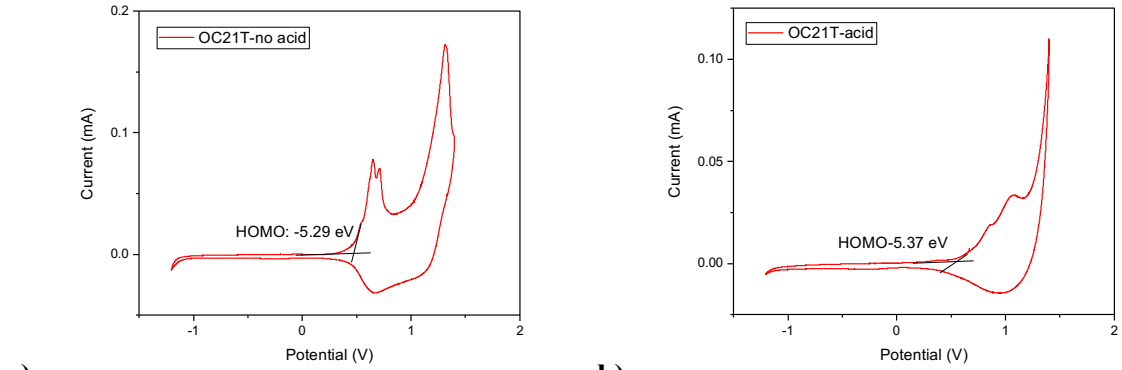


Figure 3-20. CV profiles of OC21T polymer: **a)** non-acid treated; **b)** acid treated (which is the OCH1T polymer).

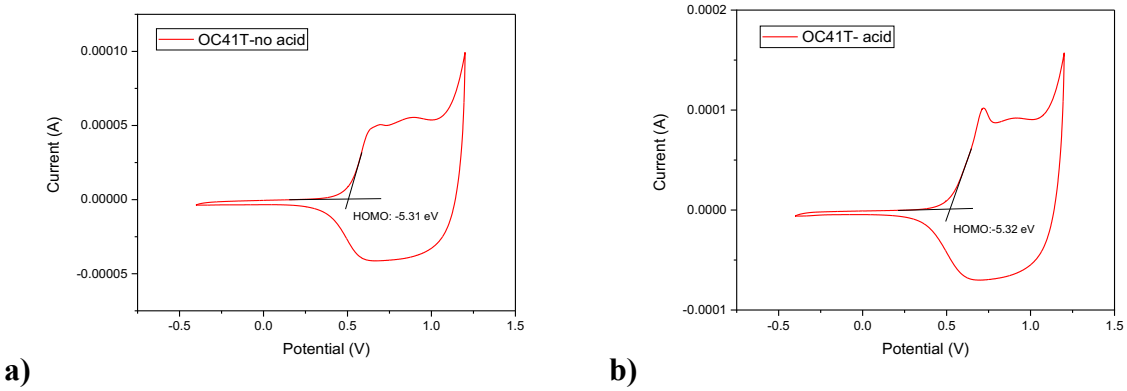


Figure 3-21. CV profiles of OC41T polymer**: a)** non-acid treated; **b)** acid treated (which is the OCH1T polymer).

Table 3-12. Summary of optical and electrochemical properties for 1T series polymers.

Polymer	$\lambda_{max\text{-}soln}$ (nm)	$\lambda_{max\text{-}TF\text{-}RT}$ (nm)	$\lambda_{max\text{-}TF\text{-}100}$ (nm)	λ_{onset} (nm)	E_g^{opt} (eV)	E_{HOMO} (eV)	E_{LUMO} (eV)
OMe1T	467	504	502	615	2.02	-5.25	-3.23
OC21T	467	506	507	548	2.26	-5.29	-3.03
OC41T	469	515	521	611	2.03	-5.31	-3.28

Table 3-13. Summary of optical and electrochemical properties for 1T series polymers after acid treatment.

Polymer	Original polymer	$\lambda_{max\text{-}TF\text{-}RT}$ (nm)	λ_{onset} (nm)	E_g^{opt} (eV)	E_{HOMO} (eV)	E_{LUMO} (eV)
OCHT1T	OMe1T	543	673	1.84	-5.39	-3.55
OCHT1T	OC21T	541	672	1.85	-5.37	-3.52
OCHT1T	OC41T	547	677	1.83	-5.32	-3.49

3.3.3 Physical and Chemical Properties

GPC of OC21T and OC41T was obtained using THF as the solvent at 70 ℃. OMe1T was not measured since it could not be fully dissolved in THF to generate a homogeneous solution for GPC. The number-average molecular weight (M_n) for OC21T and OC41T are 14,882 Da and 11,476 Da, respectively, while the weight-average molecular weights (M_w) are 21,951 Da and 14,908 Da, respectively. The PDI of OC21T and OC41T are calculated to be 1.48 and 1.30.

TGA of 1T series of polymers was measured using the identical conditions under nitrogen from 50 ℃ to 600 ℃ at a heating rate of 10℃/min. Only one thermal event was observed for all three 1T series of polymers which is shown in **Figure 3-22**. The first decomposition step occurred at 281℃, 307 ℃ and 301℃ for OMe1T, OC21T and OC41T polymers, respectively.

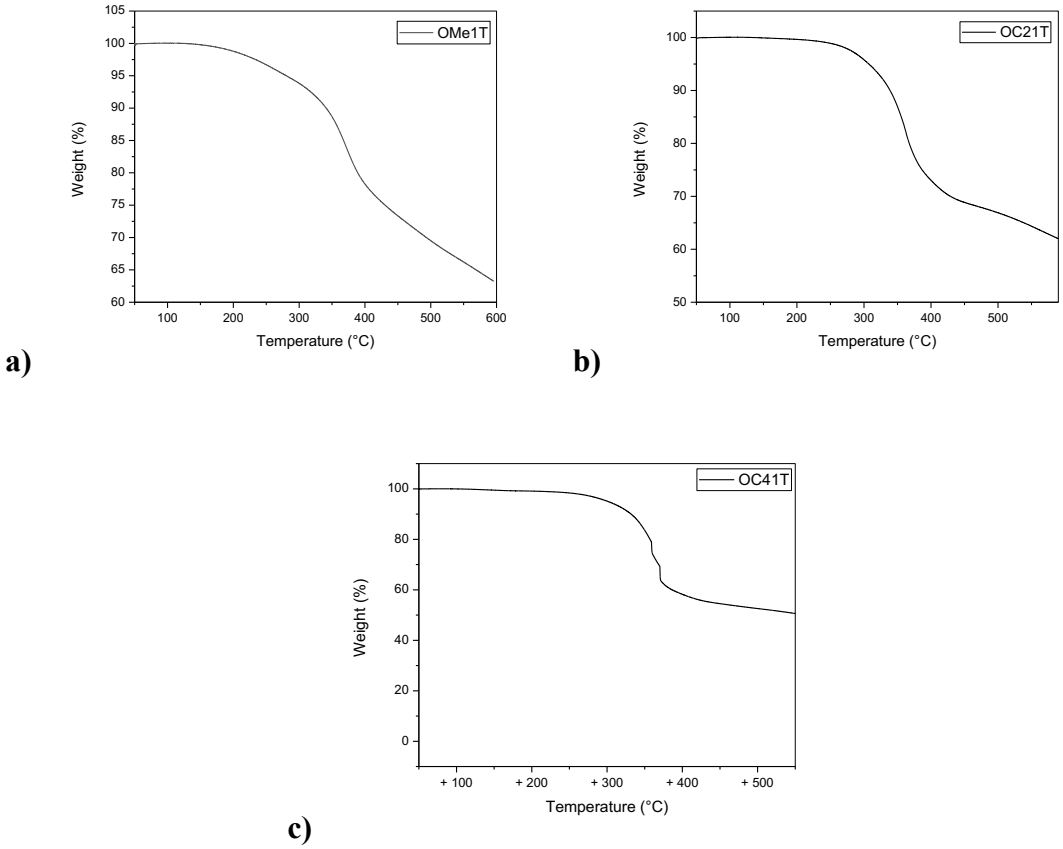


Figure 3-22. TGA curves for polymers: **a)** OMe1T; **b)** OC21T; and **c)** OC41T.

FTIR of OC21T polymer before and after acid treatment were measured to confirm the conversion of side chains. As shown in **Figure 3-23**, the peak at 1050 cm^{-1} is the C-O single bond of the acetal group. After acid treatment, the intensity of this peak dropped drastically as the acetal group was converted to aldehyde. As a result, the intensity of the peak corresponding to the C=O double bond of the aldehyde (at around 1660 cm^{-1}) increased significantly, which proved the successful conversion of side chains by the acid treatment step.

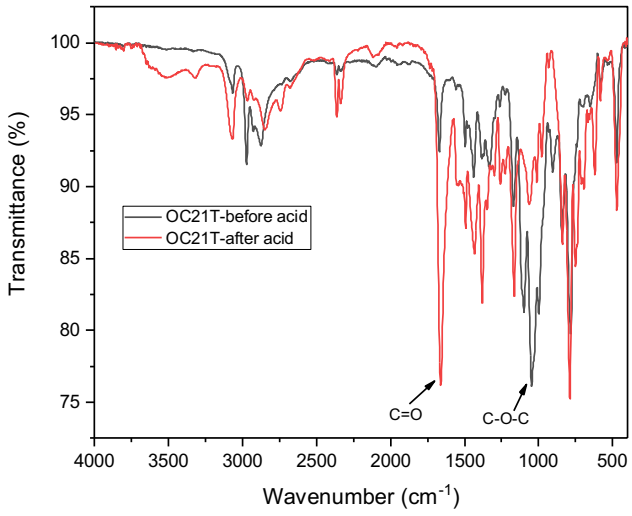


Figure 3-23. FTIR spectra of OC21T polymer before and after acid treatment.

3.3.4 Morphology and Crystallinity

XRD of OC21T and OC41T with both acetal side chains and aldehyde side chains were measured. Same acid treatment process was carried out as for preparing samples for UV-vis measurement. Since heating of polymer film at 100 °C after acid-treatment was required to remove potential residue of HCl vapor, XRD measurements for acid-treated films at temperatures below 100 °C were not conducted. Based on **Figure 3-24**, no obvious peaks are shown for both in-plane and out-of-plane at all temperatures, indicating that the OC21T polymer adopts an amorphous structure both before and after acid treatment.

For OC41T polymer which has a slightly longer side chain, the crystallinity is slightly better than that of OC21T. Weak lamellar peak at out-of-plane (OOP) was observed at 100 °C, with the intensity further increased at 150 °C and dropped at 200 °C (see **Figure 3-25**). Better polymer backbone packing was observed associated with the increased acetal chain length, which is also

the case for the other two series of polymers. However, such polymer chain packing rigidity was lost after acid treatment.

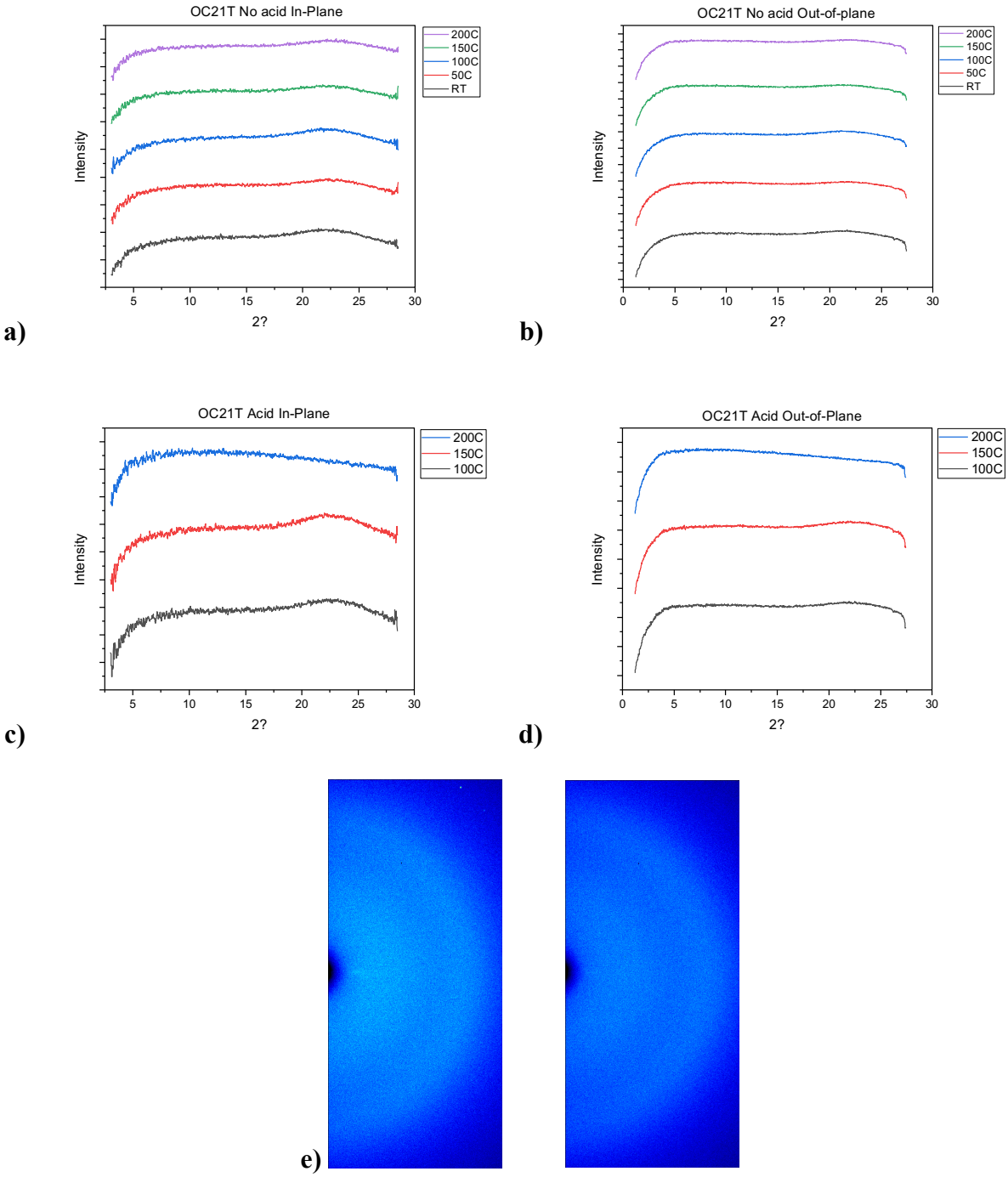


Figure 3-24. GIXD of OC21T polymer: **a)** no acid, in-plane**, b)** no acid, out-of-plane**; c)** acid, in-plane**, d)** acid, out-of-plane**, e)** 2D images for OC21T before acid treatment at 150 °C (left) and after acid at 150 °C (right).

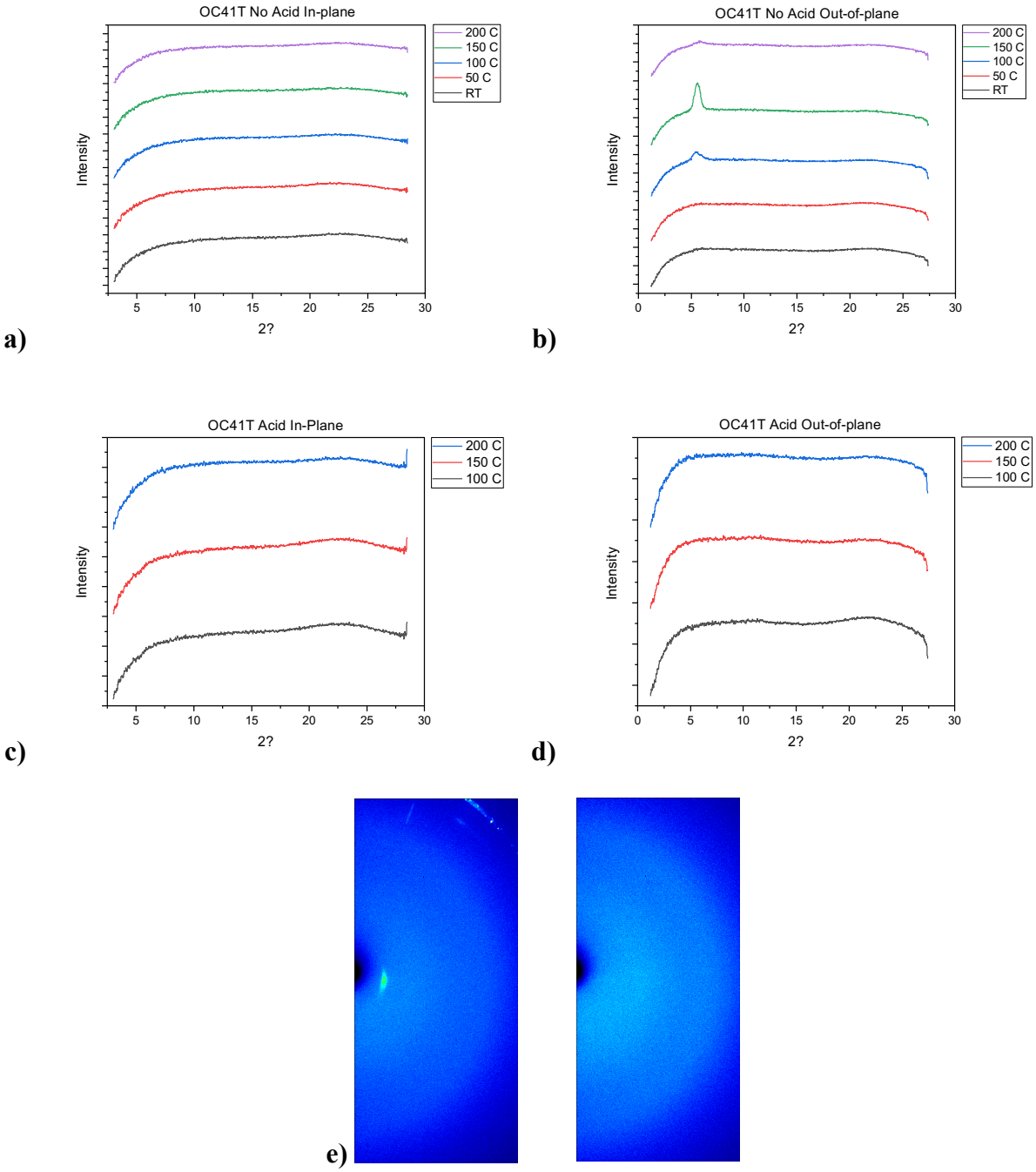


Figure 3-25. GIXD of OC41T polymer: **a)** no acid, in-plane**, b)** no acid, out-of-plane; **c)** acid, in-plane**, d)** acid, out-of-plane**, e)** 2D images for OC41T before acid treatmnet at 150 °C (left) and after acid at 150 °C (right).

Atomic force microscopy (AFM) of OC21T with and without acid treatment were measured to examine the morphology difference between the acetal and aldehyde polymer films. AFM sample preparation used a polymer solution with a concentration of 10 mg/mL in chloroform for spin coating to silicon substrate. Both films were annealed at 100 °C in glovebox before measurement, which is the same condition as for the operating OTFT devices. The dark spots shown in **Figure 3-26** may be the intrinsic defects or grain boundaries of the polymer thin film as the pore sizes of OCH1T converted from OC21T polymer might be too small to be visualized through AFM.

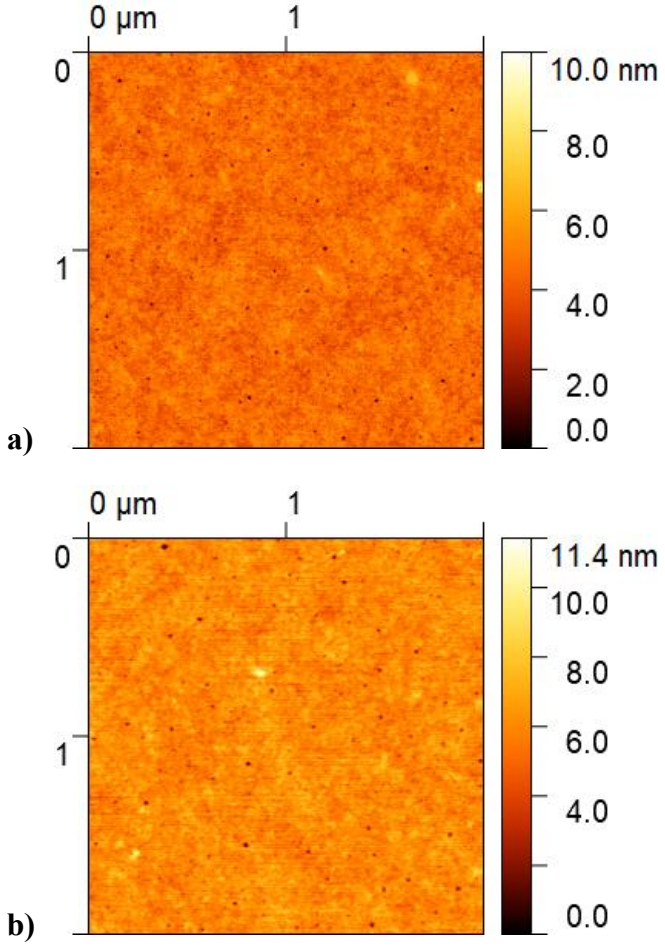


Figure 3-26. AFM images of **a)** OC21T thin film annealed at 100 °C and; **b)** OCH1T thin film which was obtained by acid treatment to OC21T film, annealed at 100 °C.

3.3.5 OTFT Performance

The OTFT performances of 1T series polymers are summarized in ***Table 3-14, 3-15*** and ***3-16***. The average mobilities of 1T polymers in general are still comparable with the BT and TT series. Highest mobility obtained for OMe1T, OC21T and OC41T are 4.08 x 10^{-4} $cm^2V^{-1}s^{-1}$, 1.08 x 10^{-3} $cm^2V^{-1}s^{-1}$, and 5.02 x 10^{-3} $cm^2V^{-1}s^{-1}$, respectively. It is worth mentioning that delamination of OMe1T film at 200 °C was observed, suggesting that the polymer was not stable enough to withstand such high temperature. It might indicate a low molecular weight associated with this polymer. Although acid treatment still leads to a decrease in average hole mobilities and an increase in absolute values of threshold voltages, the percentage changes for OMe1T and OC21T polymer based OTFTs have decreased significantly, with 56% and 45% drop in mobilities, respectively. However, OC41T still lost over 90% of mobility since 40% of molecular weight was removed after conversion into the aldehyde form. Therefore, OMe1T and OC21T were then selected as the material for further OTFT based gas sensor performance tests, which will be elaborated in the next chapter.

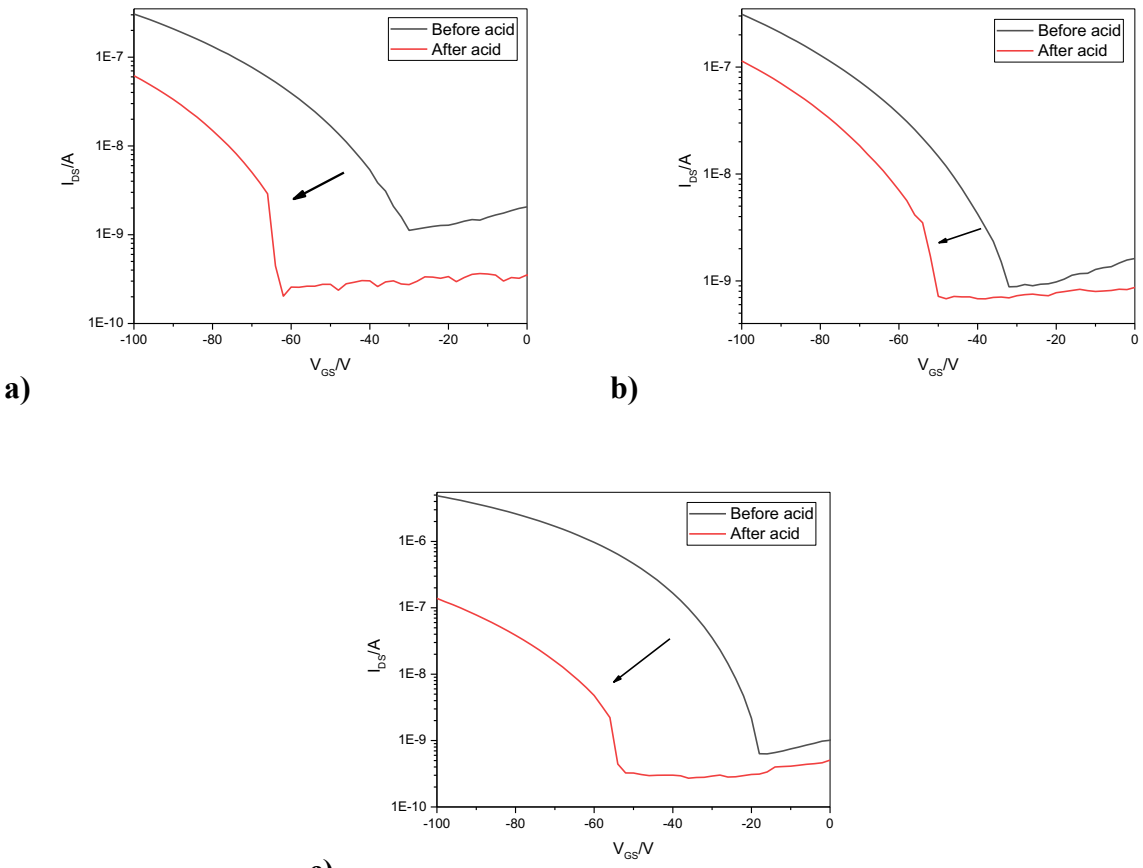
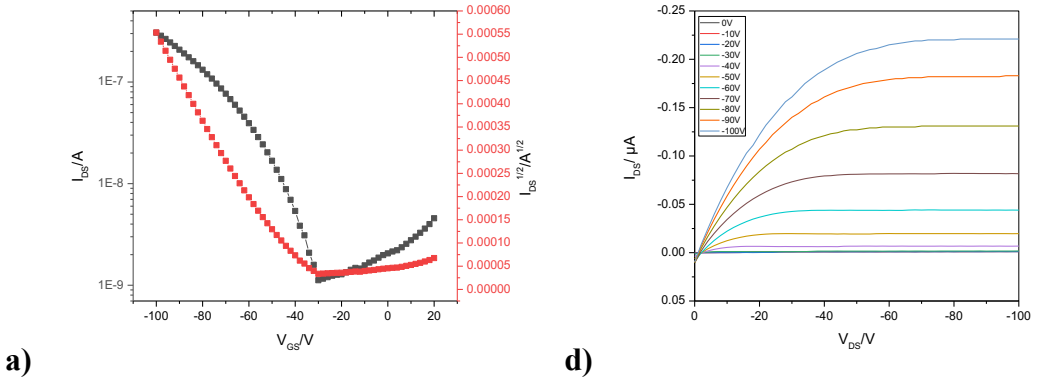


Figure 3-27. OTFT transfer curve comparisons before and after acid treatment for polymers: **a)** OMe1T; **b)** OC21T; and **c)** OC41T.



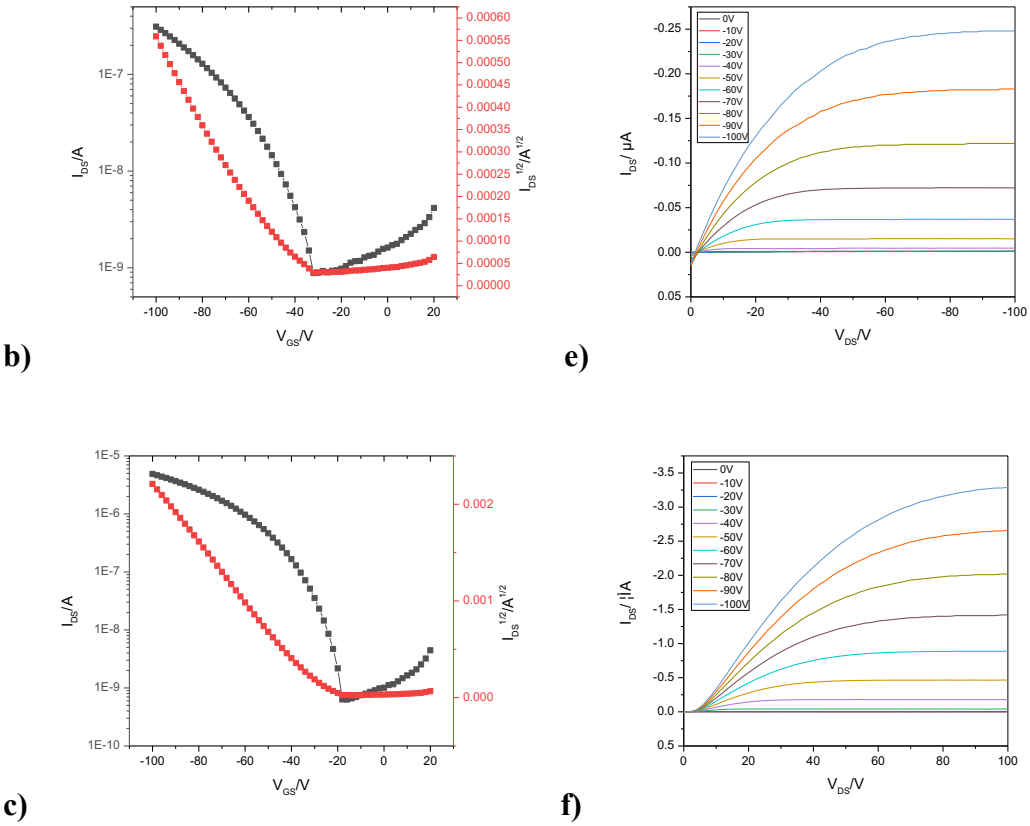


Figure 3-28. **(a-c)** OTFT transfer curves and **(d-e)** output curves for OMe1T, OC21T and OC41T at RT, 150 °C and 150 °C, respectively.

Table 3-14. OTFT performance summary for OMe1T polymer.

Polymer	Type	Temperature (°C)	Best Mobility ($cm^2V^{-1}s^{-1}$)	Avg Mobility ($cm^2V^{-1}s^{-1}$)	V_{th} (V)	$I_{on/off}$
OMe1T	***P type***	***RT***	***4.20E-04***	***4.08E-04***	***-39.29***	***100***
OMe1T	P type	50	4.19E-04	3.88E-04	-38.83	100
OMe1T	P type	100	3.72E-04	3.33E-04	-30.04	100
OMe1T	P type	150	2.17E-04	1.87E-04	-21.62	100
OMe1T	P type	200	1.62E-04	1.56E-04	-27.86	100

Table 3-15. OTFT performance summary for OC21T polymer.

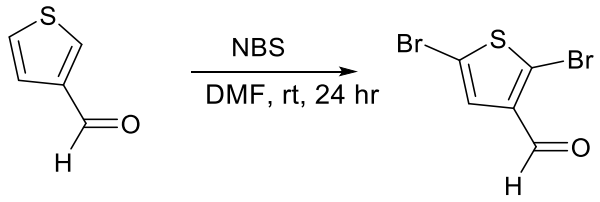
Polymer	Type	Temperature (°C)	Best Mobility ($cm^2V^{-1}s^{-1}$)	Avg Mobility ($cm^2V^{-1}s^{-1}$)	V_{th} (V)	$I_{on/off}$
OC21T	P type	RT	2.89E-04	2.78E-04	-30.41	100
OC21T	P type	50	3.36E-04	3.11E-04	-40.29	100
OC21T	P type	100	4.43E-04	3.99E-04	-40.70	1000
OC21T	***P type***	***150***	***1.21E-03***	***1.08E-03***	***-38.88***	***1000***
OC21T	P type	200	5.58E-04	5.36E-04	-33.38	1000

Table 3-16. OTFT performance summary for OC41T polymer.

Polymer	Type	Temperature (°C)	Best Mobility ($cm^2V^{-1}s^{-1}$)	Avg Mobility ($cm^2V^{-1}s^{-1}$)	V_{th} (V)	$I_{on/off}$
OC41T	P type	RT	2.87E-04	2.71E-04	-32.38	1000
OC41T	P type	50	3.42E-04	3.22E-04	-38.84	1000
OC41T	P type	100	2.89E-03	2.73E-03	-31.08	10000
OC41T	***P type***	***150***	***5.09E-03***	***4.41E-03***	***-26.11***	***10000***
OC41T	P type	200	5.06E-03	5.02E-03	-27.93	10000

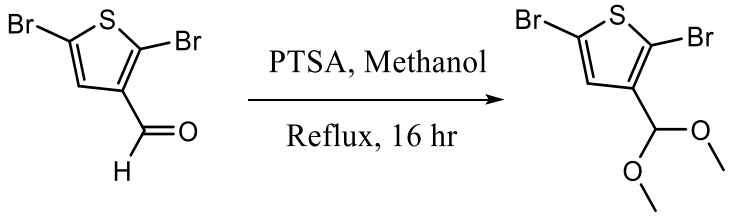
3.4 Experimental Section

Synthesis of 2,5-dibromothiophene-3-carbaldehyde



3-thiophenecarboxaldehyde (9 g, 80.25 mmol) was added to a 250 mL one-neck round-bottom flask, and it was dissolved in 120 mL DMF. Then a mixture of N-bromosuccinimide (NBS) (35.71 g, 200.63 mmol) in DMF (100 mL) was added dropwise and the solution was stirred in dark. After 24 hr, the reaction mixture was poured into DI water and extracted with diethyl ether. Then the organic phase was dried using anhydrous sodium sulfate, and the solvent was removed by rotary evaporation. The crude product was purified using column chromatography (silica gel, hexane/dichloromethane mixture = 3:1) to obtain the product as a yellow solid. (Yield: 14.84 g, 69%). ^{1}H NMR (300 MHz, $CDCl_3$, δ/ppm): 9.79 (s, 1H), 7.34 (s, 1H).

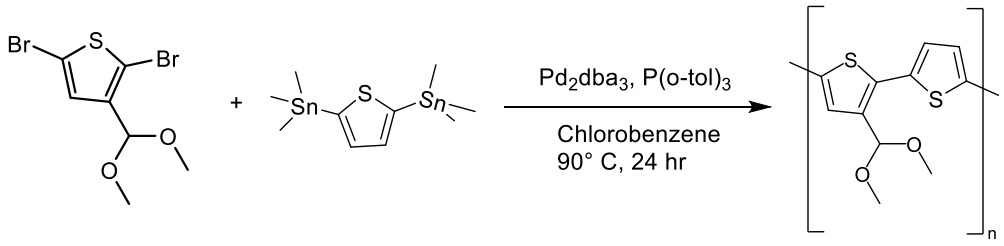
Synthesis of 2,5-dibromo-3-(dimethoxymethyl) thiophene



PTSA (5.23 mg, 0.0304mmol) and 2,5-dibromo-3-carboxyaldehydethiophene (0.2735g, 1.010 mmol) were added to a 25 mL two-neck round bottom flask equipped with a stir bar, and vacuum backfilled with nitrogen gas three times. Anhydrous methanol (10 mL) was then added to the reaction mixture and refluxed at 65 °C overnight. After 16 hours, the reaction mixture was cooled to room temperature, then it was poured into diethyl ether and washed with saturated

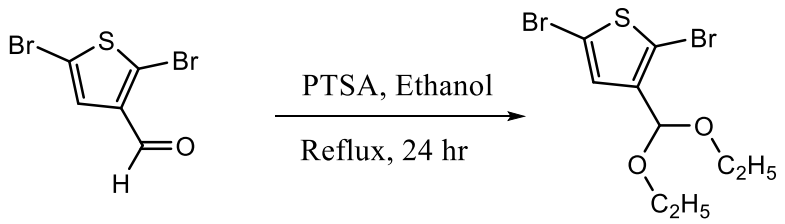
sodium bicarbonate solution (3 x 50 mL), and dried using sodium sulfate. The obtained product after evaporation of solvent was a yellow oil. (Yield: 0.31g, 97%). ^{1}H NMR (300 MHz, $CDCl_3$, δ/ppm): 7.02 (s, 1H), 5.28 (s, 1H), 3.33 (s, 6 H).

Synthesis of OMe1T polymer



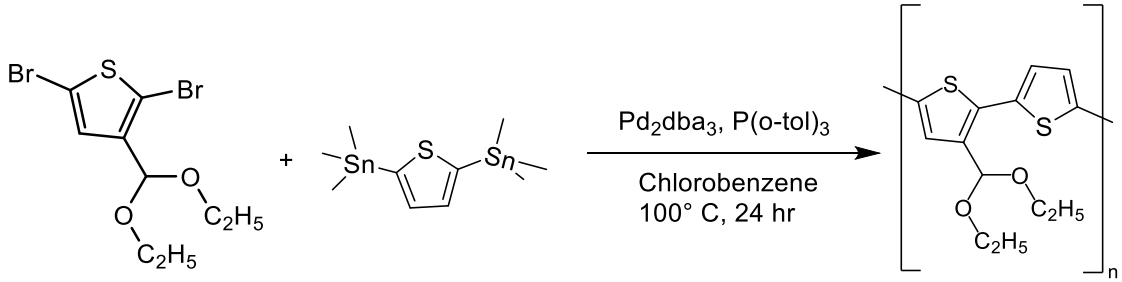
Acetal monomer (150 mg, 0.4747 mmol, 1.0 equiv.), 2,5-Bis(trimethylstannyl) thiophene (0.1945 mg, 0.4747 mmol, 1.0 equiv.) and $P(o\text{-}tol)_3$ (0.011 6g, 0.0380 mmol, 0.08 equiv) were added to a 25 mL two-neck round bottom flask along with a stir bar, then the system was purged with argon for 3 x 10-minute cycles. Tris(dibenzylideneacetone)dipalladium ($Pd_2(dba)_3$) (0.0174 mg, 0.0190 mmol, 0.04 equiv.) was measured in a benchtop glovebox under nitrogen and dissolved in 1 mL of chlorobenzene, then the catalyst solution was added to the system with a syringe, followed by additional 4 mL of anhydrous chlorobenzene as the solvent. The reaction mixture was heated at 90 °C under argon atmosphere for 24 hours. 0.5 mL of 2-(tributylstannyl) thiophene was added to the solution to stir for 1 hr. Then 0.15 mL of 2 bromothiophene (same molar equiv.) was added to the reaction mixture and stirred for another hour to end-cap the polymer. After cooling down to room temperature, the mixture was poured into stirring methanol (150 mL) for 30 mins. The solid was collected by filtration, dried, and further purified by Soxhlet extraction using acetone, hexane, chloroform. (Yield: 88 mg, 78% in chloroform).

Synthesis of 2,5-dibromo-3-(diethoxymethyl)thiophene



2,5-dibromo-3-carboxyaldehydethiophene (0.2735g, 1.010 mmol) and PTSA (5.23 mg, 0.0304mmol) were added to a 25 mL two-neck round bottom flask equipped with a stir bar and purged with nitrogen gas three times. Anhydrous ethanol (10 mL) was then added to the reaction mixture and refluxed. After 16 hours, the reaction mixture was cooled to room temperature, then it was poured into diethyl ether and washed with saturated sodium bicarbonate solution 3 times (50 mL each), and dried using sodium sulfate. After evaporation of solvent, the product was a yellow oil. Yield: 0.31g (97%). ^{1}H NMR (300 MHz, $CDCl_3$, δ/ppm): 7.05 (s, 1H), 5.40 (s, 1H), 3.61 – 3.52 (m, 4H), 1.21 (t, 6H).

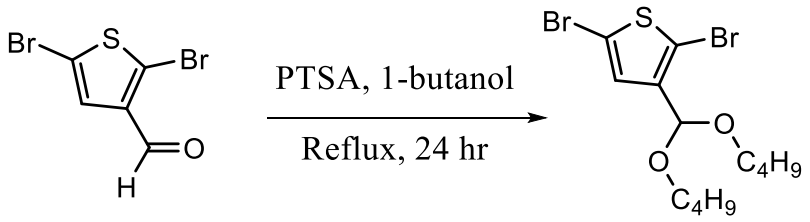
Synthesis of OC21T polymer



C2 monomer (150 mg, 0.4360 mmol, 1.0 equiv.), 2,5-Bis(trimethylstannyl) thiophene (0.1786 mg, 0.4360 mmol, 1.0 equiv.) and P(o-tol)$_3$ (0.0106g, 0.0349 mmol, 0.08 equiv) were added to a 25 mL two-neck round bottom flask along with a stir bar, then the system was purged with argon for 3 *10-minute cycles. Tris(dibenzylideneacetone)dipalladium ($Pd_2(dba)_3$)) (0.0174 mg, 0.0190 mmol, 0.04 equiv.) was measured in a benchtop glovebox under nitrogen and dissolved in 1 mL

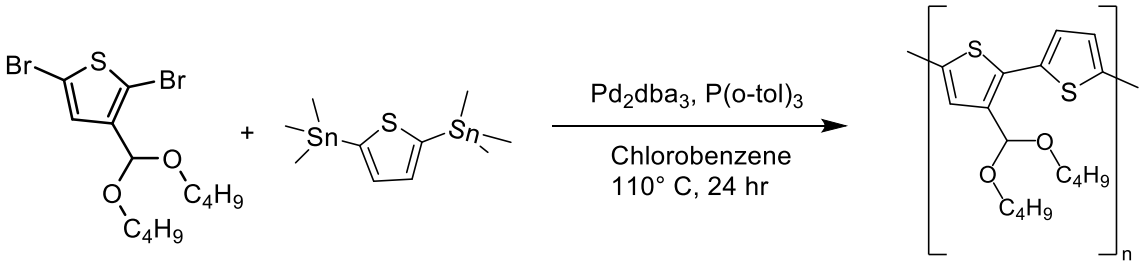
of chlorobenzene, then the catalyst solution was added to the system with a syringe, followed by additional 4 mL of anhydrous chlorobenzene as the solvent. The reaction mixture was heated at 100 °C under argon atmosphere for 24 hours. 0.5 mL of 2-(tributylstannyl) thiophene was added to the solution to stir for 1 hr. Then 0.15 mL of 2 bromothiophene (same molar equiv) was added to the reaction mixture and stirred for another hour to end-cap the polymer. After cooling down to room temperature, the mixture was poured into stirring methanol (150 mL) for 30 mins. The solid was collected by filtration, dried, and further purified by Soxhlet extraction using acetone, hexane, chloroform. (Yield: 82 mg, 71% in chloroform).

Synthesis of 2,5-dibromo-3-(dibutoxymethyl)thiophene



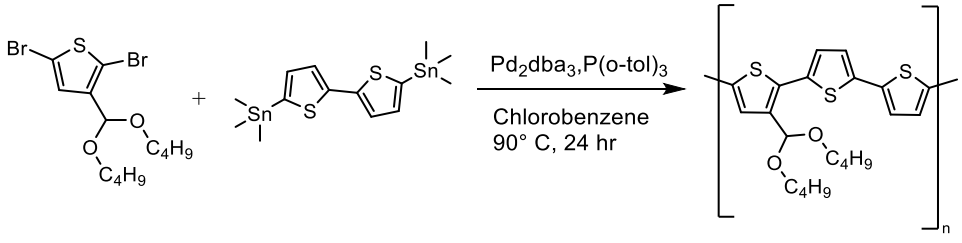
2,5-dibromo-3-carboxyaldehydethiophene (0.3373g, 1.25 mmol) and PTSA (6.5 mg, 0.04mmol) were added to a 25 mL two-neck round bottom flask equipped with a stir bar and purged with nitrogen gas three times. Butanol (10 mL) was then added to the reaction mixture and heated at 110°C. After 24 hours, the reaction mixture was cooled to room temperature, then it was poured into diethyl ether and washed with saturated sodium bicarbonate solution 3 times (50 mL each), and dried using sodium sulfate. After evaporation of solvent, the crude product was purified by column chromatography (silica gel, 12-15% DCM/hexane as the eluent). Yield: 0.42g (84%). ^{1}H NMR (300 MHz, $CDCl_3$, δ/ppm): 7.03 (s, 1H), 5.38 (s, 1H), 3.54 - 3.42 (m, 4H), 1.56 - 1.53 (m, 4H), 1.40 - 1.33 (q, 4H), 0.92 - 0.87 (t, 6H).

Synthesis of OC41T polymer



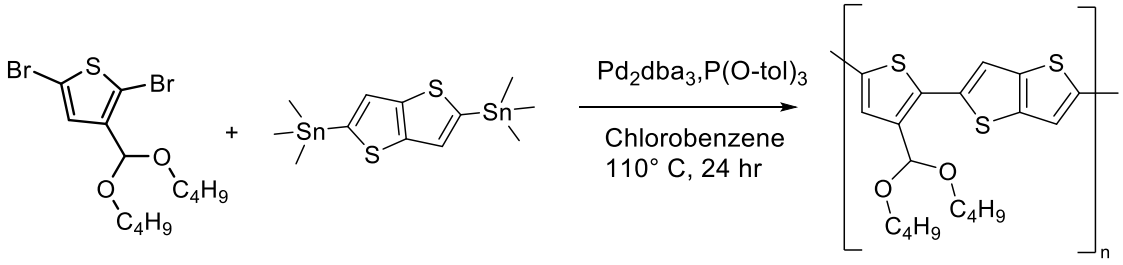
C4 monomer (130 mg, 0.3249 mmol, 1.0 equiv.), 2,5-Bis(trimethylstannyl) thiophene (0.1331 mg, 0.3249 mmol, 1.0 equiv.) and P(o-tol)$_3$ (0.079g, 0.026 mmol, 0.08 equiv.) were added to a 25 mL two-neck round bottom flask along with a stir bar, then the system was purged with argon for 3 *10-minute cycles. Tris(dibenzylideneacetone)dipalladium $Pd_2(dba)_3$ (7.9 mg, 0.013 mmol, 0.04 equiv.) was measured in a benchtop glovebox under nitrogen and dissolved in 1 mL of chlorobenzene, then the catalyst solution was added to the system with a syringe, followed by additional 4 mL of anhydrous chlorobenzene as the solvent. The reaction mixture was heated at 110 °C under argon atmosphere for 24 hours. 0.5 mL of 2-(tributylstannyl) thiophene was added to the solution to stir for 1 hr. Then 0.15 mL of 2 bromothiophene (same molar equiv) was added to the reaction mixture and stirred for another hour to end-cap the polymer. After cooling down to room temperature, the mixture was poured into stirring methanol (150 mL) for 30 mins. The solid was collected by vacuum filtration, dried, and further purified by Soxhlet extraction using acetone, hexane, chloroform. (Yield: 80 mg, 76% in hexane).

Synthesis of OC4BT polymer



C4 monomer (130 mg, 0.3249 mmol, 1.0 equiv.), 5,5'-bis(trimethylstannyl)-2,2'-bithiophene (0.1598 g, 0.3249 mmol, 1.0 equiv.) and $P(o\text{-}tol)_3$ (7.9 mg, 0.026 mmol, 0.08 equiv.) were added to a 25 mL two-neck round bottom flask along with a stir bar, then the system was purged with argon for 3 *10-minute cycles. Tris(dibenzylideneacetone)dipalladium $Pd_2(dba)_3$ (11.9mg, 0.0130 mmol, 0.04 equiv.) was measured in a benchtop glovebox under nitrogen and dissolved in 1 mL of chlorobenzene, then the catalyst solution was added to the system with a syringe, followed by additional 4 mL of anhydrous chlorobenzene as the solvent. The reaction mixture was heated at 90 °C under argon atmosphere for 12 hours, then at 100 °C for another 12 hours. 0.5 mL of 2-(tributylstannyl) thiophene was added to the solution to stir for 1 hr. Then 0.15 mL of 2 bromothiophene (same molar equiv.) was added to the reaction mixture and stirred for another hour to end-cap the polymer. After cooling down to room temperature, the mixture was poured into stirring methanol (150 mL) for 30 mins. The solid was collected by vacuum filtration, dried, and further purified by Soxhlet extraction using acetone, hexane, chloroform. (Yield: 100 mg, 77% in chloroform).

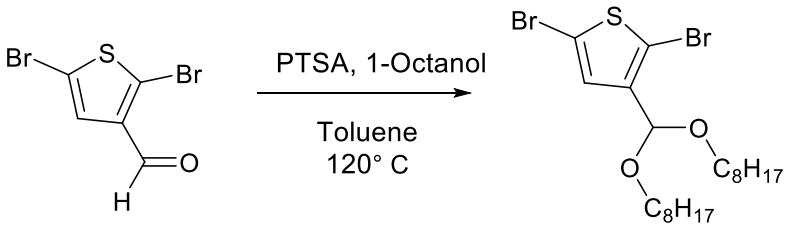
Synthesis of OC4TT polymer



C4 monomer (120 mg, 0.2999 mmol, 1.0 equiv.), 2,5-Bis(trimethylstannyl)-thieno[3,2-b]thiophene (0.1397 mg, 0.2999 mmol, 1.0 equiv.) and $P(o\text{-}tol)_3$ (7.3 mg, 0.024 mmol, 0.08 equiv) were added to a 25 mL two-neck round bottom flask along with a stir bar, then the system

was purged with argon for 3 * 10-minute cycles. Tris(dibenzylideneacetone)dipalladium $Pd_2(dba)_3$ (11.0 mg, 0.0110 mmol, 0.04 equiv.) was measured in a benchtop glovebox under nitrogen and dissolved in 1 mL of chlorobenzene, then the catalyst solution was added to the system with a syringe, followed by additional 4 mL of anhydrous chlorobenzene as the solvent. The reaction mixture was heated at 110 °C under argon atmosphere for 24 hours. 0.5 mL of 2-(tributylstannyl) thiophene was added to the solution to stir for 1 hr. Then 0.15 mL of 2 bromothiophene (same molar equiv.) was added to the reaction mixture and stirred for another hour to end-cap the polymer. After cooling down to room temperature, the mixture was poured into stirring methanol (150 mL) for 30 min. The solid was collected by vacuum filtration, dried, and further purified by Soxhlet extraction using acetone, hexane, chloroform. (Yield: 110 mg, 92% in chloroform).

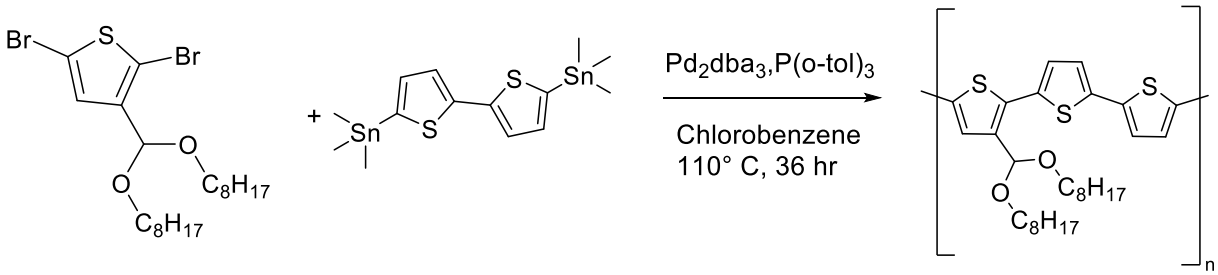
Synthesis of 3-(bis(octyloxy)methyl)-2,5-dibromothiophene



2,5-dibromo-3-carboxyaldehydethiophene (0.7902 g, 2.9746 mmol) and PTSA (0.015g, 0.0878 mmol) were added to a 50 mL two-neck round bottom flask with a stir bar. A Dean-Stark apparatus (10 mL) setup was used. The reaction system was purged of oxygen and carried out under N_2 atmosphere. Anhydrous toluene (25 mL) was added to the reaction mixture as the solvent. Then 1-octanol (0.92 mL, 5.8549 mmol) was added, and the reaction mixture was refluxed for 24 hours. After 24 hours, the reaction mixture was washed with saturated sodium bicarbonate solution 3 times (50 mL each) and the organic layer was dried using sodium sulfate.

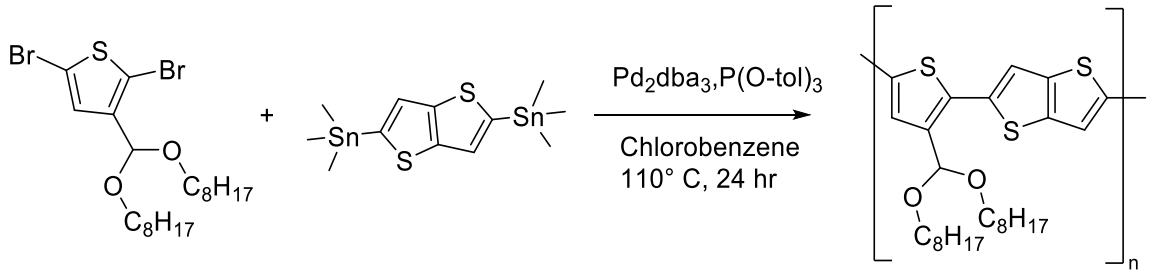
The organic solvent was removed by rotary evaporation. Purification of the crude product was performed by column chromatography using 8-10% DCM/Hexane as the eluent. (Yield: 1.13g 75%). ^{1}H NMR (300 MHz, $CDCl_3$, δ/ppm): 7.03 (s, 1H), 5.38 (s, 1H), 3.54 - 3.41 (m, 4H), 1.59 - 1.52 (m, 4H), 1.34 – 1.25 (m, 20H), 0.88 – 0.84 (t, 6H).

Synthesis of OC8BT polymer



C8 monomer (150 mg, 0.2927 mmol, 1.0 equiv.), 5,5'-bis(trimethylstannyl)-2,2'-bithiophene (144.0 mg, 0.2927 mmol, 1.0 equiv.) and P(o-tol)$_3$ (7.1 mg, 0.016 mmol, 0.08 equiv) were added to a 25 mL two-neck round bottom flask along with a stir bar, then the system was purged with argon for 3 x 10-minute cycles. Tris(dibenzylideneacetone)dipalladium $Pd_2(dba)_3$ (9.4 mg, 0.008 mmol, 0.04 equiv.) was measured in a benchtop glovebox under nitrogen and dissolved in 1 mL of chlorobenzene, then the catalyst solution was added to the system with a syringe, followed by additional 4 mL of anhydrous chlorobenzene as the solvent. The reaction mixture was heated at 110°C under argon atmosphere for 36 hours. 0.5 mL of 2-(tributylstannyl) thiophene was added to the solution to stir for 1 hr. Then 0.15 mL of 2-bromothiophene (same molar equiv.) was added to the reaction mixture and stirred for another hour to end-cap the polymer. After cooling down to room temperature, the mixture was poured into stirring methanol (150 mL) for 30 mins. The solid was collected by vacuum filtration, dried, and further purified by Soxhlet extraction using acetone, hexane, chloroform. (Yield: 130 mg, 87% in hexane).

Synthesis of OC8TT polymer



C8 Monomer (150 mg, 0.2927 mmol, 1.0 equiv.), 2,5-Bis(trimethylstannyl)-thieno[3,2-b]thiophene (0.1364 g, 0.2927 mmol, 1.0 equiv.) and P(o-tol)$_3$ (7.1 mg, 0.016 mmol, 0.08 equiv.) were added to a 25 mL two-neck round bottom flask along with a stir bar, then the system was purged with argon for 3 x 10-minute cycles. Tris(dibenzylideneacetone)dipalladium $Pd_2(dba)_3$ (7.1 mg, 0.008 mmol, 0.04 equiv.) was measured in a benchtop glovebox under nitrogen and dissolved in 1 mL of chlorobenzene, then the catalyst solution was added to the system with a syringe, followed by additional 4 mL of anhydrous chlorobenzene as the solvent. The reaction mixture was heated at 110 °C under argon atmosphere for 24 hours. 0.5 mL of 2-(tributylstannyl) thiophene was added to the solution to stir for 1 hr. Then 0.15 mL of 2 bromothiophene (same molar equiv.) was added to the reaction mixture and stirred for another hour to end-cap the polymer. After cooling down to room temperature, the mixture was poured into stirring methanol (150 mL) for 30 mins. The solid was collected by vacuum filtration, dried, and further purified by Soxhlet extraction using acetone, hexane, chloroform. (Yield: 108 mg, 77% in chloroform).

Chapter 4 OTFT Based Gas Sensor Performances Using OMe1T and OC21T Polymers

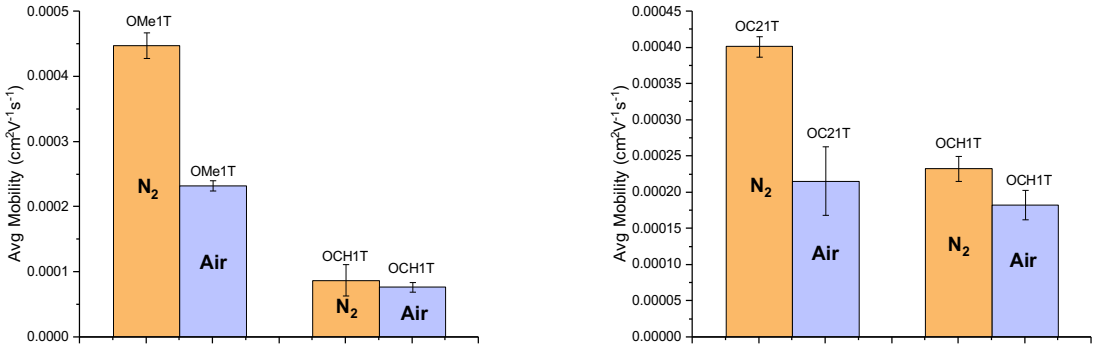
4.1 Introduction

The 1T polymers discussed in the previous chapter demonstrated great potential to be used as gas sensors. An ideal gas sensor should have high sensitivity and selectivity while maintaining good stability. The performance of 1T series of polymers behaving as OTFT based gas sensors will be explored in this chapter. First, the stability of sensor under ambient condition should be evaluated as the moisture in air may affect the device performance or cause device degradation. I-V measurements for OTFT devices should be performed both inside and outside of glovebox for comparison. In addition, a thorough screening of volatile organic compound (VOC) gas exposures will be conducted to evaluate the selectivity of 1T polymers as gas sensor materials. Same sensing tests should be carried out for polymers both before and after acid treatment to prove the need of side chain conversion and generation of nanopores. Moreover, I_{DS} vs. time curves should also be obtained to gain insights regarding the real-time sensing performance.

4.2 Stability of 1T Polymers in Air

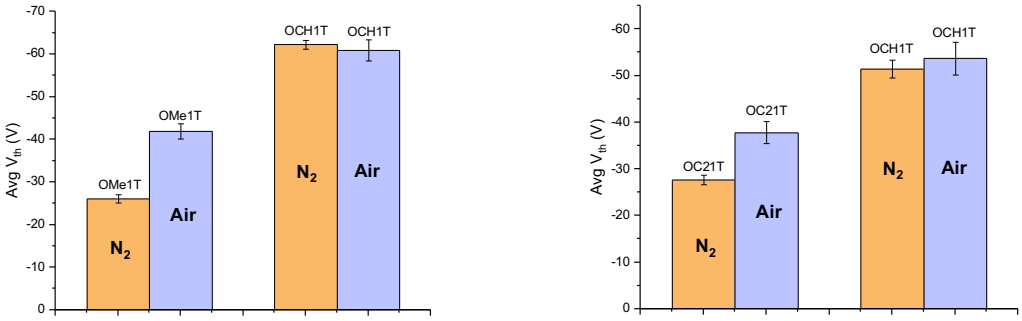
Polymer's stability in air is essential for application as gas sensors. To examine the air stability of the polymers, OTFT performances of 1T polymers were measured both in air and nitrogen glovebox to examine the difference, which are summarized in **Figure 4-1** and **Figure 4-2**. It is shown that without acid removal of side chains, mobilities of both OMe1T and OC21T devices dropped significantly when measured in air with an increase in the absolute values of threshold voltage (shifting away from 0). This might be due to the interaction of acetal side chains with moisture, suggesting that the pristine polymer was not stable in air. However, after acetal was converted to aldehyde, the drop in mobility in air was not as large as observed for the non-acid

treated case. Moreover, the threshold voltage only changed slightly when measured in air for both polymers, suggesting that the polymer was more stable in the aldehyde substituted form, thus can be potentially used as a gas sensor. It is noteworthy that the pores generated by OMe1T should be smaller in size than that from OC21T polymer in theory, but a larger threshold voltage (more negative value) was observed for OMe1T which may be caused by the poor quality or grain boundaries of the polymer film or low molecular weight of the polymer.



a) **b)**

Figure 4-1. Mobilities of OTFT device measured in N_2 glovebox and air for polymers before acid treatment (left) and after acid treatment (right): **a)** OMe1T; **b)** OC21T.



a) b)

Figure 4-2. Threshold voltages of OTFT device measured in N_2 glovebox and air for polymer before acid treatment (left) and after acid treatment (right): **a)** OMe1T; **b)** OC21T.

Table 4-1. OMe1T OTFT performance comparison in glovebox and air.

OMe1T	**Glovebox**		**Air**	
No acid	Avg Mobility ($cm^2V^{-1}s^{-1}$)	4.48E-04 ±1.93E-05	Avg Mobility ($cm^2V^{-1}s^{-1}$)	2.33E-04 ± 7.90E-06
	Avg V_{th} (V)	-26.11 ± 0.95	Avg V_{th} (V)	-41.91 ± 1.78
Acid	Avg Mobility ($cm^2V^{-1}s^{-1}$)	8.75E-05 ± 2.40E-05	Avg Mobility ($cm^2V^{-1}s^{-1}$)	7.71E-05 ±7.60E-06
	Avg V_{th} (V)	-62.25 ± 0.97	Avg V_{th} (V)	-61.00 ± 2.49

Table 4-2. OC21T OTFT performance comparison in glovebox and air.

OC21T	**Glovebox**		**Air**	
No acid	Avg Mobility ($cm^2V^{-1}s^{-1}$)	4.02E-04 ± 1.42E-05	Avg Mobility ($cm^2 V^{-1}s^{-1}$)	2.16E-04 ± 4.73E-05
	Avg V_{th} (V)	-27.73 ± 1.03	Avg V_{th} (V)	-37.87 ± 2.38
Acid	Avg Mobility ($cm^2V^{-1}s^{-1}$)	2.33E-04 ± 1.74E-05	Avg Mobility ($cm^2V^{-1}s^{-1}$)	1.11E-04 ± 2.00E-05
	Avg V_{th} (V)	-51.53 ± 1.91	Avg V_{th} (V)	-53.74 ± 3.48

4.3 OTFT Based Sensing Performances

Various saturated volatile organic compound (VOC) vapors were injected to the OTFT device surface to briefly examine the influence on device performances. The impact of gas interaction with the semiconducting material was evaluated based on three main parameters, which are mobility, V_{th} and $I_{ON/OFF}$. Ideally, the polymer should be sensitive to alcohol vapors with sizes equal to or smaller than the size of nanopores generated by the acid cleavage step. Only the molecule with size that is small enough will be able to fill the vacancies of the OCH1T polymer film and restore the conductive pathway that was interrupted by the loss of the side chains for charge carriers to transport. Therefore, an increase in mobility and decrease in absolute value of threshold voltage should be expected. Methanol, ethanol, and IPA were the three alcohols selected to examine the size exclusion effect. For acid treated OMe1T polymer (OCH1T), it is

ideal to show response upon interaction with methanol gas only; while the aldehyde OCH1T polymer obtained by acid treatment to OC21T is expected to let both ethanol and methanol gas molecules to pass through. IPA should have no impact on the OTFT performance due to its relatively large size compared to the nanopores generated. Other VOCs were also tested to further investigate the selectivity of the aldehyde polymers as gas sensors. It is ideal that other VOCs with sizes larger than the pores cause no change in the OTFT performances.

4.3.1 Gas Injection Method

The same I-V characterization method was carried out as the regular OTFT measurements conducted previously. Saturated gas vapor was prepared using the method indicated in **Section 2.5.** Three injections of gas vapor (5mL each time) to the device surface were performed during the I-V scanning process to ensure that the device was operating under an atmosphere containing the analyte gas. Injection was performed about 1 cm above the active channel area every 5 s for 3 times in total. Common volatile solvents including acetone, DCM, hexane, and diethyl ether with various polarities and sizes were tested to examine the selectivity.

4.3.2 Results and Discussion

Results revealed that acetone, DCM, hexane, and diethyl ether all had no effect on OCH1T based OTFT devices (through acid treatment to both OMe1T and OC21T). OCH1T converted from OC21T demonstrated expected results regarding the injection of alcohol gases. Methanol and ethanol gases brought back the device mobility slightly with a decrease in threshold voltage (closer to 0). However, the aldehyde polymer converted from OMe1T showed response to all types of alcohol. This might be related to the intrinsic large threshold voltage of the device that

was potentially caused by the poor quality of film, which was observed during the previous air stability test as well. The grain boundaries of the OMe1T polymer thin film might be large enough for IPA and ethanol gas molecules to pass through. As a result, only the OC21T polymer is suitable to be used as OTFT based gas sensors. All the OTFT performances related to the gas injection to the OCH1T polymers (from acid cleavage of both OMe1T and OC21T) are summarized in ***Table 4-3*** and ***Table 4-4.*** Further investigation regarding the sensing performance of OC21T specifically will be discussed in the next subsection with a focus on the immediate current change as a response with respect to the gas injection.

Table 4-3. OTFT Summary for OCH1T polymer (converted from OMe1T) with injection of various gases.

Original polymer	Polymer	Vapor	Avg Mobility ($cm^2V^{-1}s^{-1}$)	Avg V_{th} (V)	$I_{on/off}$
OMe1T	OCH1T	None	8.63E-05	-55.66	1000
OMe1T	OCH1T	Hexane	8.17E-05 ± 7.31E-07	-59.77 ± 3.46	1000
OMe1T	OCH1T	Acetone	6.09E-05 ± 6.17E-06	-55.03 ± 3.66	1000
OMe1T	OCH1T	DCM	7.88E-05 ± 1.29E-05	-62.02 ± 2.57	1000
OMe1T	OCH1T	***IPA***	***9.92E-05 ±5.39E-06***	***-39.21 ± 10.56***	***1000***
OMe1T	OCH1T	***Methanol***	***8.61E-05 ± 8.68E-06***	***-38.75 ± 5.25***	***100***
OMe1T	OCH1T	***Ethanol***	***1.02E-04 ± 9.55E-06***	***-37.88 ± 10.27***	***100***

Table 4-4. OTFT Summary of OCH1T polymer (converted from OC21T) with injection of various gases.

Original polymer	Polymer	Vapor	Avg Mobility ($cm^2V^{-1}s^{-1}$)	Avg V_{th} (V)	$I_{on/off}$
OC21T	OCH1T	None	8.04E-05	-58.01	1000
OC21T	OCH1T	Hexane	7.68E-05 ± 2.90E-06	-56.91 ± 2.34	1000
OC21T	OCH1T	Ether	6.43E-05 ± 3.07E-06	-58.45 ± 0.27	1000
OC21T	OCH1T	Acetone	5.91E-05 ± 7.49E-06	-61.08 ±1.09	1000
OC21T	OCH1T	DCM	6.97E-05 ± 2.75E-06	-62.65 ± 1.05	1000
OC21T	OCH1T	IPA	7.36E-05 ± 2.23E-06	-60.41 ± 1.17	1000
OC21T	OCH1T	***Methanol***	***8.90E-05 ± 7.43E-06***	***-47.55 ± 6.21***	***100***
OC21T	OCH1T	***Ethanol***	***9.22E-05 ± 8.30E-06***	***-48.98 ± 6.96***	***100***

4.4 Real Time Sensing of OC21T Polymer Pair

To gain a better understanding of the polymer's sensing performance, the current change of the pristine OC21T and the corresponding OCH1T polymer upon gas injection should be investigated. Responses of polymers both before and after acid cleavage were tested to confirm the necessity of side chain removal for sensor application and to serve as supporting evidence for the successful formation of the porous structure. The pore sizes of the proposed structure should be the same as the size of ethanol molecules, with only 4.4 Angstroms (0.44 nm) in diameter, which is hard to be detected using SEM or TEM. The current change responding to various concentrations of analyte exposure were studied to evaluate the sensitivity of the polymer device.

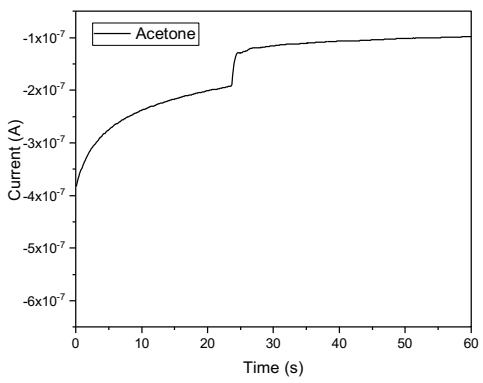
4.4.1 Sensing Method

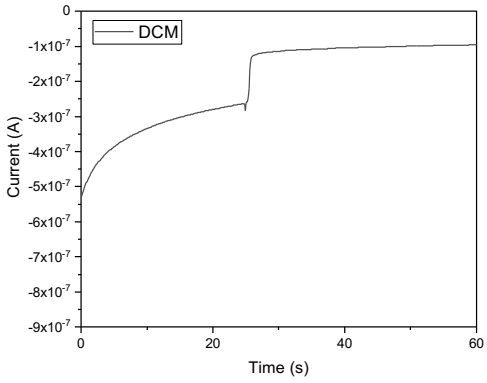
Saturated solvent vapors of acetone, DCM, EA, diethyl ether, hexane and toluene were prepared using the method outlined in **Section 2.5**. 5 mL of vapor was injected directly above the channel area of OTFT devices to observe the current change and examine the gas selectivity. For alcohol vapors, various concentrations of gases were prepared by the volume percentage dilution method as described in **Section 2.5**. Five replicates were conducted for each gas concentration to ensure the reproducibility and reliability of the results.

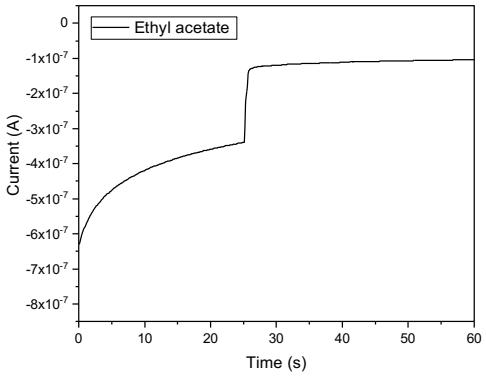
4.4.2 OC21T Polymer Sensitivity (Before Acid Treatment)

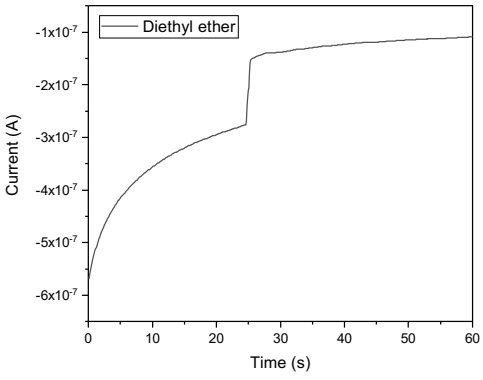
OTFT based sensor performance of the pristine acetal polymer was investigated first. It is known that DCM and toluene can dissolve the acetal polymer, therefore a change in current could be expected. However, for all the remaining solvents, the polymer had no solubility in them. But results revealed that vapor exposure still leads to significant change in current, indicating that the

pristine acetal polymer has no selectivity towards different gases. Combined with the air stability results outlined in **Section 4.2**, it is essential to convert the acetal polymer to the aldehyde form even though removal of acetal side chains may lead to a decrease in mobility and increase in threshold voltage. In addition, OC21T exhibited responses to all three alcohols (methanol, ethanol, and IPA) as well. Exposure of OC21T based sensor device to all the listed gases caused a decrease in current, making it unsuitable to be used as a sensor material directly. The gas sensing profiles of OC21T are listed below:









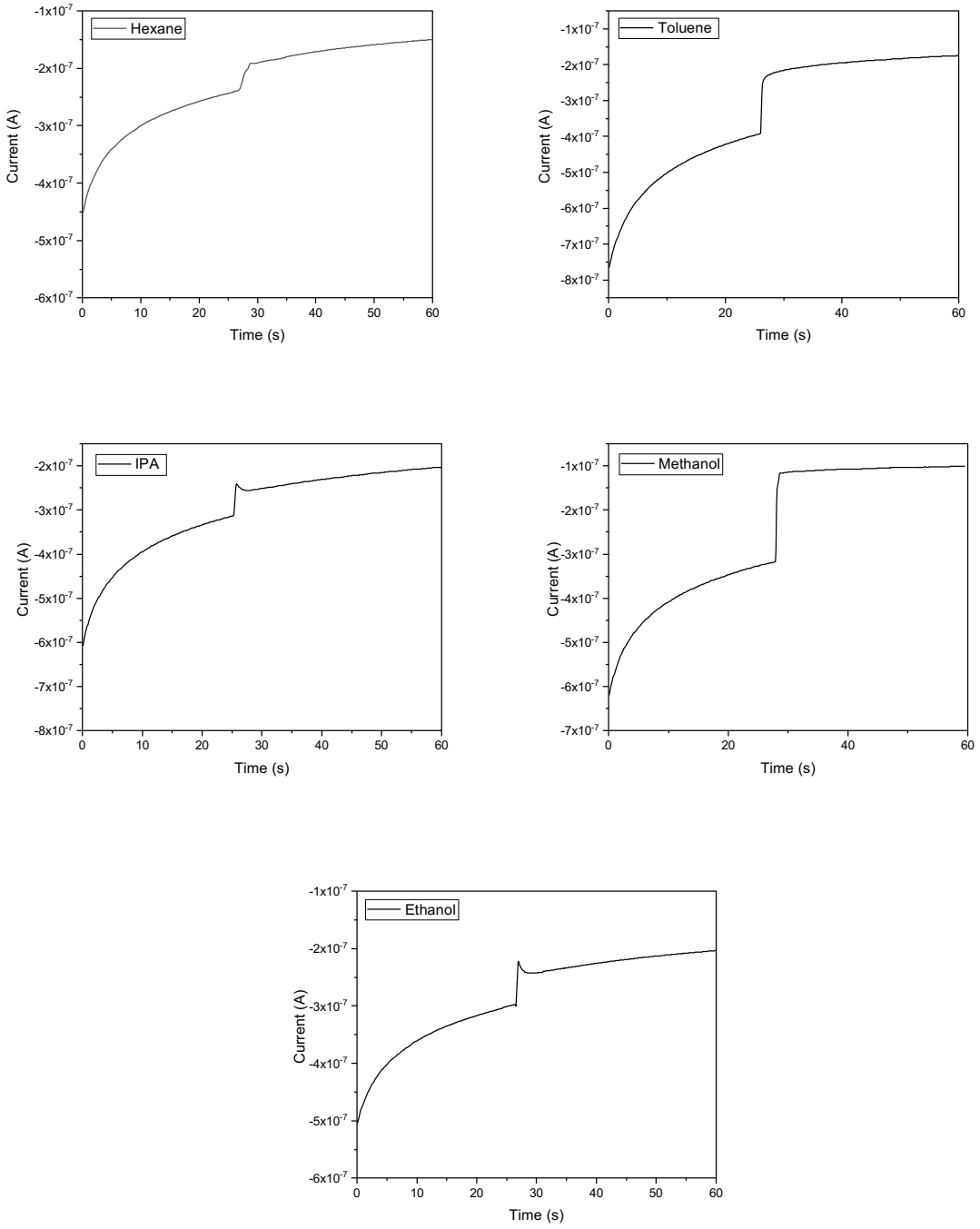


Figure 4-3. Gas sensing profiles of OC21T based OTFT sensor being exposed to various gas vapors.

4.4.3 OCH1T based OTFT Sensor Performance

4.4.3.1 Alcohol Vapor Sensing

Based on the results shown in **Section 4.3**, it is known that OCH1T was sensitive to methanol, ethanol, and IPA (slightly). Therefore, the responses to different concentrations of target analyte vapors should be examined. 20%, 40%, 60%, 80% and 100% of saturated alcohol vapors were prepared following the method described in **Section 2.5**. For methanol and ethanol, an obvious increase in current was observed in the I_{DS} vs. T profile as the analyte concentration went higher. But for IPA, there was no obvious positive correlation between the concentration of vapor and the current change as observed for methanol and ethanol gases. Based on the pore size theory proposed, IPA molecules are larger than the film vacancies created by the acid treatment process, therefore they are unable to enter the nanopores to influence the OTFT device performance. The slight response might be mainly attributed to the intrinsic grain boundaries of the polymer film that allows for molecules to enter. The change in current is the parameter used to evaluate the response level. The relative response is calculated as follows:

$$Relative\ response\ ratio = \frac{(I - I_0)}{I_0}$$

Where I represents the largest current reached after gas introduction, and I_0 is the current right before gas was injected. The summary of relative responses of OCH1T polymer to methanol, ethanol and IPA with various concentrations is shown in **Figure 4-4**. Moreover, the sensitivity of the device can be calculated by dividing the relative response by the concentration of the analytes, which is summarized in **Figure 4-5**.

For all three alcohols tested, increase in current (more negative I_{DS} value) was observed upon each alcohol vapor injection regardless of the concentration. This is opposite to what has been

observed for the pristine acetal form of polymer. The increase in current implies that better charge carrier transport could be achieved due to the introduction of alcohol molecules that fill up the gaps within the active channel. Moreover, the response time is very short as a sharp peak was shown in the I_{DS} vs. T curve with a fast recovery time. It is observed that for ethanol and methanol vapors, after passing a certain point of concentration threshold, the relative response increased almost linearly with the analyte concentration. For methanol gases, when concentration is above 0.00353 mol/L or 113 mg/L, relative response increases linearly with the increased concentration. The sensitivity was calculated to be around 4.6% when the concentration is larger than 113 mg/L. The turning point for ethanol, where the relative response begins to be linearly proportional to concentration, is 73.98 mg/L (0.00161 mol/L), with the highest sensitivity reaching 5.8%. But for IPA, the sensitivity is much lower than that of ethanol and methanol with a value of 0.4% only. The relative response of IPA for all concentrations is shown to be around the same as the portion of ethanol and methanol when the threshold concentration was not reached. This might also suggest the presence of grain boundaries, and interaction of IPA stimuli with polymer film might happen mainly at these defects which are larger than the size of pores created. The higher sensitivity towards methanol and ethanol gases further proved the formation of nano pores with desired size.

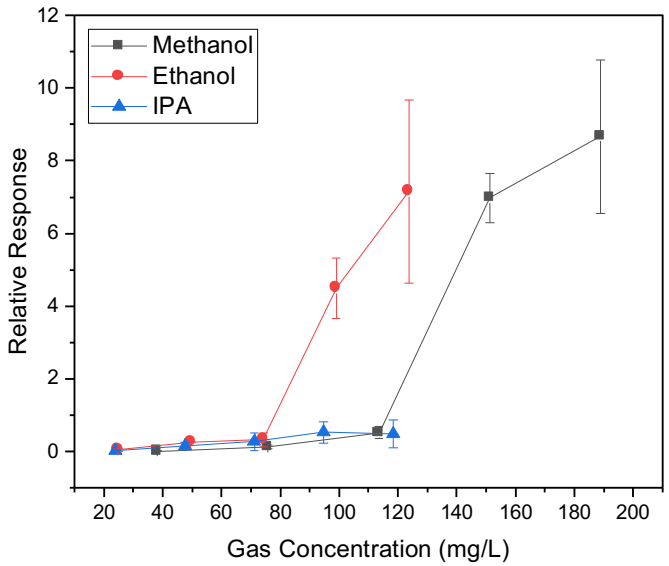


Figure 4-4. Relative response ratio summary of OCH1T based OTFT device (from OC21T polymer) towards methanol, ethanol, and IPA gases with different concentrations.

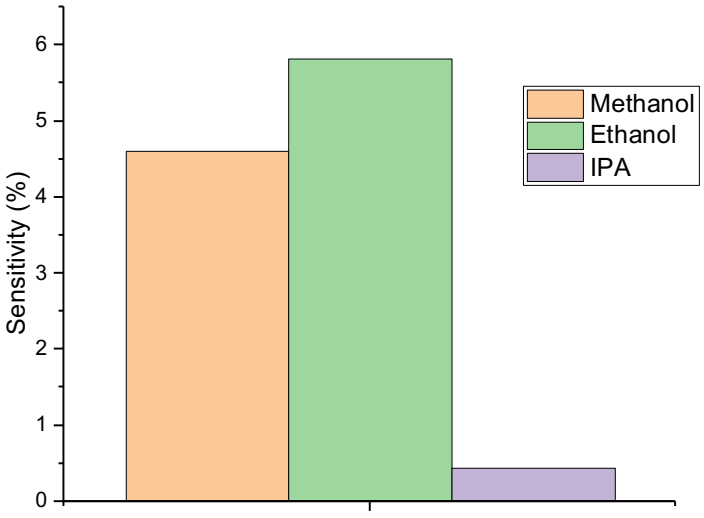


Figure 4-5. Sensitivity summary for OCH1T (from OC21T polymer) based OTFT device upon exposure to methanol, ethanol and IPA gases.

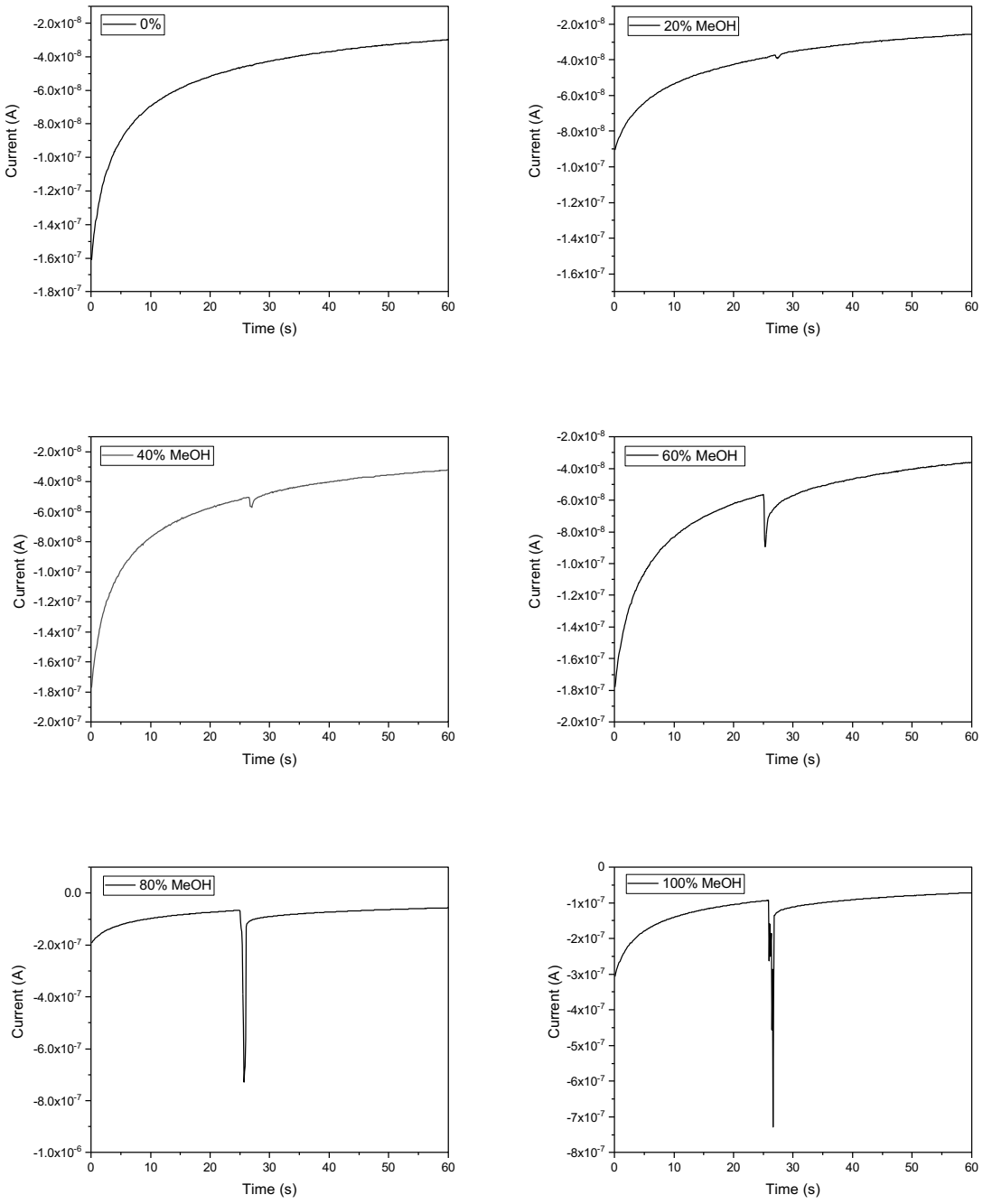


Figure 4-6. I_{DS} vs. time measurment of OCH1T polymer being exposed to various concentrations of methanol vapors.

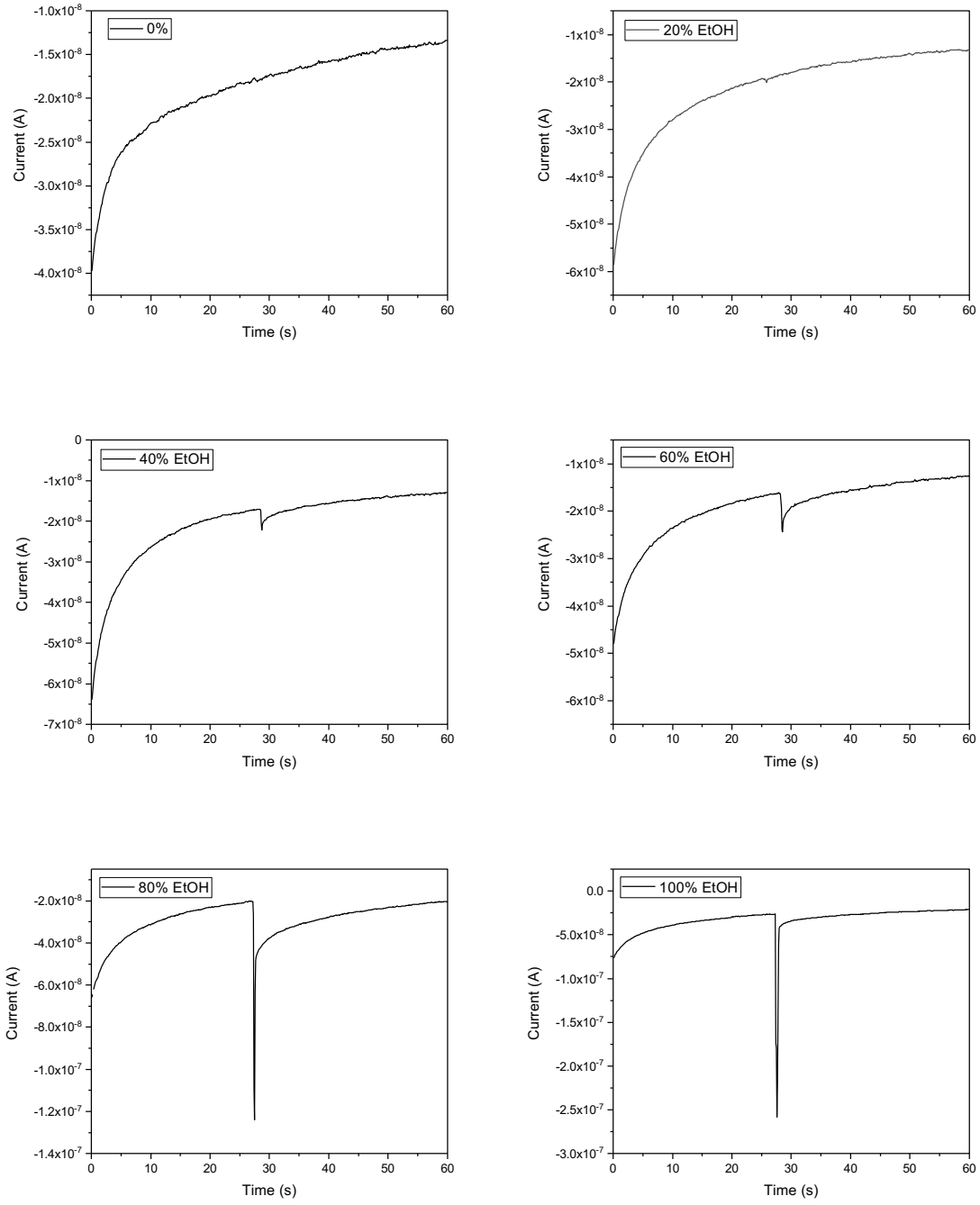


Figure 4-7. I_{DS} vs. time measurment of OCH1T polymer being exposed to various concentrations of ethanol vapors.

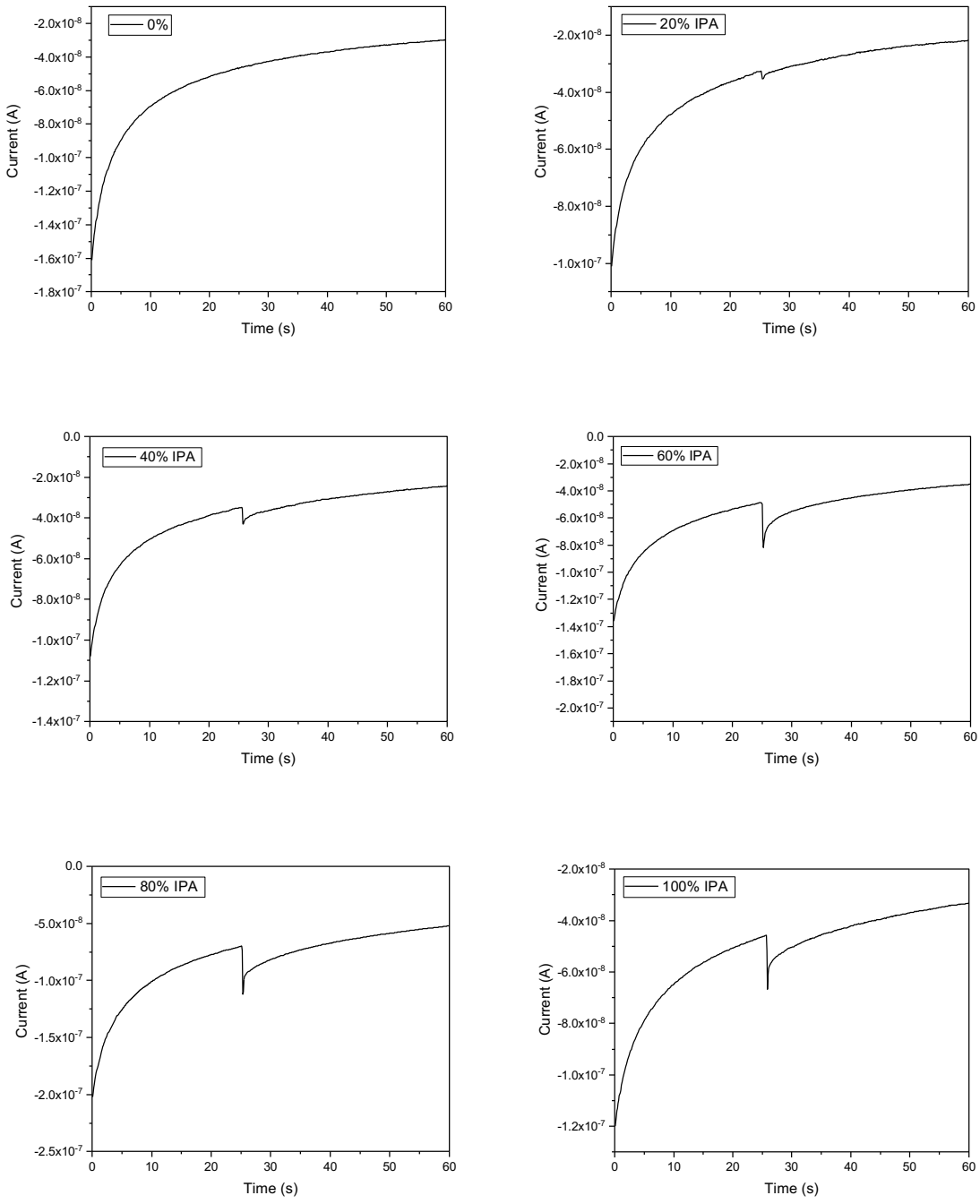


Figure 4-8. I_{DS} vs. time measurment of OCH1T polymer being exposed to various concentrations of ispropanol vapors.

4.4.3.2 Other Solvent Sensing

I_{DS} vs. time measurements of other volatile solvent vapors being injected to the device surface were also performed to further evaluate the selectivity of the polymer device. Based on **Figure 4-9,** no change in current was observed when the solvent vapor was applied to the surface of the OTFT device, indicating that the polymer sensor is inert to DCM, ethyl acetate, diethyl ether, hexane, and toluene. Compared to its acetal counterpart, which gives response to all solvent vapors, the aldehyde polymer exhibited sensitivity towards desired alcohol gases only with great selectivity. This result also proves the need to remove the acetal side chains for sensor applications. Despite the sacrifice in OTFT performances including mobilities and threshold voltages associated with the cleavage of side chains, the relative change in OTFT performances upon analyte exposure is of greater interest. High mobilities might not be useful for sensor applications as the relative change in signal might be hard to observe.

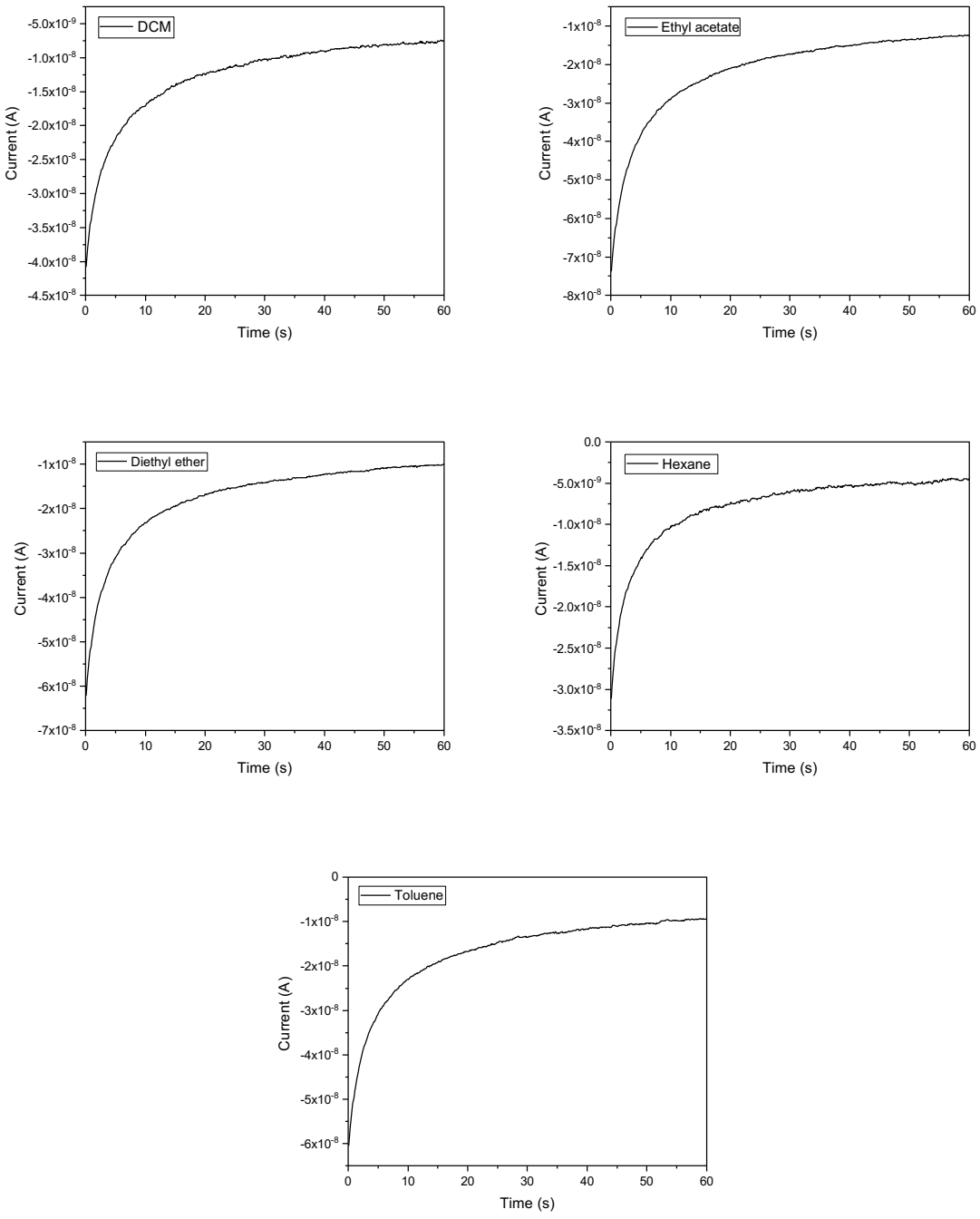


Figure 4-9. Real-time gas sensing profiles of OCH1T based OTFT sensor being exposed to various gas vapors.

4.5 Conclusions

In this chapter, the potential of OCH1T polymer to work as an OTFT based gas sensor was explored and evaluated. Even though acid treatment to both OMe1T and OC21T polymers can lead to formation of OCH1T film with the same chemical structure, the quality and molecular chain packing of film obtained still vary with different interchain spaces. Therefore, selection of the pristine polymer subjected for acid treatment became crucial. The air stability of OCH1T obtained from both acetal polymers was studied by comparing the mobility and threshold voltage change when measured in glovebox and in air. Results showed that the threshold voltage of OMe1T shifted to a more negative threshold voltage value when measured in air, indicating that the interface of semiconducting film and dielectric layer might be interrupted due to the poor quality of polymer film or low polymer molecular weight thus making the device more vulnerable to the presence of moisture in air. The OCH1T polymer obtained by acid treatment to OC21T polymer exhibited better mobility and threshold voltage with relatively smaller changes when measured in air.

The smaller OTFT device was firstly used for screening of VOC gases that may lead to a change in the OTFT performances. Based on the results, it is shown that the interaction of alcohol gases with the device would lead to a slight increase in mobility and cause the V_{th} to shift to the direction closer to 0. Both signs suggest that improved OTFT performance and charger carrier transport could be expected due to the exposure to alcohol gases. OC21T was chosen for further OTFT sensing measurements. I_{DS} vs. time measurement was then carried out for detailed study related to the selectivity and sensitivity of the polymer device. Results showed that before acid treatment, the pristine acetal polymer based OTFT device could be affected by all the gases tested (including DCM, acetone, diethyl ether, hexane, toluene, IPA, ethanol, and methanol) with

decrease in current upon all gas exposures. Meanwhile, after the acetal side chain was converted to the corresponding aldehyde group, no change in current was observed for injection of common solvent vapors, and only alcohol gases caused increase in I_{DS} of the device. Furthermore, an increase in relative response was observed as the concentration of the ethanol and methanol gases went higher. The device showed some sensitivity towards IPA, but the sensitivity was much lower compared to that of the other two alcohols, which may be caused by the grain boundaries of polymer or intrinsic defects. In addition, the relative response is considerably constant regardless of the concentration of IPA gases applied, which further proves that the signal change may not be due to the interaction at porous sites generated within the structure. Instead, the IPA stimuli interacted primarily with the defects or grain boundaries in the polymer film as they couldn't pass the nanopores created.

Chapter 5 Conclusions and Future Steps

5.1 Conclusions

This thesis focused on the design of porous semiconducting polymers for potential use in size-selective OTFT-based gas sensors for alcohol vapor detection. Different polymer backbones with various comonomer units have been explored to find the most appropriate candidate. The porous structure was achieved through a simple acid treatment process, resulting in a robust aldehyde substituted thiophene based polymer with excellent solvent resistance and considerable air stability.

In chapter 3, a series of acetal substituted thiophene monomers with various chain lengths were synthesized, and copolymerized with bithiophene, thienothiophene or one-thiophene unit. The obtained polymers were characterized using CV, UV-Vis, GPC, TGA, AFM, XRD and FTIR. Easy and effective conversion of these acetal substituted thiophene polymers to aldehyde substituted thiophene polymers was achieved through acid cleavage of side chains by HCl vapor. Successful and complete conversion was confirmed by UV-Vis, CV, FTIR and XRD. OTFT performances using both acetal and aldehyde forms of polymer were measured as well. For bithiophene and thienothiophene series of polymers, acetals with C4 and C8 lengths were employed to render polymers with good solubility. The mobilities dropped drastically as an outcome of the acid treatment process, with larger absolute values of threshold voltages observed as well. This negative impact on the OTFT performance could be explained by the large percentage of weight loss associated with the acid treatment step. As a result, one-thiophene series of polymers were designed to potentially resolve this issue. Smaller relative OTFT performance drop was observed for OMe1T and OC21T polymers, which were selected as the

candidates for further gas sensing measurements. In chapter 4, the ability of OCH1T polymers (converted from OMe1T and OC21T polymers) for application as OTFT based gas sensors were evaluated. Due to the significant influence of moisture on OMe1T polymer and its poor selectivity caused by film quality issues, the polymer selection was narrowed down to OC21T. I_{DS} vs. time measurement was conducted to examine the selectivity and sensitivity. OCH1T polymer (after acid-treatment to OC21T polymer) showed selectivity toward ethanol and methanol only, which proved the formation of pores with desired sizes. Even though slight sensitivity of polymer to IPA vapors was also observed, the relative response level was much lower than that of ethanol and methanol. This is likely due to the grain boundaries in the polymer film being large enough for IPA molecules to enter.

5.2 Future Steps

Future work can focus on the following aspects:

1. The same concentration of different alcohol gases could be prepared to investigate their impact on current changes, allowing for direct comparison. In other words, equal concentration of alcohol gases could be used rather than the same volume percentage.
2. Gas sensing tests for aldehyde substituted thiophene polymers obtained from other acetal polymers with different chain lengths should be performed to further validate pore formation and size tunability.
3. The polymer film quality should be improved by optimizing either the polymer synthesis conditions or the fabrication process.
4. The impact of film thickness on device sensitivity could be investigated.
5. High-resolution imaging techniques could be explored to visualize pore formation.
6. Long term stability of devices in air can be monitored over time.

References

(1) Jayendran, A.; Jayendran, R. Conductors, Insulators and Semiconductors. In *Englisch für Elektroniker: Ein Lehr- und Übungsbuch für das technische Englisch*; Jayendran, A., Jayendran, R., Eds.; Vieweg+Teubner Verlag: Wiesbaden, 1996; pp 1–7. https://doi.org/10.1007/978-3-322-84907-6_1.

(2) Brütting, W. Introduction to the Physics of Organic Semiconductors. In *Physics of Organic Semiconductors*; John Wiley & Sons, Ltd, 2005; pp 1–14. https://doi.org/10.1002/3527606637.ch.

(3) Singh, Y. *Semiconductor Devices*; I. K. International Pvt Ltd, 2013.

(4) Bronstein, H.; Nielsen, C. B.; Schroeder, B. C.; McCulloch, I. The Role of Chemical Design in the Performance of Organic Semiconductors. *Nat. Rev. Chem.* **2020**, *4* (2), 66–77. https://doi.org/10.1038/s41570-019-0152-9.

(5) Morab, S.; Sundaram, M. M.; Pivrikas, A. Review on Charge Carrier Transport in Inorganic and Organic Semiconductors. *Coatings* **2023**, *13* (9), 1657. https://doi.org/10.3390/coatings13091657.

(6) Tilli, M.; Haapalinna, A. Chapter 1 - Properties of Silicon. In *Handbook of Silicon Based MEMS Materials and Technologies (Second Edition)*; Tilli, M., Motooka, T., Airaksinen, V.-M., Franssila, S., Paulasto-Kröckel, M., Lindroos, V., Eds.; Micro and Nano Technologies; William Andrew Publishing: Boston, 2015; pp 3–17. https://doi.org/10.1016/B978-0-323-29965-7.00001-4.

(7) Pisula, W. Inorganic Semiconductors in Electronic Applications. *Electron. Mater.* **2023**, *4* (3), 136–138. https://doi.org/10.3390/electronicmat4030011.

(8) Vidor, F. F.; Meyers, T.; Hilleringmann, U. Flexible Electronics: Integration Processes for Organic and Inorganic Semiconductor-Based Thin-Film Transistors. *Electronics* **2015**, *4* (3), 480–506. https://doi.org/10.3390/electronics4030480.

(9) Le, T.-H.; Kim, Y.; Yoon, H. Electrical and Electrochemical Properties of Conducting Polymers. *Polymers* **2017**, *9* (4), 150. https://doi.org/10.3390/polym9040150.

(10) Yan, Y.; Zhao, Y.; Liu, Y. Recent Progress in Organic Field-Effect Transistor-Based Integrated Circuits. *J. Polym. Sci.* **2022**, *60* (3), 311–327. https://doi.org/10.1002/pol.20210457.

(11) King, B.; Lessard, B. H. Review of Recent Advances and Sensing Mechanisms in Solid-State Organic Thin-Film Transistor (OTFT) Sensors. *J. Mater. Chem. C* **2024**, *12* (16), 5654–5683. https://doi.org/10.1039/D3TC03611A.

(12) Zou, S.-J.; Shen, Y.; Xie, F.-M.; Chen, J.-D.; Li, Y.-Q.; Tang, J.-X. Recent Advances in Organic Light-Emitting Diodes: Toward Smart Lighting and Displays. *Mater. Chem. Front.* **2020**, *4* (3), 788–820. https://doi.org/10.1039/C9QM00716D.

(13) Yi, J.; Zhang, G.; Yu, H.; Yan, H. Advantages, Challenges and Molecular Design of Different Material Types Used in Organic Solar Cells. *Nat. Rev. Mater.* **2024**, *9* (1), 46–62. https://doi.org/10.1038/s41578-023-00618-1.

(14) Horowitz, G. Organic Field-Effect Transistors. *Adv. Mater.* **1998**, *10* (5), 365–377. https://doi.org/10.1002/(SICI)1521-4095(199803)10:5<365::AID-ADMA365>3.0.CO;2-U.

(15) Li, Y.; Huang, W.; Zhao, D.; Wang, L.; Jiao, Z.; Huang, Q.; Wang, P.; Sun, M.; Yuan, G. Recent Progress in Organic Solar Cells: A Review on Materials from Acceptor to Donor. *Molecules* **2022**, *27* (6), 1800. https://doi.org/10.3390/molecules27061800.

(16) Ates, M. A Review Study of (Bio)Sensor Systems Based on Conducting Polymers. *Mater. Sci. Eng. C* **2013**, *33* (4), 1853–1859. https://doi.org/10.1016/j.msec.2013.01.035.

(17) Forrest, S. R.; Thompson, M. E. Introduction: Organic Electronics and Optoelectronics. *Chem. Rev.* **2007**, *107* (4), 923–925. https://doi.org/10.1021/cr0501590.
(18) Zhao, X.; Zhan, X. Electron Transporting Semiconducting Polymers in Organic Electronics. *Chem. Soc. Rev.* **2011**, *40* (7), 3728–3743. https://doi.org/10.1039/C0CS00194E.
(19) Shaw, J. M.; Seidler, P. F. Organic Electronics: Introduction. *IBM J. Res. Dev.* **2001**, *45* (1), 3–9. https://doi.org/10.1147/rd.451.0003.
(20) Chason, M.; Brazis, P. W.; Zhang, J.; Kalyanasundaram, K.; Gamota, D. R. Printed Organic Semiconducting Devices. *Proc. IEEE* **2005**, *93* (7), 1348–1356. https://doi.org/10.1109/JPROC.2005.850306.
(21) Bracciale, M. P.; Kim, C.; Marrocchi, A. Organic Electronics: An Overview of Key Materials, Processes, and Devices. In *Sustainable Strategies in Organic Electronics*; Marrocchi, A., Ed.; Woodhead Publishing Series in Electronic and Optical Materials; Woodhead Publishing, 2022; pp 3–71. https://doi.org/10.1016/B978-0-12-823147-0.00001-X.
(22) Luo, N.; Ren, P.; Feng, Y.; Shao, X.; Zhang, H.-L.; Liu, Z. Side-Chain Engineering of Conjugated Polymers for High-Performance Organic Field-Effect Transistors. *J. Phys. Chem. Lett.* **2022**, *13* (4), 1131–1146. https://doi.org/10.1021/acs.jpclett.1c03909.
(23) Shirakawa, H.; Louis, E. J.; MacDiarmid, A. G.; Chiang, C. K.; Heeger, A. J. Synthesis of Electrically Conducting Organic Polymers: Halogen Derivatives of Polyacetylene, (CH)x. *J. Chem. Soc. Chem. Commun.* **1977**, No. 16, 578–580. https://doi.org/10.1039/C39770000578.
(24) Ravichandran, R.; Sundarrajan, S.; Venugopal, J. R.; Mukherjee, S.; Ramakrishna, S. Applications of Conducting Polymers and Their Issues in Biomedical Engineering. *J. R. Soc. Interface* **2010**, *7* (suppl_5), S559–S579. https://doi.org/10.1098/rsif.2010.0120.focus.
(25) Singh, N.; Riaz, U. Recent Trends on Synthetic Approaches and Application Studies of Conducting Polymers and Copolymers: A Review. *Polym. Bull.* **2022**, *79* (12), 10377–10408. https://doi.org/10.1007/s00289-021-03987-1.
(26) Shahabuddin, S.; Mazlan, N. A.; Baharin, S. N. A.; Sambasevam, K. P. Introduction to Conducting Polymers. In *Advances in Hybrid Conducting Polymer Technology*; Shahabuddin, S., Pandey, A. K., Khalid, M., Jagadish, P., Eds.; Springer International Publishing: Cham, 2021; pp 1–18. https://doi.org/10.1007/978-3-030-62090-5_1.
(27) Bajpai, M.; Srivastava, R.; Dhar, R.; Tiwari, R. S. Review on Optical and Electrical Properties of Conducting Polymers. *Indian J. Mater. Sci.* **2016**, *2016* (1), 5842763. https://doi.org/10.1155/2016/5842763.
(28) Dimitrakopoulos, C. d.; Malenfant, P. r. l. Organic Thin Film Transistors for Large Area Electronics. *Adv. Mater.* **2002**, *14* (2), 99–117. https://doi.org/10.1002/1521-4095(20020116)14:2<99::AID-ADMA99>3.0.CO;2-9.
(29) Koezuka, H.; Tsumura, A.; Ando, T. Field-Effect Transistor with Polythiophene Thin Film. *Synth. Met.* **1987**, *18* (1), 699–704. https://doi.org/10.1016/0379-6779(87)90964-7.
(30) Reese, C.; Roberts, M.; Ling, M.; Bao, Z. Organic Thin Film Transistors. *Mater. Today* **2004**, *7* (9), 20–27. https://doi.org/10.1016/S1369-7021(04)00398-0.
(31) Klauk, H. Organic Thin-Film Transistors. *Chem. Soc. Rev.* **2010**, *39* (7), 2643–2666. https://doi.org/10.1039/B909902F.
(32) Zhang, C.; Chen, P.; Hu, W. Organic Field-Effect Transistor-Based Gas Sensors. *Chem. Soc. Rev.* **2015**, *44* (8), 2087–2107. https://doi.org/10.1039/C4CS00326H.

(33) Guo, Y.; Yu, G.; Liu, Y. Functional Organic Field-Effect Transistors. *Adv. Mater.* **2010**, *22* (40), 4427–4447. https://doi.org/10.1002/adma.201000740.
(34) Katz, H. E.; Bao, Z. The Physical Chemistry of Organic Field-Effect Transistors. *J. Phys. Chem. B* **2000**, *104* (4), 671–678. https://doi.org/10.1021/jp992853n.
(35) Valizadeh, P. *Field Effect Transistors, A Comprehensive Overview: From Basic Concepts to Novel Technologies*; John Wiley & Sons, 2016.
(36) Cavallari, M. R.; Pastrana, L. M.; Sosa, C. D. F.; Marquina, A. M. R.; Izquierdo, J. E. E.; Fonseca, F. J.; Amorim, C. A. de; Paterno, L. G.; Kymissis, I. Organic Thin-Film Transistors as Gas Sensors: A Review. *Materials* **2021**, *14* (1), 3. https://doi.org/10.3390/ma14010003.
(37) Chandar Shekar, B.; Lee, J.; Rhee, S.-W. Organic Thin Film Transistors: Materials, Processes and Devices. *Korean J. Chem. Eng.* **2004**, *21* (1), 267–285. https://doi.org/10.1007/BF02705409.
(38) Horowitz, G.; Lang, P.; Mottaghi, M.; Aubin, H. Extracting Parameters from the Current–Voltage Characteristics of Organic Field-Effect Transistors. *Adv. Funct. Mater.* **2004**, *14* (11), 1069–1074. https://doi.org/10.1002/adfm.200305122.
(39) Li, S.; Tang, W.; Chen, S.; Si, Y.; Liu, R.; Guo, X. Flexible Organic Polymer Gas Sensor and System Integration for Smart Packaging. *Adv. Sens. Res.* **2023**, *2* (11), 2300030. https://doi.org/10.1002/adsr.202300030.
(40) Lin, P.; Yan, F. Organic Thin-Film Transistors for Chemical and Biological Sensing. *Adv. Mater.* **2012**, *24* (1), 34–51. https://doi.org/10.1002/adma.201103334.
(41) Pang, C.; Lee, C.; Suh, K.-Y. Recent Advances in Flexible Sensors for Wearable and Implantable Devices. *J. Appl. Polym. Sci.* **2013**, *130* (3), 1429–1441. https://doi.org/10.1002/app.39461.
(42) Crone, B.; Dodabalapur, A.; Gelperin, A.; Torsi, L.; Katz, H. E.; Lovinger, A. J.; Bao, Z. Electronic Sensing of Vapors with Organic Transistors. *Appl. Phys. Lett.* **2001**, *78* (15), 2229–2231. https://doi.org/10.1063/1.1360785.
(43) Gold, H.; Haase, A.; Fian, A.; Prietl, C.; Striedinger, B.; Zanella, F.; Marjanović, N.; Ferrini, R.; Ring, J.; Lee, K.-D.; Jiawook, R.; Drost, A.; König, M.; Müller, R.; Myny, K.; Genoe, J.; Kleb, U.; Hirshy, H.; Prétôt, R.; Kraxner, J.; Schmied, R.; Stadlober, B. Self-Aligned Flexible Organic Thin-Film Transistors with Gates Patterned by Nano-Imprint Lithography. *Org. Electron.* **2015**, *22*, 140–146. https://doi.org/10.1016/j.orgel.2015.03.047.
(44) Roberts, M. E.; Sokolov, A. N.; Bao, Z. Material and Device Considerations for Organic Thin-Film Transistor Sensors. *J. Mater. Chem.* **2009**, *19* (21), 3351–3363. https://doi.org/10.1039/B816386C.
(45) Lim, S.; Nguyen, K. V.; Lee, W. H. Enhancing Sensitivity in Gas Detection: Porous Structures in Organic Field-Effect Transistor-Based Sensors. *Sensors* **2024**, *24* (9), 2862. https://doi.org/10.3390/s24092862.
(46) Nketia-Yawson, B.; Noh, Y.-Y. Organic Thin Film Transistor with Conjugated Polymers for Highly Sensitive Gas Sensors. *Macromol. Res.* **2017**, *25* (6), 489–495. https://doi.org/10.1007/s13233-017-5108-7.
(47) Deng, P.; Ren, S.; Cao, K.; Li, H.; Zhang, Q. A Comparative Study of Bithiophene and Thienothiophene Based Polymers for Organic Field-Effect Transistor Applications. *J. Mater. Sci. Mater. Electron.* **2016**, *27* (9), 9143–9151. https://doi.org/10.1007/s10854-016-4950-2.

(48) Zhang, X.; Wang, B.; Huang, L.; Huang, W.; Wang, Z.; Zhu, W.; Chen, Y.; Mao, Y.; Facchetti, A.; Marks, T. J. Breath Figure–Derived Porous Semiconducting Films for Organic Electronics. *Sci. Adv.* **2020**, *6* (13), eaaz1042. https://doi.org/10.1126/sciadv.aaz1042.
(49) Wu, M.; Hou, S.; Yu, X.; Yu, J. Recent Progress in Chemical Gas Sensors Based on Organic Thin Film Transistors. *J. Mater. Chem. C* **2020**, *8* (39), 13482–13500. https://doi.org/10.1039/D0TC03132A.
(50) Thomson, G. Wm. The Antoine Equation for Vapor-Pressure Data. *Chem. Rev.* **1946**, *38* (1), 1–39. https://doi.org/10.1021/cr60119a001.
(51) *Vapor Pressure Calculation by Antoine Equation (Methanol)*. http://ddbonline.ddbst.com/antoinecalculation/antoinecalculationcgi.exe (accessed 2024-07-17).
(52) Ionin, B. I.; Ershov, B. A. The Fundamentals of NMR Spectroscopy. In *NMR Spectroscopy in Organic Chemistry*; Ionin, B. I., Ershov, B. A., Eds.; Springer US: Boston, MA, 1970; pp 1–59. https://doi.org/10.1007/978-1-4684-1785-2_1.
(53) Lambert, J. B.; Mazzola, E. P.; Ridge, C. D. *Nuclear Magnetic Resonance Spectroscopy: An Introduction to Principles, Applications, and Experimental Methods*; John Wiley & Sons, 2019.
(54) Smith, I. C. P.; Blandford, D. E. Nuclear Magnetic Resonance Spectroscopy. *Anal. Chem.* **1995**, *67* (12), 509–518. https://doi.org/10.1021/ac00108a037.
(55) Yang, R. Gel Permeation Chromatography. In *Analytical Methods for Polymer Characterization*; CRC Press, 2018.
(56) Goedhart, D.; Opschoor, A. Polymer Characterization by Coupling Gel-Permeation Chromatography and Automatic Viscometry. *J. Polym. Sci. Part -2 Polym. Phys.* **1970**, *8* (7), 1227–1233. https://doi.org/10.1002/pol.1970.160080716.
(57) Ng, H. M.; Saidi, N. M.; Omar, F. S.; Ramesh, K.; Ramesh, S.; Bashir, S. Thermogravimetric Analysis of Polymers. In *Encyclopedia of Polymer Science and Technology*; John Wiley & Sons, Ltd, 2018; pp 1–29. https://doi.org/10.1002/0471440264.pst667.
(58) Saadatkhah, N.; Carillo Garcia, A.; Ackermann, S.; Leclerc, P.; Latifi, M.; Samih, S.; Patience, G. S.; Chaouki, J. Experimental Methods in Chemical Engineering: Thermogravimetric Analysis—TGA. *Can. J. Chem. Eng.* **2020**, *98* (1), 34–43. https://doi.org/10.1002/cjce.23673.
(59) Yadav, L. D. S. Ultraviolet (UV) and Visible Spectroscopy. In *Organic Spectroscopy*; Yadav, L. D. S., Ed.; Springer Netherlands: Dordrecht, 2005; pp 7–51. https://doi.org/10.1007/978-1-4020-2575-4_2.
(60) Elgrishi, N.; Rountree, K. J.; McCarthy, B. D.; Rountree, E. S.; Eisenhart, T. T.; Dempsey, J. L. A Practical Beginner's Guide to Cyclic Voltammetry. *J. Chem. Educ.* **2018**, *95* (2), 197–206. https://doi.org/10.1021/acs.jchemed.7b00361.
(61) Pandey, A.; Dalal, S.; Dutta, S.; Dixit, A. Structural Characterization of Polycrystalline Thin Films by X-Ray Diffraction Techniques. *J. Mater. Sci. Mater. Electron.* **2021**, *32* (2), 1341–1368. https://doi.org/10.1007/s10854-020-04998-w.
(62) Freychet, G.; Gann, E.; Zhernenkov, M.; McNeill, C. R. Anisotropic Resonant X-Ray Diffraction of a Conjugated Polymer at the Sulfur K-Edge. *J. Phys. Chem. Lett.* **2021**, *12* (15), 3762–3766. https://doi.org/10.1021/acs.jpclett.1c00532.

(63) Osaka, I.; Takimiya, K. Backbone Orientation in Semiconducting Polymers. *Polymer* **2015**, *59*, A1–A15. https://doi.org/10.1016/j.polymer.2014.12.066.
(64) Berthomieu, C.; Hienerwadel, R. Fourier Transform Infrared (FTIR) Spectroscopy. *Photosynth. Res.* **2009**, *101* (2), 157–170. https://doi.org/10.1007/s11120-009-9439-x.
(65) Barnes, G.; Yau, C. P. Poly(Thiophene)s. In *Encyclopedia of Polymeric Nanomaterials*; Kobayashi, S., Müllen, K., Eds.; Springer: Berlin, Heidelberg, 2021; pp 1–15. https://doi.org/10.1007/978-3-642-36199-9_120-1.
(66) Kaloni, T. P.; Giesbrecht, P. K.; Schreckenbach, G.; Freund, M. S. Polythiophene: From Fundamental Perspectives to Applications. *Chem. Mater.* **2017**, *29* (24), 10248–10283. https://doi.org/10.1021/acs.chemmater.7b03035.
(67) Chan, H. S. O.; Ng, S. C. Synthesis, Characterization and Applications of Thiophene-Based Functional Polymers. *Prog. Polym. Sci.* **1998**, *23* (7), 1167–1231. https://doi.org/10.1016/S0079-6700(97)00032-4.
(68) McCullough, R. D. The Chemistry of Conducting Polythiophenes. *Adv. Mater.* **1998**, *10* (2), 93–116. https://doi.org/10.1002/(SICI)1521-4095(199801)10:2<93::AID-ADMA93>3.0.CO;2-F.
(69) Deng, P.; Ren, S.; Cao, K.; Li, H.; Zhang, Q. A Comparative Study of Bithiophene and Thienothiophene Based Polymers for Organic Field-Effect Transistor Applications. *J. Mater. Sci. Mater. Electron.* **2016**, *27* (9), 9143–9151. https://doi.org/10.1007/s10854-016-4950-2.
(70) Flynn, S.; Yuan, Y.; Cui, S.; Liu, H.; Li, X.; Wang, J.; Li, Y. Acetal- and Aldehyde-Substituted Thiophene-Benzodithiophene Copolymers for Organic Solar Cells. *ACS Appl. Energy Mater.* **2024**, *7* (3), 1277–1286. https://doi.org/10.1021/acsaem.3c02921.